DEVELOPMENT OF ALKYL POLYGLUCOSIDES (APG) NANOEMULSIONS CONTAINING IBUPROFEN AS A DELIVERY SYSTEM FOR PHARMACEUTICS

NURUL SHAHIDAH BINTI MOHAMAD SHAHRIPODDIN

FACULTY OF SCIENCE
UNIVERSITI MALAYA
KUALA LUMPUR

2022

DEVELOPMENT OF ALKYL POLYGLUCOSIDES (APG) NANOEMULSIONS CONTAINING IBUPROFEN AS A DELIVERY SYSTEM FOR PHARMACEUTICS

NURUL SHAHIDAH BINTI MOHAMAD SHAHRIPODDIN

DISSERTATION SUBMITTED IN FULFILMENT OF THE REQUIREMENTS FOR THE DEGREE OF MASTER OF SCIENCE

DEPARTMENT OF CHEMISTRY
FACULTY OF SCIENCE
UNIVERSITI MALAYA
KUALA LUMPUR

2022

UNIVERSITI MALAYA
ORIGINAL LITERARY WORK DECLARATION

Name of Candidate: **NURUL SHAHIDAH BINTI MOHAMAD SHAHRIPODDIN**

Matric No: **SGR160038 / 17028042/3**

Name of Degree: **MASTER OF SCIENCE**

Title of Dissertation:

DEVELOPMENT OF ALKYL POLYGLUCOSIDES (APG) NANOEMULSIONS CONTAINING IBUPROFEN AS A DELIVERY SYSTEM FOR PHARMACEUTICS

Field of Study:

PHYSICAL CHEMISTRY (COLLOIDAL CHEMISTRY)

I do solemnly and sincerely declare that:

(1) I am the sole author/writer of this Work;
(2) This Work is original;
(3) Any use of any work in which copyright exists was done by way of fair dealing and for permitted purposes and any excerpt or extract from, or reference to or reproduction of any copyright work has been disclosed expressly and sufficiently and the title of the Work and its authorship have been acknowledged in this Work;
(4) I do not have any actual knowledge nor do I ought reasonably to know that the making of this work constitutes an infringement of any copyright work;
(5) I hereby assign all and every rights in the copyright to this Work to the University of Malaya ("UM"), who henceforth shall be owner of the copyright in this Work and that any reproduction or use in any form or by any means whatsoever is prohibited without the written consent of UM having been first had and obtained;
(6) I am fully aware that if in the course of making this Work I have infringed any copyright whether intentionally or otherwise, I may be subject to legal action or any other action as may be determined by UM.

    Candidate's Signature   Date: 28/02/2022

Subscribed and solemnly declared before,

    Witness's Signature   Date: 28/02/2022

Name:

Designation:

DEVELOPMENT OF ALKYL POLYGLUCOSIDES (APG) NANOEMULSIONS CONTAINING IBUPROFEN AS A DELIVERY SYSTEM FOR PHARMACEUTICS

ABSTRACT

Green, nonionic and biomimicking properties of alkyl polyglucosides (APGs) have contributed to the re-emergence of sugar-based surfactants recently. This research aims to investigate the influence of alkyl polyglucoside (APG) as a co-surfactant in nanoemulsion formulation containing ibuprofen, as a model drug, which is intended to be used for topical application. The phase behaviour of oil/surfactant/water system containing ibuprofen, stability properties and comparison of preliminary particle size were investigated. The results showed that the ternary phase diagram of the CrEL:APG12 system with a ratio of 9:1 has the largest transparent isotropic region. When comparing nanoemulsion formulations with and without APG, it showed that the system with APG exhibited higher emulsifying ability than CrEL surfactant alone which due to the APG co-surfactant could decrease the water affinity and increased the oil affinity of the systems. Several formulations with different surfactant mixtures (CrEL only, CrEL:APG08, CrEL:APG10, and CrEL:APG12) were prepared. The particle sizes ranged between 20-200 nm and polydispersity index of less than 0.25 were obtained. The cytotoxicity results of nanoemulsion with APG12 and nanoemulsion without APG12 showed no toxic effect against 3T3 cell line. Thus, APG co-surfactants prolonged the storage stability, improved the structural morphology, and enhanced ibuprofen permeation. This suggests that APG could be used as an alternative stabilizing agent and the formulated nanoemulsion system could be used as a drug carrier system for pharmaceutical applications.

Keywords: Alkyl polyglucoside, Nanoemulsion, Ternary phase diagram, Stability.

PEMBANGUNAN NANOEMULSI ALKIL POLIGLUKOSIDA (APG) MENGANDUNGI IBUPROFEN SEBAGAI SISTEM PENGHANTAR UNTUK FARMASEUTIK

ABSTRAK

Alkil poliglukosida (APG) yang bersifat hijau, tidak berion dan biomimik telah menyumbang ke arah kebangkitan surfaktan berasaskan gula baru-baru ini. Penyelidikan ini bertujuan untuk mengkaji pengaruh alkil poliglukosida (APG) sebagai surfaktan bersama dalam formulasi nanoemulsi yang mengandungi ibuprofen, sebagai model ubat, yang bertujuan untuk digunakan bagi aplikasi topikal. Fasa tingkah laku sistem minyak/surfaktan/air yang mengandungi ibuprofen dengan nisbah campuran surfaktan yang berbeza, sifat kestabilan dan perbandingan saiz awal partikel telah dikaji. Hasil kajian menunjukkan bahawa gambar rajah fasa pertigaan bagi sistem CrEL:APG12 dengan nisbah 9:1 mempunyai kawasan isotropik lutsinar yang terbesar. Apabila dibandingkan formulasi nanoemulsi dengan dan tanpa APG, ini menunjukkan bahawa sistem dengan APG menunjukkan kemampuan pengemulsi yang lebih tinggi berbanding surfaktan CrEL sahaja yang disebabkan oleh surfaktan bersama APG dapat menurunkan afiniti air dan meningkatkan afiniti minyak sistem tersebut. Beberapa formulasi dengan campuran surfaktan yang berbeza (CrEL sahaja, CrEL:APG08, CrEL:APG010, dan CrEL:APG12) telah disediakan. Saiz partikel antara 20-200 nm dan indeks polidispersiti kurang daripada 0.25 telah diperoleh. Hasil ujian sitotoksik bagi nanoemulsi dengan APG12 dan nanoemulsi tanpa APG12 menunjukkan tiada kesan toksik terhadap titisan sel 3T3. Oleh itu, surfaktan bersama APG memanjangkan kestabilan penyimpanan, mengukuhkan struktur morfologi, dan meningkatkan penyerapan ibuprofen. Ini menunjukkan bahawa APG dapat digunakan sebagai agen penstabil alternatif dan sistem nanoemulsi yang diformulasikan boleh digunakan sebagai sistem pembawa ubat bagi aplikasi farmaseutik.

Kata kunci: Alkil poliglukosida, Nanoemulsi, Gambar rajah fasa pertigaan, Kestabilan.

TABLE OF CONTENTS

LIST OF FIGURES

LIST OF TABLES

LIST OF EQUATIONS

LIST OF SYMBOLS AND ABBREVIATIONS

$°C$	:	Celsius
a	:	Coefficient of temperature
A	:	Absorbance
a_0	:	Cross-sectional area of hydrophilic headgroup
A_{CO}	:	Interaction between surfactant and oil molecules
A_{CW}	:	Interaction between surfactant and water molecules
A_{HH}	:	Interaction between surfactant hydrophilic groups
A_{LL}	:	Interaction between surfactant lipophilic groups
A_{OO}	:	Interaction between oil molecules
A_{WW}	:	Interaction between water molecules
c	:	Molar concentration
C_∞	:	Solubility of the bulk phase
Cc	:	Characteristic curvature of surfactant
D	:	Diffusion coefficient
d	:	Hydrodynamic diameter
$EACN$	:	Effective alkane carbon number of oil
$f(S)$	:	Function of salinity
f_a	:	Mass fraction of the main surfactant
H	:	Total cell height
H_h	:	Hydrophilicity contributed by hydrophilic group
H_l	:	Hydrophilicity contributed by lipophilic group
HLB_a	:	HLB value of the main surfactant
HLB_b	:	HLB value of the co-surfactant
HLB_{EO}	:	HLB value for ethoxylated surfactants

HLB_{mix}	:	Total HLB value of the mixed surfactants
HLB_{PEG}	:	HLB value for PEG surfactants
I	:	Intensity of transmitted light
I_0	:	Intensity of incident light
k_0	:	Kinetic constant for zero order model
k_1	:	Kinetic constant for first order model
k_a	:	Ratio of particle radius to Debye length
k_B	:	Boltzmann constant
k_{EACN}	:	Scaling factor of effective alkane carbon number
k_H	:	Kinetic constant for Higuchi model
k_{HC}	:	Kinetic constant for Hixson–Crowell model
k_{KP}	:	Kinetic constant for Korsmeyer–Peppas model
l	:	Length of lipophilic tail
L	:	Path length of light through a solution
M	:	Molecular mass of the whole surfactant molecule
M_h	:	Molecular mass of the surfactant hydrophilic group
p	:	Packing parameter
Q_0	:	Initial amount of drug loaded
Q_t	:	Amount of drug released
Q_t/Q_∞	:	fraction of drug released
R	:	Winsor's R ratio
r	:	Radius
R^2	:	Correlation of determination
r_o	:	Initial droplet radius
S	:	Ester saponification value
$scan_i$	:	Turbiscan scan value at initial time

scan$_{i-1}$	:	Turbiscan scan value at given time
T	:	Temperature
t	:	Time
U$_e$	:	Electrophoretic mobility
v	:	Volume of the lipophilic tail
V$_m$	:	Molar volume of the internal phase
ΔBS	:	Changes in backscattering intensity
ΔBS$_{mean}$	:	Relative backscattering at mid segment of cell height
ΔBS$_{top}$	:	Relative backscattering at top segment of cell height
ε	:	Molar absorption coefficient
η	:	Viscosity
λ	:	Wavelength
ξ	:	Zeta potential value
ω	:	Frequency of rupture per unit of the film surface
1Φ	:	Monophasic region
APG	:	Alkyl polyglucoside
APG08	:	Octyldecyl polyglucoside (Oramix^{TM} CG110)
APG10	:	Decyl polyglucoside (Oramix^{TM} NS10)
APG12	:	Dodecyl polyglucoside (Glucopon® 600 CS UP)
API	:	Active pharmaceutical ingredients
BS	:	Backscattered light
CER	:	Cohesive energy ratio
CMC	:	Critical micelle concentration
CO	:	Coconut oil
CPP	:	Critical packing parameter
CrEL	:	Cremophor EL

CTAB	:	Cetyltrimethylammonium bromide
DDAB	:	Dimethyldidodecylammonium bromide
DLS	:	Dynamic light scattering
EIP	:	Emulsion inversion point
ELS	:	Electrophoretic light scattering
GRAS	:	Generally regarded as safe
HLB	:	Hydrophilic-lipophilic balance
HLD	:	Hydrophilic-lipophilic deviation
HPLC	:	High-performance liquid chromatography
IB	:	Ibuprofen drug
IC_{50} value	:	Drug concentration causing 50% growth inhibition
LAC	:	Limiting association concentration
LBS	:	Light backscattering technique
LCT	:	Long-chained triglycerides
MCT	:	Medium-chained triglycerides
ME	:	Microemulsion
MΦ	:	Multiphasic region
NE	:	Nanoemulsion
NE0	:	Nanoemulsion without any APG
NE1	:	Nanoemulsion with APG08
NE2	:	Nanoemulsion with APG10
NE3	:	Nanoemulsion with APG12
NE-highS	:	High-surfactant nanoemulsion with S:O ratio of 9:1
NE-lowS	:	Low-surfactant nanoemulsion with S:O ratio of 1:9
NIBS	:	Non-invasive backscattering
NLC	:	Nanostructured lipid carriers

NSAID	:	Nonsteroidal anti-inflammatory drug
O	:	Oil
O/W	:	Oil-in-water
O/W/O	:	Oil-in-water-in-oil
PBS	:	Phosphate-buffered saline
PDI	:	Polydispersity index
PEG	:	Polyoxyethylene glycol
PIC	:	Phase inversion composition
PIT	:	Phase inversion temperature
rpm	:	Rotations per minute
S	:	Surfactant
S:O ratio	:	Surfactant-to-oil ratio
SAD	:	Surfactant affinity difference
SANS	:	Small angle neutron scattering
SCT	:	Short-chained triglycerides
SD	:	Standard deviation
SDS	:	Sodium dodecyl sulfate
SE	:	Spontaneous emulsification
SLN	:	Solid lipid nanoparticle
SLS	:	Sodium lauryl sulfate
S_{mix} ratio	:	Mixed surfactants ratio
SOW	:	Surfactant-oil-water system
T	:	Transmitted light
TEM	:	Transmission electron microscopy
TSI	:	Turbiscan stability index
UV-Vis	:	Ultraviolet-visible

W	:	Water
W/O	:	Water-in-oil
W/O/W	:	Water-in-oil-in-water
wt.%	:	Weight percentage
ZP cell	:	Zeta potential cell

LIST OF APPENDICES

CHAPTER 1: INTRODUCTION

1.1   Research Background

Sustainable technology is never more crucial in this 21st century. Other than reducing environmental footprint, the slow or/and toxic biodegradability issue is addressed with development using natural-origin materials free from sulphate, phosphate, alkylphenol ethoxylate (Pantelic & Cuckovic, 2014). In contrast with petroleum-based surfactants, alkyl polyglycoside (APG) are biodegradable and eco-friendly sugar-based surfactants (Hato, 2001; Sulek et al, 2013; Pantelic, 2014). In comparison with its polyethoxylated counterpart, an APG is less susceptible to oxidation and elevated temperature. The mild character of APG is suitable for cosmetic and pharmaceutical applications (Keck et al., 2014). However, this versatile glycolipid surfactant group has a complex structure. Naturally extracted APG are difficult to be procured, hence synthetic APG such as Hashim's novel branched alkyl glycosides are promising amphiphilic designs (Hashim et al., 2012; Ahmad et al., 2012). Other than that, there are plenty of commercial APG surfactants such as product lines by Seppic (e.g. Montanov™, Fluidanov™, Simulsol™, and Oramix™) and also by BASF-Cognis (e.g. Glucopon®, Plantacare®, Agnique®, and Disponil®). The usage of commercial APG surfactants is versatile and cost-effective but APG surfactants exist as mixtures with different carbon chain lengths at heads and tails. Therefore, it is hard to make the head or tail of its phase behaviour (Jurado et al., 2008). However, this should be seen as a research opportunity to discover interesting APG-stabilized nanostructures such as nanoemulsions (Ahmad et al., 2014), hexosomes (Sazalee et al., 2017) and solid lipid nanoparticles (Keck et al., 2014). APG is continuously studied for its structural variations, phase behaviours (Fukuda et al., 2001, Ahmad et al., 2012), and compatibility in binary (Han et al., 2015) and ternary (Lim et al., 2012) mixtures.

Applications of APG ranging from emulsifying, foaming, wetting agent in day-to-day products to nanomaterial synthesis. The APG-stabilized formulation is also studied for the delivery of drugs such as ibuprofen (Djekic et al., 2011; Ahmad et al., 2014), lactobionic acid (Tasić-Kostov et al., 2011), adapalene and sertaconazole nitrate (Pajić et al., 2019) and spironolactone (Ilic et al., 2020). There are also APG-based drug carrier systems formulated that utilized the synergistic effect of surfactant and oil of the same carbons in the alkyl chain, such as C12/14 (myristyl glucoside and myristyl alcohol) and C16/18 (cetearyl glucoside and cetearyl alcohol) APG-mixed surfactants (Tasić-Kostov et al., 2011).

The selection of components depends on the purpose and the physicochemical properties of the desired formulation. In most cases, a single surfactant is insufficient for the formulation of the optimum and stable dispersion system. In order to provide hydrophilicity and lipophilicity effectively and to improve drug delivery, surfactant-stabilized formulations are incorporated with complementary excipients namely co-surfactants, co-solvent, humectant, hydrocolloid and polymer such as propylene glycol (Pajic et al., 2019; Vo et al., 2021), and xanthan gum (Salim et al., 2012). Excipients can be selected based on the targeted component. Suitable surfactants possess good oil solubilization capacity (the maximum amount of desired oil phases solubilized) (Matsaridou et al., 2012; Salim et al., 2011), surfactant efficiency (the minimum amount of surfactant required to completely homogenize equal masses of oil and water, S_{min}) and water solubilization capacity (the maximum amount of water solubilized surfactant/oil mixture, W_{max}) (Djekic et al., 2008). The selection of excipients may also depend on the drug solubilization capacity in order to elucidate possible drugs distribution in the formulated system (Pajić et al, 2017). Either drug solubility in each component or drug solubilizing power of the system, the latter is argued to be more dominant (Rahman et al., 2012). Thus, optimum compatibility is crucial, and this warrants the phase behaviour analysis during the pre-formulation phase.

Colloidal systems are mixtures of two or more components that are microscopically dispersed evenly in each other. An emulsion is a type of colloidal dispersion of liquid droplet in another liquid medium, bridged together by a surfactant forming a monophasic solution. The main categories of nanosized colloidal systems are nanoemulsion and microemulsion which can be unanimously defined based on their intrinsic energy profiles (Clements, 2012). The thermodynamically unstable nanoemulsion requires energy input to be formed as it has a higher energy state than its starting components. Therefore, nanoemulsions are formed with internal energy input from low-energy or formed with external energy input from high-energy methods. Low-energy methods are preferable as they are less disruptive, less expensive and produce finer and more stable nanoemulsions than high-energy methods. (Solans et al., 2005; Tadros et al, 2014: Jasmina et al., 2017). On the other hand, the thermodynamically stable microemulsion does not require energy input to be formed as it has a lower energy state than its starting components. Hence, the microemulsion is spontaneously formed (Solans & Sole, 2012). Another defining property of microemulsion is its ultralow interfacial tension that is generated with the specific surfactant, higher surfactant-to-oil ratio (McClements, 2012) and usually a shorter co-surfactant (Rosen & Kujanppu, 2012). This research aims to investigate the effect of APG in the formation of nanoemulsions containing a poorly water-soluble drug, ibuprofen, as a model drug. The in-vitro cytotoxicity and drug release study of the nanoemulsions were also evaluated.

1.2 Problem Statement

Alkyl polyglucoside (APG) surfactant group is a nonionic, biodegradable, and biocompatible glycolipid, making it is a greener alternative than conventional surfactants. APG is also utilized and patented in varying applications from emulsifying, foaming, wetting agent in day-to-day products to nanomaterial synthesis. However, phase behaviour study may be tricky due to APG complexity in structure and mixture. While the potential of APG as the main surfactant has been extensively studied (Ahmad et al., 2014; Pajić et al., 2017, Banerjee et al., 2020, Wei et al., 2020, and Ilic et al., 2021), the potential of APG as a co-surfactant in oil-in-water nanoemulsion system still has gaps to be explored.

Cremophor EL (CrEL) or PEG-35 castor oil is a commonly used drug vehicle with a notorious reputation in the pharmaceutical field. It was found to exhibit toxicity (Kiss et al., 2013) and hypersensitivity and to reduce the efficacy of paclitaxel anti-tumor drug (Gelderblom, et al., 2001, Skwarczynski et al., 2006, Mao et al., 2018, Caloguiri et al., 2019). In lieu of this, albumin-based Abraxane formulation served as a more tolerable chemotherapy substitute than CrEL-based Taxol formulation (Gonzalez-Valdivieso, et al., 2021). Other than using alternative, the dose-dependent toxicity of CrEL surfactant is tackled by lowering its proportion in formulation with compatible nanoparticles, surfactants, co-surfactant or co-solvent (Bergonzi et al., 2016, Piazzini et al., 2017, Zeng et al., 2017, and Reddy, 2020). This research aims to obtain a formulation with less than 20% surfactant mixture of CrEL surfactant and different APG co-surfactants. The concern related to CrEL surfactant is addressed with proper selection of compositional parameters and cytotoxicity study. We developed and investigated nanoemulsions stabilized with CrEL main surfactant (HLB 13.90) mixed with APG08, APG10 and APG12 co-surfactants (HLB 16.0, 12.6 and 11.2 respectively) as mixed surfactants may exhibit synergistic effect in reducing interfacial tension of nanoemulsion system.

Coconut oil is an inexpensive, readily available, and edible oil with a high solubilizing capacity for hydrophobic drugs. Ibuprofen (α-methyl-4-(2-methylpropyl)benzeneacetic acid) is a nonsteroidal anti-inflammatory drug (NSAID) with poor aqueous solubility, low molecular weight of 205.28 Daltons and short elimination half-life of 2-4 hours (Djekic et al., 2015). In this research, the model drug is to be encapsulated in coconut oil-in-water nanoemulsions with and without APGs. There is also the possibility of synergistic effect between surfactant and oil phases as APG08, APG10 and APG12 co-surfactants (8, 10, 12 carbon length respectively) possess similar alkyl chain length with the medium-chained triglycerides (6-12 carbon length) in coconut oil.

1.3   Motivations of Research

This research filling in the gap in the APG field especially its potential to be used in drug delivery systems. The problems in terms of structural complexity, economical practicality and cumulative toxicity are addressed in the development of the oil-in-water nanoemulsion. The formulation would also have high functionality and practicality values by using green and commercially available materials and a low-energy emulsification method. Therefore, this study is crucial to investigate the phase behaviour, physicochemical characteristics, and drug delivery properties of APG-incorporated nanoemulsion systems towards pharmaceutical application.

1.4   Objectives of Research

The objectives of this research are to:

1. screen the components and investigate the phase behaviour of water, Cremophor EL (CrEL), alkyl polyglucosides (APG) and coconut oil (CO) systems;

2. prepare and characterize the physicochemical properties and stability of nanoemulsion containing ibuprofen; and

3. evaluate the cytotoxicity and release of ibuprofen from nanoemulsions.

1.5   Dissertation Outline

Chapter 1 describes the general introduction of the phase behaviour and stability of APG-incorporated nanoemulsion and its potential as drug carrier systems. It covers topics such as introduction to amphiphiles, structure of amphiphiles, applications of amphiphiles, micelle, vesicle and mixed amphiphiles. Other than that, it states the research problem statement, motivations, objectives, and dissertation outline.

Chapter 2 represents the literature review and a more in-depth discussion of the research. It covers the reviews on surfactant, oil, emulsion and drug delivery system.

Chapter 3 describes the materials used throughout this work. It also covers the methodology and instrumentation used in this research.

Chapter 4 describes the results and discussions of the phase behaviour, nanoemulsion characterization, stability evaluation, cytotoxicity test and drug delivery study on the APG-incorporated drug carrier systems.

Chapter 5 gives general conclusions, including some ideas and recommendations for future research.

CHAPTER 2: LITERATURE REVIEW

2.1 Review on Surfactant

2.1.1 Classification of Surfactants

Surfactants, or also known as emulsifiers or tensides, can be classified in numbers of ways. Based on the molecular weight of the surfactants (Jahan et al., 2020), surfactants are classified into two general groups: (a) low molecular weight surfactants comprised of small molecule surfactants, polysaccharides, phospholipids, and proteins (McClements & Jafari, 2018); (b) high molecular weight surfactants comprised of polymeric and particulate surfactants (Pal et al., 2021). Based on the headgroups charge of the surfactants, conventional surfactants can be categorized into four types: nonionic (without any charge), cationic (carrying positive charge), anionic (carrying positive charge) and zwitterionic (carrying positive charge), as summarized in **Table 2.1**. The ionic surfactants i.e. cationic, anionic and zwitterionic are surfactants that have headgroups with electrically charged. The nonionic surfactants are surfactants that have headgroups are not electrically charged. (Myers, 2006; Jahan et al., 2020; Moldes, et al., 2021).

Table 2.1: Types, characteristics and examples of surfactants.

Types	Characteristics	Examples
Nonionic surfactants	Neutral-charged headgroup	· Polyoxyethylene glycol (PEG) · Polyoxyethylene sorbitan ester (Tween) · Sorbitan ester (Span) · Alkyl polyglucoside (APG)
Cationic surfactants	Positively charged headgroup	· Cetyltrimethylammonium bromide (CTAB) · Dimethyldidodecylammonium bromide (DDAB) · Benzalkonium chloride · Quarternary ammonium salts
Anionic surfactants	Negatively charged headgroup	· Sodium dodecyl sulfate (SDS) · Sodium lauryl sulfate (SLS)

		· Alkylbenzene sulfonates (detergents)
		· Salts of higher fatty acids (soaps)
Zwitterionic surfactants	Dual-charged headgroup	· Alkylcarboxylates (natural soaps)
		· Phospholipids
		· Betaines
		· Amphoacetate

Nonionic surfactants are chosen over ionic surfactants for their mild nature, high biocompatibility and low toxicity (Bastian, 2017; Chen et al., 2019). In contrast with ionic surfactants, nonionic surfactants are not sensitive towards electrolyte and pH fluctuation (Sheth et al., 2020). However, they are sensitive towards temperature fluctuations as ethoxylates become more hydrophobic at higher temperatures due to the decrease of the hydration of the headgroup. This characteristic property of nonionic surfactants leads to rich phase behaviour due to the variety of liquid crystal mesophases formed throughout the continuous change in spontaneous curvature hydrophilic-hydrophobic interface (Ferreira et al., 2013; Holmberg et al., 2014). Thus, the phase behaviour of APG-incorporated systems is one of the objectives in this research.

2.2   Behaviour of Surfactants

Surfactants, or emulsifiers are surface-active molecules composed of hydrophilic (water-loving) polar head and hydrophobic (water-hating) non-polar tail (Ali et al., 2020). Surfactants have different water solubility or affinity due to the slightest difference in structural variation in the hydrophobic and hydrophilic moieties. A surfactant with high water affinity will preferentially partition into water phase while a surfactant with low water affinity will preferentially partition into oil phase. The combination of surfactants with different solubilities may lower the water-oil interfacial tension differently than the individual surfactants (McClements & Jafari, 2018).

Adsorption is the tendency of surfactant molecules to partition themselves in specific orientation at the hydrophilic-hydrophobic interface, in order to reduce the unfavourable interactions between oil and water molecules. A surfactant molecule can adsorb at oil-water interface which leads to a decrease in interfacial tensions (Kronberg et al., 2014). There are different adsorption mechanisms: monomolecular adsorption (forming monolayer film), multimolecular adsorption (forming multilayer film) or solid particle adsorption (forming particulate film) (Marhamati et al., 2021). Adsorption is a dynamic process as both transfer of surfactant molecules from the bulk phase to the interface (adsorption) and the transfer of surfactant molecules from the interface to the bulk phase (desorption) occur quickly and simultaneously. Adsorption occurs spontaneously because the adsorption-desorption equilibrium tends towards the adsorption as adsorbed surfactant molecules possess lower free energy than surfactant molecules in bulk phase (Henríquez et al., 2009). However, a surfactant with insufficient non-polar groups will not adsorb to the interface, whereas a surfactant with excess non-polar groups will form insoluble aggregates (McClements, 2017). Therefore, a desirable surfactant must be able (1) to adsorb to oil-water interface hence effectively decrease the interfacial tension; and (2) to create a protective layer surrounding the dispersed droplets (Li et al., 2020).

Self-assembly, is the tendency of the surfactant molecules to assemble themselves. to reduce the unfavourable interactions between non-polar groups of surfactant molecules and the surrounding water molecules (McClements & Jafari, 2018). At diluted surfactant concentration, the molecules exist as monomers. As surfactant concentration increases, the molecules saturate the interface and accumulate in the bulk. At limiting association concentration (LAC), certain surfactants may form into oligomers. At critical micelle concentration (CMC), the molecules form into micelles. Surfactant molecules behave differently at different surfactant concentration (Rosenholm, 2020).

2.2.1 Characteristics of Surfactant

Surfactant characteristics needs to be understood to determine the optimal conditions of surfactant-oil-water (SOW) system. Over the years, several theories to describe surfactant characteristics and predict the SOW system: Bancroft's rule, Langmuir's oriented wedge theory, hydrophilic-lipophilic balance (HLB) by Griffin and Davies, Winsor-R ratio, solubility parameters by Hildebrand and Hansen, phase inversion temperature (PIT), cohesive energy ratio (CER), surfactant affinity difference (SAD), critical packing parameters (CPP), spontaneous curvature and bending elasticity, and hydrophilic-lipophilic deviation (HLD). The Hansen's solubility parameter and normalized HLD approached are urged to be utilized. However, the trial-and-error and practical surfactant mixing experimental works are still widely used (Perazzo et al., 2015; Abbott, 2020; Salager et al., 2020).

2.2.1.1 Bancroft's Rule

Bancroft postulated that the continuous phase is the phase in which surfactant is the most soluble. This means that hydrophilic surfactants will produce oil-in-water (O/W) emulsion while hydrophobic surfactants will form a water-in-oil (W/O) emulsion. In explaining the Bancroft Rule, Taylor's theory stated that deformable droplets can approach each other more quickly. When the hydrophilic surfactant is present, water droplets coalesce more quickly than oil droplets, thus causing O/W emulsion formation. However, anti-Bancroft O/W emulsion formed with very low concentrations of hydrophobic surfactant shows that the Bancroft rule has limitations (Abbott, 2017).

2.2.1.2 Winsor's R Ratio

Winsor's R theory pioneered the understanding that the intermolecular interactions can be related to the behaviour of the SOW system. Surfactant affinity can be described from the ratio of the attractive interactions between surfactant molecules and oil molecules A_{CO} and water A_{CW} molecules (**Equation 2.1**). Bourrel and Schechter extended the original Winsor's R ratio to include the repulsive interactions between oil molecules A_{CO}, between water molecules A_{WW}, between lipophilic tails A_{LL}, and between hydrophilic heads A_{HH} (**Equation 2.2**). $R << 1$ corresponds to Winsor system type I where surfactant interacts more with water phase thus forming micelles solubilizing oil inside. $R < 1$ indicates the increased relative miscibility with water (decreased relative miscibility with oil). On the other spectrum, $R >> 1$ corresponds to Winsor system type II where surfactant interacts more with oil phase thus forming reverse micelles solubilizing water inside. $R > 1$ indicates the decreased relative miscibility with water (increased relative miscibility with oil). $R = 1$ corresponds to Winsor system type III where surfactant equally interacts with both oil and water forming middle phase structure. Type I system appears as biphasic mixture composed of micellar layer with excess oil layer at the top. Type II system appears as biphasic mixture composed of reverse micellar layer with excess water layer at the bottom. Type III system appears as triphasic mixture composed of structured middle phase sandwiched between excess oil and water layers. Type IV system appears a monophasic mixture as there is sufficiently high surfactant concentration to cosolubilize both oil and water into true microemulsion (Sheng, 2010; Salager et al., 2020).

$$R = \frac{A_{CO}}{A_{CW}} \qquad (2.1)$$

$$R = \frac{A_{CO} - A_{OO} - A_{LL}}{A_{CW} - A_{SO} - A_{HH}} \qquad (2.2)$$

2.2.1.3 Hydrophilic-Lipophilic Balance (HLB)

Hydrophilic-lipophilic balance (HLB) is the historical first useful empirical guide to utilize surfactants efficiently. According to Griffin (1949), the HLB values for ethoxylated surfactants HLB_{EO} are calculated based on the molecular masses of the hydrophilic group, M_h and the whole surfactant, M (**Equation 2.3**) while the HLB values for PEG surfactants HLB_{PEG} are calculated based on the ester saponification value, S and the fatty acid value, A (**Equation 2.4**). On the other hand, HLB values according to Davies (1957) are calculated based on the cumulative hydrophilicity contributed by hydrophilic H_h and lyophilic H_l groups (**Equation 2.5**). From, HLB values of mixed surfactants can be calculated based on the HLB values of individual surfactants where f_a is the mass fraction of the main surfactant while HLB_a and HLB_b are the HLB values of the main surfactant and co-surfactant respectively (**Equation 2.6**). The determined HLB of surfactant is then matched with the required HLB of oil to obtain the desired emulsion (**Figure 2.1**). Surfactants with high HLB show affinity towards water (hydrophilic) and are used to formulate oil-in-water (O/W) emulsions. Surfactants with low HLB show affinity towards oil (lipophilic) and are used as formulate water-in-oil (W/O) emulsions.

$$HLB_{EO} = 20\left(\frac{M_h}{M}\right) \tag{2.3}$$

$$HLB_{PEG} = 20\left(1 - \frac{S}{A}\right) \tag{2.4}$$

$$HLB = \sum H_h - \sum H_l + 7 \tag{2.5}$$

$$HLB_{mix} = f_a(HLB_a) + (1 - f_a)(HLB_b) \tag{2.6}$$
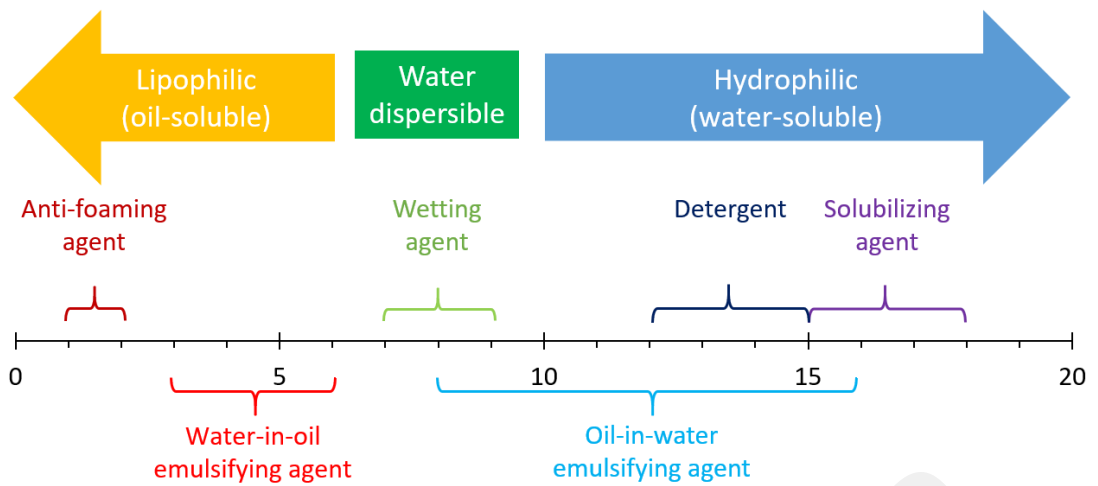
Figure 2.1 Hydrophilic-lipophilic balance (HLB) scale with example materials and the type of emulsifying agents.

HLB has been a useful and highly utilised reference for formulators. However, HLB is not perfect and may give inaccurate predictions. There is no correlation that can be found between Davies' and Griffin's HLB values, especially for polyoxyethylene surfactants (Ontiveros et al., 2014). HLB is not applicable to surfactants of different polarities and complexities such as molecular weight of surfactant, branching of lipophilic tail, aromaticity of oil, presence of electrolyte, additives, temperature, pressure and specific interactions in the system which have significant impact in applications such as enhanced oil recovery application. As such, hydrophilic-lipophilic deviation (HLD) is a better alternative (Pasquali et al., 2008, McClements & Jafari, 2018; Salager et al., 2020).

2.2.1.4 Hydrophilic-Lipophilic Deviation (HLD)

Hydrophilic-lipophilic deviation (HLD) is the empirical description of the relationship between variables in a surfactant-oil-water system (Salager, 2020). While the HLB describes the property of the surfactant, the HLD describes the property of the system. HLD is adapted from surfactant affinity difference and is a more comprehensive alternative as oil, temperature and salinity components are also factored in the empirical calculation of solubility characteristics (Perazzo et al., 2015). **Equation 2.7** shows that in the HLD calculation (**Figure 2.2**): (1) the surfactant component is denoted by the characteristic curvature of surfactant, Cc; (2) the oil component is denoted by the effective alkane carbon number of oil $EACN$ with 0.17 scaling factor k_{EACN}; (3) the temperature component is denoted by the temperature deviation ΔT from the standard temperature 25°C and the coefficient of temperature a which is 0 for APG; and (4) the salinity component is denoted by the $f(S)$ which is 0.13S and ln(S) for nonionic and ionic electrolytes respectively (Abbott, 2017).

$$HLD = Cc - k.EACN - \alpha.\Delta T + f(S) \tag{2.7}$$

HLD terms			
(1) Surfactant	**(2) Oil**	**(3) Temperature**	**(4) Electrolyte**
Cc	$k.EACN$	$\alpha \Delta T$	$f(S)$

HLD models		
HLD < 0	**HLD = 0**	**HLD > 0**
O/W emulsion	Bicontinuous or true emulsion	W/O emulsion
Winsor Type I	Winsor Type III or IV	Winsor Type II
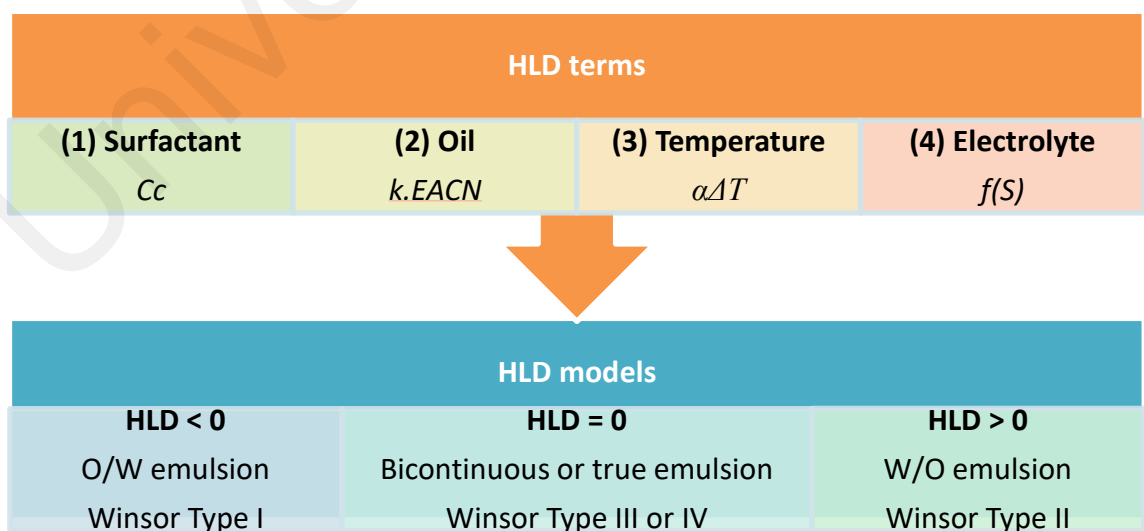
Figure 2.2: Hydrophilic-lipophilic deviation (HLD) terms and models.

2.2.1.5 Critical Packing Parameter (CPP)
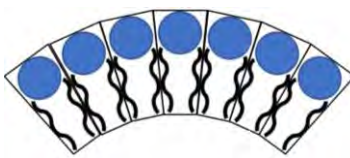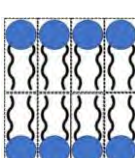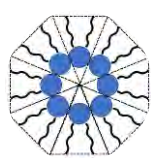
Critical packing parameter (CPP) is a theoretical frame to measure of the preferred geometry adopted when surfactant molecules pack themselves and it is used to predict aggregate morphology (**Table 2.2**). The dimensionless packing parameter, *p* is calculated from the ratio of the volume of the lipophilic tail, *v* over the length of lipophilic tail, and the cross-sectional area of hydrophilic headgroup, a_0 (**Equation 2.8**).

$$p = \frac{v}{a_0 l} \tag{2.8}$$

Repulsive interaction between aggregates may induce packing into ordered cubic phases. Attractive interaction between aggregates may induce clouding phenomena, followed by phase separation above a critical point (Langevin, 1992). The role of interactions between aggregates is significant when its concentration or growth is substantial enough, but CPP is not a constant and it may be influenced by surfactant concentration, temperature and salinity. The length of cylindrical micelles increases with the increase of surfactant concentration or/and increase of alkyl chain tail (Pantelic et al., 2014). In certain conditions, wormlike or threadlike micelles are formed as micelles elongate to minimize excess free energy (Acharya et al., 2006).

In regard to this research, the packing parameters of alkyl polyglucoside (APG) surfactants are not known due to their structural complexity and polymeric nature. However, the packing parameters of APG08, APG10 and APG12 may be similar to their simpler counterparts C8, C10, C12 glucosides which formed spherical geometries in a small-angle neutron scattering (SANS) study (Moore et al., 2018). Another SANS study showed that Cremophor EL (CrEL) also formed spherical micelles (Jadhav et al., 2021). Therefore, it can be deduced that $p < 1/3$ for CrEL and APG surfactants used.

Table 2.2: Morphologies of monomer and aggregate predicted by critical packing parameter (CPP).

Monomer shape	Packing parameter	Aggregate structure
Cone	$p < \frac{1}{3}$	Normal micelle
Truncated cone	$\frac{1}{3} < p < \frac{1}{2}$	Elongated micelle
Slightly truncated cone	$\frac{1}{2} < p < 1$	Vesicle
Cylinder	$p \sim 1$	Planar bilayer
Wedge	$p > 1$	Reversed micelle

2.2.2 Alkyl Polyglucoside Surfactants

Alkyl polyglucosides (APG) are nonionic, non-ethoxylated, mild, biodegradable glycolipids. Other than the advantages as a nonionic surfactant, the biodegradability and ease of availability (can be synthesized from renewable resources and in mild condition) of APG deem it superior in comparison with other surfactants. Synthetic APG compensates for the difficulties in extraction and purification of its natural counterpart (Pantelic et al., 2014). However, most APG are commercially available as complex blends differing in alkyl chain length, degree of polymerization and stereochemistry (Fukuda et al., 2001; Ahmad et al., 2012; Ahmad et al., 2014). They are studied in their structural variations or/and synergism/compatibility with other surfactants or additives, mostly either in binary mixtures (Zhang R. et al., 2004; Wang et al., 2005; Ruiz & Molina-Bolivar, 2011; Han et al., 2015; Sazalee et al., 2017) or in ternary mixtures (Zhang J. et al., 2004; Nainggolan et al., 2009; Jiang et al., 2011; Lim et al., 2012).

An APG molecule is made up of a relatively rigid polar sugar head and a relatively flexible a polar alkyl chain tail. APG with short (i.e. 6-14 carbon atoms) chain length is more soluble in polar solvents, while APG with long (i.e. 16-22 carbon atoms) chain length is more soluble in non-polar solvents. APG with too long or too short chains exhibit low surface activity (Sulek et al., 2006). The longer the alkyl chain tail, the lower the critical micelle concentration (CMC) value (Pantelic et al., 2014). Increasing degree of polymerization or increasing size of sugar headgroup renders the APG to be more soluble in polar medium, e.g. glucoside and maltoside headgroups study by Ahmad et al. (2014).

2.3   Review on Oil

The main components of nanoemulsions are surfactant, aqueous, and oil phases. The importance of oil lies in its lipophilicity to increase the solubilization, availability and absorption of lipophilic active ingredients (Rajpoot & Tekade, 2019). Oils are composed of fatty acid derivatives, phospholipid, sterols, tocols and hydrocarbons like alkane squalene and carotene. The composition and proportion of fatty acids vary intrinsically. Therefore, the fatty acid profile is the thumbprint of oil. Fatty acids have specified Cm:n shorthand whereby m and n is the number of carbon the number of the double bond in the alkyl tail of the fatty acid. Common fatty acids have common names that are usually based on the fatty acid origin: caproic (C6:0), caprylic (C8:0), capric (C10:0), lauric (C12:0), myristic (C14:0), palmitic (C16:0), stearic (C18:0), oleic (C18:1) and linoleic (C18.2) (Marina et al, 2009). Fatty acids in oils can be categorized based on the saturation degree: saturated fatty acid (SFA) with no double bond, monounsaturated fatty acid (MUFA) with a double bond, and polyunsaturated fatty acid (PUFA) with multiple double bonds.

Fatty acid derivatives are free fatty acid, monoacylglycerol, diacylglycerol and triacylglycerol or also known as triglycerides (Amri et al., 2011) which make up 95% of oil. Since most fatty acid derivatives are triglycerides, both terms are sometimes interchangeably used. Triglycerides are esters of 1 glycerol molecule and 3 fatty acid molecules and esterification renders triglycerides to be non-polar (Lusas et al., 2017). Triglycerides can be categorized based on the alkyl tail: short-chained triglycerides (SCT) with less than 6 carbon atoms, medium-chained triglycerides (MCT) with 6-12 carbon atoms, and long-chained triglycerides (LCT) with more than 12 carbon atoms.

The oil used in this research is coconut oil. Coconut oil is composed of minor portion of PUFA (4.04%) and MUFA (16.65%) and major portion of SFA with low SCT (0.78%) and high MCT (78.53%) percentages. MCT which is predominantly found in coconut oil has a lower molecular weight, high water solubility, lower interfacial tension, and higher solvent capacity than LCT (Anderson & Marra, 1999; Cao et al., 2004). Due to the advantages of MCT, a number of MCT-based commercial products such as Miglyol are commonly used in pharmaceuticals formulation. However, coconut oil is less utilized as compared to its constituent MCT. Examples of studies utilizing coconut oil in nanoemulsion systems are unloaded, cyclosporine-loaded and curcuminoid-loaded coconut oil-based nanoemulsions (Hasan et al., 2015; Musa et al., 2017; Jintapattanakit et al., 2018). Coconut oil-based systems have also been manufactured using low-energy emulsification method and high-energy emulsification method such as ultrasound-assisted and high-shear-homogenized (Ramisetty et al., 2015; Pengon et al., 2018).

2.4   Review on Colloidal Systems

Colloidal systems are mixtures of two or more components that are microscopically dispersed evenly in each other. The different kinds of colloidal systems vary in terms of the content, dimension and structure. There are (a) emulsion systems: equilibrium micelles and microemulsions, non-equilibrium nanoemulsions and emulsions (McClements, 2020; Feng et al., 2020; Sheth et al., 2020); (b) vesicular systems: liposomes, niosomes, ethosomes, and phytosomes (Doost et al., 2020); (c) lipid nanoparticle systems: solid lipid nanoparticles and nanostructured lipid carriers (Keck et al., 2014; Samimi et al., 2019; Duan et al, 2020); and (d) gel systems: microgels and hydrogels (de Lima et al., 2020; Li et al., 2021). Emulsions are colloidal dispersion of liquid droplet in another liquid medium, bridged together by surfactant forming monophasic   solution.   The   three   conventional   emulsion-based   systems   are

macroemulsions, nanoemulsions and microemulsions. As nanosized emulsions are of interest, nanoemulsions and microemulsions will be the highlights of this brief review. which can be characterized based on their type, size, method of formation, and stability characteristics. (McClements et al., 2012; Callender et al., 2017).

2.4.1   Characteristics of Nanoemulsion and Microemulsion

Nanoemulsions are non-equilibrium thermodynamically unstable colloidal dispersions. The energy profiles of the nanoemulsions are at higher energy state than the energy profiles of the starting components. Nanoemulsions contain droplets with mean diameters of less than 100 nm, whereas macroemulsions contain droplets with mean diameters of 100 nm to 100 μm (Vincekovic et al., 2017; McClements 2020). conventional emulsions with particle size in the range of hundreds above the particles size limit of nanoemulsion. Due to its smaller size, nanoemulsions possess higher resistance to coalescence thus can remain stable long enough before the reversion process occurs. Nanoemulsions are previously referred to as mini-emulsions (El-Aasser et al., 1988), submicron emulsion (Benita et al., 1993), translucent emulsion (Sing et al., 1999), or ultrafine emulsions (Callender et al., 2017). On the other hand, macroemulsions appear opaque or turbid, thus commonly referred to as coarse or opaque emulsions.

Microemulsion are isotropic thermodynamically stable colloidal dispersions. The energy profiles of the microemulsions are at lower energy state than the energy profiles of the starting components. This causes microemulsion to be thermodynamically stable, hence able to be formed spontaneously. The microemulsion is sometimes interchangeably known as swollen micelle or micellar emulsion or micellar solution. This is despite arguments that micellar solution term should be exclusive to surfactant in a solvent thus not applicable to ternary systems, and swollen micelle has less distinct smaller core and less stability than microemulsion (Siano, 1983; Langevin, 1992).

Macroemulsions, nanoemulsions and microemulsions appear differently based on the diameter of particles that scatter light, as shown in **Table 2.3**. Nanoemulsion usually appears bluish because the shorter-wavelength (blue) light is reflected while longer-wavelength (red) light is transmitted. This is commonly referred to as the Tyndall effect which was proposed to explain the colour of the sky. However, the sky is blue due to light scattering by air molecules (smaller than the wavelength of light) as described by Rayleigh; and not contaminant particles (larger than the wavelength of light) as described by Tyndall (He et al., 2009; Rootman et al., 2014). Rayleigh and Mie scatterings are mathematically precise, as opposed to Tyndall scattering of which exclusive category is debatable. In terms of long-term stability, it may be difficult to differentiate between highly kinetically stable nanoemulsion and thermodynamically stable microemulsion. In terms of size, other than the confusion regarding micro- (10^{-6}) and nano- (10^{-9}) prefixes, there is no clearly defined size ranges to distinguish microemulsion and nanoemulsion. There is no consensus to distinguish nanoemulsion from macroemulsion; whether on the size limit (whether 100 nm, 200 nm, or 500 nm) or the size parameter (whether radius or diameter). Nanosized particles, including nanoemulsions, exhibited diameters of 1-100 nm (McClements, 2021) define nanoemulsion having a radius less than 100 nm. David McClements proposed to clearly define the radius mean *i.e.* Z-average, number-weighted average (r_{10}), surface-weighted average (r_{32}), or volume-weighted average (r_{43}). Practical methods can be done to investigate long-term storage, sample history, particle size, and particle shape (McClements, 2012).

Microemulsions and nanoemulsions can be composed of the oil phase, aqueous phase, and surfactant(s). However, certain types of surfactants, higher surfactant-to-oil ratio (McClements, 2012) and usually a shorter co-surfactant (Rosen & Kunjappu, 2012) are required to generate ultralow interfacial tension in microemulsion. To know the nature of the dispersed and continuous phases, the emulsion can be tested using simple

experiments such as dye test (O/W emulsion is uniformly coloured with water-soluble dye), filter paper test (O/W emulsion which is not highly viscous can spread out rapidly when dropped on filter paper), fluorescence test (spotty fluorescence when O/W emulsion is exposed to UV light), and conductance test (O/W emulsion conducts electricity and circuit is completed).

2.4.2 Formation of Nanoemulsion and Microemulsion

Emulsion-based systems are fabricated with oil, water, and surfactant and are added with auxiliary agents for the purposes of physicochemical modification or/and stability enhancement (McClements, 2018). Emulsification can be done using high- and low-energy methods which are driven by external and internal forces respectively. Examples of high-energy methods are sonication, ultrasonic cavitation, microfluidization, and high-pressure homogenization (Jaiswal et al., 2015 & Sarheed et al., 2020). High-energy methods can be used for wider range of ingredients but require costly specialized equipment. Examples of low-energy methods are spontaneous/self-emulsification (SE), emulsion inversion point (EIP) which is a catastrophic phase inversion process, phase inversion temperature (PIT) and phase inversion composition (PIC) which are transitional phase inversion processes (Kumar et al., 2015). Low-energy method is preferable over high-energy methods due the cost-effectiveness and produce nanoemulsions with smaller and more uniformed size, without the risk interfacial film rupture (Solans & Sole, 2012).

2.5   Review on Drug Delivery System

An active pharmaceutical ingredient or more specifically drug is delivered by carrier systems A good drug delivery system can maximize therapeutic effect while minimizing toxicity. Nanoemulsion is a good delivery vector because it does not only make up of generally regarded as safe (GRAS) components. It also protects drugs during delivery and so hinders patient variability. The advantage of nanoemulsion mostly lies in its small droplet size and stability which facilitates loading, solubilization capacity, bioavailability, targeting and controlled release of targeted drugs (Chime et al., 2014, Sabjan et al., 2020). Hence, nanoemulsions are used in a variety of drug delivery routes.

Enteral ('through the intestines') administration usually includes drug delivery through oral (mouth) and rectal (rectum). Oral delivery is the oldest delivery route that involves placing a drug under the tongue (sublingual) or placing a drug between the tongue or cheek (buccal). Poorly water-soluble drugs require sufficient aqueous solubility against gastrointestinal conditions during the gastrointestinal passage. Nanoemulsions meet this prerequisite as drugs are encapsulated and preserved within the dispersed phase of nanoemulsion. The nanosized nanoemulsion has a higher surface-area-to-volume ratio than coarser emulsion, hence drug uptake is more readily available.   Liquid-state emulsions such as vesicles and nanoemulsions (NE) show a higher lipid digestion rate than solid-state emulsions such as solid lipid nanoparticles (SLN) and nanostructured lipid carriers (NLC) (Yukuyama et al., 2017). Examples of drugs used for oral nanoemulsion are cyclosporine, ritonavir, saquinavir (Zhao et al., 2013), aspirin, cilostazol, ezetimibe (Yukuyama et al., 2017), amlodipine besylate, curcumin, pitavastatin (Patel et al., 2018), tacrolimus (Rosso et al., 2020), rosuvastatin and silybinin (Wu et al., 2020).

Parenteral ('not through the intestines') administration is the oldest non-oral delivery and it includes injection of drug directly to the targeted site for rapid action. Common parenteral routes are intradermal (into the skin), intravenous (into the bloodstream), subcutaneous (under the skin), and intramuscular (into the muscle) routes. Hydrophobic drugs require sufficient solvent solubility (Patel et al., 2018) and non-charged rod-like particles with hydrophilic PEG chain are preferable for this administration route. Parenteral drug carriers must be small enough (less than 100 nm) to escape cell phagocytosis, yet large enough (more than 30 nm) to avoid leaking into blood capillaries (Yukuyama et al., 2017). Examples of drugs used for parenteral nanoemulsions are risperidone, sorafenib, diazepam, indinavir, thalidomide (Patel et al., 2018), carbamazepine, clotrimazole, docetaxel, insulin, paclitaxel, (Nikam et al., 2018), cefuroxime (Harun et al., 2018), and ciprofloxacin (Said Suliman et al., 2020)

Topical administration involves drug diffusion across the skin for local action while transdermal administration involves drug diffusion across the skin for systemic action (Patel et al., 2018). Topical drug carriers must be able to penetrate skin barriers through hair follicles, intercellular routes, and external routes. These three pathways across the stratum corneum layer are not mutually exclusive and permeation-enhanced nanoemulsions can permeate through a combination of pathways (Robert, 1997). Oil-based nanoemulsion enhances its permeation, possesses sufficient viscosity to distribute evenly and avoid being washed away. Other than the aesthetically pleasing clear appearance of nanoemulsions, there is a slight accumulation of drugs on the targeted area (Salim et al., 2016). Examples of drugs used for topical nanoemulsions are aceclofenac, celecoxib, diclofenac, flurbiprofen, ibuprofen, ketoprofen, meloxicam, piroxicam (Shakeel et al., 2010), lacidipine, ropinirole, voriconazole (Chellapa et al., 2015), propranolol (da Silva Marques et al., 2018), and naringenin (Akrawi et al., 2020).

The stability of a drug delivery system is crucial as it needs to be resistant throughout the delivery administration. Stability is defined as the capability of a formulation in a system to retain its specifications (Bajaj et al, 2012) against destabilizatio. It is important to understand how and why destabilization phenomena occur in order to formulate a stable drug carrier system. Creaming can be hindered when particles are lower than 90 nm in radius. Ostwald ripening can be hindered by using an oil phase with minimal water solubility. Flocculation and coalescence can be hindered by using surfactants with strong interdroplet repulsion (McClements, 2012).

Generally, a delivery system carries drugs at its core. Therefore, the continuous phase must be compatible with the drug nature and able to solubilize the maximum drug amount. Mixtures of surfactants or surfactant/alcohol or surfactant/hydrocolloid are commonly used to provide both hydrophilicity and lipophilicity effectively. In this research, the oil pre-mixture blend was consisting of ibuprofen (a hydrophobic compound) solubilized in coconut oil (CO), while the surfactant pre-mixture blend was made of Cremophor EL (CrEL) and alkyl polyglucoside (APG). Once the blends were completely homogenized, water was added to make up the final mixture, as shown in **Figure 2.3**.
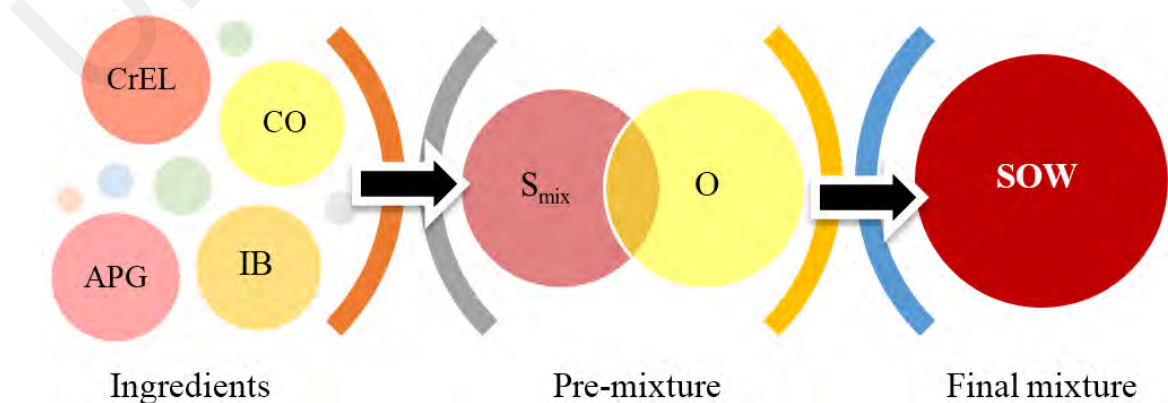
Figure 2.3: Flow of surfactant-oil-water preparation.

CHAPTER 3: METHODOLOGY

3.1 Materials

Octyl decyl polyglucoside (Oramix^{TM} CG110) and decyl polyglucoside (Oramix^{TM} NS10) were purchased from Seppic (Milan, Italy). Dodecyl polyglucoside (Glucopon® 600 CS UP), coconut oil of certified organic grade and polyethoxylated castor oil (Cremophor® EL) were purchased from Sigma-Aldrich (Missouri, US). Ibuprofen [α-methyl-4-(2-methyl propyl)benzene acetic acid] was purchased from Eurochem (China). Materials were used as received without purification. Sample preparations utilised deionised water produced from Diamond Nano-pure deioniser (Sartorius) with an ionic conductivity of 18.2 µS cm^{-1}. n-Dodecyl β-D-glucopyranoside with 98% purity was sparingly done and only highlighted in the morphological study. It was represented by inexpensive commercial blend Glucopon® 600 CS UP with 50% purity due to the similarities in general properties. Cremophor® EL, Oramix^{TM} CG110, Oramix^{TM} NS10, Glucopon® 600 CS UP, coconut oil, and ibuprofen were referred to as CrEL, APG08, APG10, APG12, CO, and ibuprofen.

Table 3:1: General properties of surfactants used

Code	Trade name	Main chemical component	Active content (%)	HLB value	Approx. alkyl chain length
APG08	Oramix^{TM} CG110	C8 alkyl polyglucoside	-	16.0	8
APG10	Oramix^{TM} NS10	C10 alkyl polyglucoside	55	12.6	10
APG12	Glucopon® 600 CS UP	C12 alkyl polyglucoside	50	11.2	12
CrEL	Cremophor EL® (or Kolliphor EL®)	Polyethoxylene glycol-35 castor oil	-	12-14	17

3.2   Methodology

3.2.1   Phase Behaviour Study

Ternary phase diagrams were constructed at room temperature to illustrate the equilibrium composition of components in the system (Hadzir et al., 2015). The oil phase was prepared by dissolving 0.25 g of ibuprofen in 2.5 g of coconut oil (CO) until a clear mixture formed. A surfactant mixture was prepared by mixing Cremophor EL (CrEL) and dodecyl polyglucosides (APG12) at a CrEL:APG12 ratio of 9:1 using vortex-mixer (VM-300, Gemmy Industrial CORP, Taiwan) for 5 min. The surfactant mixture and oil phase at different surfactant-to-oil (S:O) ratios of 10:0, 9:1, 8:2, 7:3, 6:4, 5:5, 4:6, 3:7, 2:8, 1:9 and 0:10 were prepared in 10-mL screw-cap glass tubes and homogenized using a benchtop centrifuge EBA 20 (Hettich, Germany) at 4000 rpm for 5 min. Water (5 wt.%) was added dropwise into the mixtures and the samples were vortexed for homogenization. Then, samples were then centrifuged at 4000 rpm for 15 min. The appearance of the mixture was visually observed: clear single-phase mixtures were denoted as monophasic region, 1Φ whereas cloudy or separated phases were denoted as multiphasic region, MΦ. The steps were repeated with 5 wt.% increments until a total of 90 wt.% water was added. These experiments were repeated without the addition of APG, and different mixture ratios of CrEL:APG12 (8:2 and 6:4) and different APG (APG08 and APG10). Ternary phase diagrams were constructed using the Chemix School v3.50 Software (Arne Standnes, Norway) and denoted with respective hydrophilic-lipophilic balance, HLB values (calculation are shown in Appendix).

3.2.2   Preparation of Nanoemulsions

Based on the ternary phase diagrams, several sets of nanoemulsion formulations were selected and prepared. The nanoemulsions were prepared by the phase inversion composition method at room temperature. The effect of the presence of ibuprofen, the presence of APG, the different concentrations of ibuprofen, and the different types of APG were investigated. A mixture of surfactant and coconut oil was homogenized first in a screw-capped vial at a specified weight ratio using a vortex mixer. The vial was then sealed with parafilm and left in a water bath at 40°C overnight. On the next day, water was then added dropwise into the mixture. The sample was sealed with parafilm again and left equilibrated in a 25°C water bath overnight then kept for further analysis.

3.2.3   Characterization of Nanoemulsions

3.2.3.1 Particle Size and Polydispersity Index Measurement

Particle sizes of the samples were measured using dynamic light scattering (DLS) at 25°C using Malvern Zetasizer Nano-ZS (Malvern Instruments Ltd., UK) equipped with 633 nm laser with a detector at 173° angle. Particle size measurement was repeated thrice. Z-average mean diameter size and polydispersity index (PDI) values obtained were shown as mean ± standard deviation (n = 5). As a measure of the narrowness of particle size distribution, PDI of less than 0.25 indicated a monodisperse system (Salim et al., 2018).

3.2.3.2 Zeta Potential Measurement

Zeta potential (ZP) values of the selected nanoemulsion formulations were determined by measuring the electrophoretic mobility of the dispersed particles in a charged field. Optimized nanoemulsions were diluted with deionized water at different dilution factors (1x, 10x, 100x, and 1000x dilution) and were injected into the ZP cell. Three measurements of 20 sub-runs were performed using Malvern Zetasizer Nano-ZS (Malvern Instruments Ltd., UK).

3.2.3.3 Morphology Measurement

Morphology of ibuprofen-loaded formulations was visualized using a high-resolution transmission electron microscope HRTEM H-7100 (Hitachi Ltd, Japan). Samples were placed on a 200 mesh formvar carbon-coated copper grid (Polyscience Inc, US) and the excess samples were removed after 10 min incubation. Then, samples were negatively stained with phosphotungstic acid solution, and the excess samples were removed after 5 min incubation. Excess liquid removal was done using Whatman filter paper No. 1 (Whatman International Ltd, UK) followed by drying at room temperature.

3.2.4 Stability Study

3.2.4.1 Centrifugation Test

The formulations were centrifuged using a benchtop centrifuge EBA 20 (Hettich, Germany) at 4000 rpm for 15 minutes. Centrifugal field served to accelerate creaming/sedimentation directly instead of accelerated ageing by storing the samples (Badolato et al., 2008).

3.2.4.2 Cooling-Heating Cycling Test

The physical stability of the formulations was carried out under cooling-heating cycle test for 5 cycles (24 hours at 5 ± 1°C, 24 hours at 25 ± 1°C, and back to 24 hours at 5 ± 1°C, for one cycle). The test was assessed based on the visual inspection of optical clarity and homogeneity of the system (Djekic et al., 2015).

3.2.4.3 Stability via Light Backscattering Measurement

The destabilization of the formulations was evaluated using Turbiscan Classic MA 2000 Stability Analyzer (Formulaction Co, France). Samples were scanned every 30 minutes for 72 hours in backscattering mode at room temperature. Backscattered light profile as a function of samples height was analysed. Changes in backscattering intensity (ΔBS) were plotted as a function of time. Relative backscattering at middle (10-50 mm) ΔBS_{mean} and top (50-55 mm) ΔBS_{peak} segments of cell height was plotted to evaluate mean and peak value kinetics. Turbiscan stability index (TSI) was calculated (**Equation 3.1**).

$$TSI = \sum_{i} \frac{\sum_{h}|scan_i(h) - scan_{i-1}(h)|}{H} \tag{3.1}$$

where $scan_i$ and $scan_{i-1}$ are scan value initial and given time respectively, H is the total height and TSI is the sum of scan differences in the measurement time.

3.2.4.4 Stability via Dynamic Light Scattering Measurement

Triplicates of nanoemulsion formulations were kept at storage temperatures of 4, 25 and 40°C representing common temperature limits for pharmaceutical storage and application (Djekic et al., 2015). The particle sizes were measured every week for 3 months using Malvern Zetasizer Nano-ZS (Malvern Instruments Ltd., UK). Triplicates samples were then measured in three consecutive measurements.

3.2.4.5 Kinetic Analysis of Destabilization

Based on the changes in particle size over time, Ostwald ripening, and coalescence rates were analysed to identify the cause of particle size change. The coefficients of determination were obtained from the graphs to determine the best-fit equation.

Coalescence is the creation of larger droplets due to the rupture of thin film hence the merging of droplet interfaces. In **Equation 3.2**, t is the storage time in seconds, r is the average droplet radius, r_0 is the initial droplet radius at $t=0$, and ω is the frequency of rupture per unit of the film surface. A graph of $(1/r^2)$ against time (seconds) was plotted to evaluate the coalescence rate.

$$\frac{1}{r^2} = \frac{1}{r_0{}^2} - \left(\frac{8\pi}{3}\right)\omega t \tag{3.2}$$

Ostwald ripening is the creation of larger droplets due to the diffusive transfer of the oil phase through the aqueous phase. Ostwald ripening rate is derived from the Lishitz-Slyozov-Wagner theory. In **Equation 3.3**, t is the storage time in seconds, r is the average radius, ω is the frequency of rupture per unit of the film surface, C_∞ is the solubility of the bulk phase, V_m is the molar volume of the internal phase, D is the diffusion coefficient of the dispersed phase in the continuous phase, k_B is Boltzmann constant and T is the

absolute temperature. A graph of (r^3) against time (seconds) was plotted to evaluate the Ostwald ripening rate.

$$\omega = \frac{dr^3}{dt} = \frac{8}{9}\left[\frac{C_\infty \gamma V_m D}{kT}\right]$$ (3.3)

3.2.5 *In-vitro* Drug Release Study

In-vitro drug release of ibuprofen from nanoemulsion formulations was studied using dialysis bag technique according to Arbain et al (2018). The dialysis bag used was hydrophilic cellulose with cut-off of 5000 molecular weight, which would allow the passage of ibuprofen of 206.28 molecular weight. The membrane was rinsed thoroughly with water and dilute (0.2%) sulphuric acid to get rid of any glycolipid present, thus eliminating any possible influence of membrane nature on the diffusion of the target molecules (Clement et al, 2000). Then, it was immersed in phosphate-buffered saline (PBS; pH 7.4) solution, overnight for equilibrium. 8.0 g of samples were filled into dialysis bags, which were then submerged in PBS and maintained at 37°C and stirred constantly at 300 rpm. Every hour, aliquots were withdrawn and were replaced with the same volume of PBS at each sampling times (0, 1, 2, 3, 4, 5, 6, 7, 8, 9, 10, 12 and 24 hours) to maintain sink condition. Spectrophotometric determination of ibuprofen concentration was done using a UV-Vis Spectrophotometer (Varian, Cary 50, Varian, USA) at a wavelength of maximum absorption of ibuprofen (220 nm). The calibration curve of ibuprofen-in-coconut oil solutions versus absorbance was used to estimate the ibuprofen concentration by applying Beer's law. The linear equation of the calibration curve determined was y = 0.0322x + 0.0469 with r^2 of 0.9918. The experiment was performed in triplicates for all samples and with respect to the percentage of cumulative ibuprofen detected.

3.2.5.1 Kinetics Release

The kinetic release was evaluated with respect to several drug release kinetic models. A graph of the percentage of the cumulative drug released versus time was plotted for the zero-order model (**Equation 3.4**). A graph of log percentage of the cumulative drug remained versus time was plotted for the first-order model (**Equation 3.5**). A graph of the percentage of the cumulative drug released versus square root of time was plotted for the Higuchi model **(Equation 3.6)**. A graph of log percentage of the cumulative drug released versus log time was plotted for the Korsmeyer–Peppas model (**Equation 3.7**). A graph of the cube root of the drug remained versus time was plotted for the Hixson–Crowell model (**Equation 3.8**).

$$Q_0 - Q_t = k_0 t \tag{3.4}$$

$$\ln(Q_0/Q_t) = -k_1 t \tag{3.5}$$

$$Q_t = k_H t^{1/2} \tag{3.6}$$

$$Q_t/Q_\infty = k_{KP} t^n \tag{3.7}$$

$$Q_0^{1/3} - Q_t^{1/3} = k_{HC} t \tag{3.8}$$

where Q_0 is the initial drug amount loaded, Q_t is the amount of drug released, Q_t/Q_∞ is the fraction of drug released, t is time, and $k_0, k_1, k_H, k_{KP},$ and k_{HC} are the kinetic constants for zero order, first order, Higuchi, Korsmeyer–Peppas, and Hixson–Crowell models.

3.2.6 *In-vitro* Cytotoxicity Study

Cytotoxicity test was performed using MTT (3-[4,5-dimethylthiazol-2-yl]-2,5 diphenyl tetrazolium bromide) assay. The concentrations of 2×10^4 cells/mL of 3T3 cell culture were plated onto 96-well sterile plates concentration (100 µL/well). Diluted sample extracts with concentrations of 500, 100, 50, 20, 10, 5 and 1 µg/mL were prepared and incubated for 72 hr. Incubated samples were then stained with MTT solution and further incubated for 3 hr. Dissolution of the resulting purple was done using DMSO and then incubated in dark for 2 hr. Measurement of absorbance at 570 mm wavelength was done using ELISA reader (Hidex, Turku, Finland) and reported as the average of three replicates. Cell viability was calculated using the formula in **Equation 3.9** below. Cytotoxicity was recorded as drug concentration causing 50% growth inhibition of the fibroblast 3T3 cells (IC_{50} value).

$$\text{Cell viability} = \frac{\text{Absorbance of sample}}{\text{Absorbance of control}} \times 100\% \tag{3.9}$$

3.2.7 Statistical Analysis

All experiments were carried out in triplicate and data were shown as mean ± SD (n = 3), unless otherwise indicated. The models were confirmed by analysis of goodness-of-fit correlation of determination (R^2) where R^2 values need to be more than 0.95.

3.3 Instrumentation

3.3.1 Particle Size Analyzer

Zetasizer Nano-ZS (Malvern Instruments Ltd., UK) is used for particle size analysis. Dynamic light scattering (DLS) method quantifies the Brownian motion of dispersed particle in the form of average hydrodynamic size and polydispersity of particles. The fluctuating scattering signals from the Brownian motion (Babick, 2019) is detected at 173° angle (**Figure 3.1**). At this angle, non-invasive backscattering (NIBS) allows measurement of more concentrated sample and less multiple scattering.
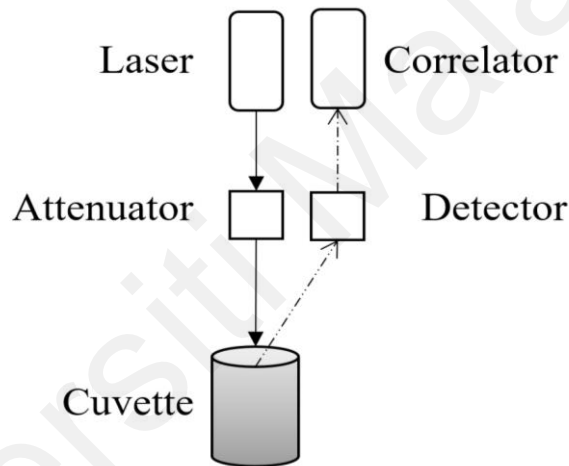
Figure 3.1: A schematic diagram of the operating principle of Zetasizer.

DLS measurement of particle size is not direct measurement as it is based on the movement of the particles. The faster the velocity of Brownian motion, the smaller the size of the dispersed particle. Hence, the particle size is calculated using the Stokes-Einstein equation. as shown in **Equation 3.10.**

$$D = \frac{k_B T}{3\pi\eta d} = \frac{k_B T}{6\pi\eta r} \tag{3.10}$$

where D is the translational diffusion coefficient, r and d are the hydrodynamic radius and hydrodynamic diameter, k_B is the Boltzmann constant, T is the absolute temperature, and η is the viscosity (Instrument, 2004). The factors that affect the diffusion speed of dispersed particles are the particle concentration, particle shape, particle surface and ion in medium. Samples must be in low concentration or diluted prior to measurement to prevent multiple scattering effect. Technique such as multi-angle depolarized dynamic light scattering, static light scattering, and microscopy need to be employed to identify possible non-sphericity of samples.

Polydispersity index (PDI) is a fundamental parameter to determine the quality of successful, stable, and safe formulation. The polydispersity (or non-uniformity or broad distribution) of particle sizes is indicated by PDI values of more than 0.3 for lipid-based carriers (Danaei et al., 2018) or PDI values of more than 0.25 for nanoemulsions (Salim, et al., 2018). PDI values higher than 0.5 indicate severe polydispersity that renders the data unreliable (Babick 2019).

Zetasizer Nano-ZS instrument is also used for zeta potential analysis which provides information on surface functionality and dispersion stability as electrostatic repulsion between particles is reflected. Zeta potential, or also known as electrokinetic potential, can be determined when mobility is induced by streaming potential, sedimentation potential, electroosmosis or electrophoresis (Instrument, 2004). Electrophoretic light scattering (ELS) method determines the movement of charged particles suspended in a medium. Calculation of electrophoretic mobility is based on the Henry equation (as shown in **Equation 3.11**).

$$U_e = \frac{2\varepsilon \cdot \xi \cdot f(ka)}{3\eta} \tag{3.11}$$

where U_e is the electrophoretic mobility. ξ is the zeta potential, ε is the dielectric constant, η is the viscosity, k_a is the ratio of particle radius to Debye length and $f(k_a)$ is the Henry's function, which value is: (a) 1.5 following Smoluchowski approximation for large particles in high dielectric constant media; (b) 1.0 following Huckel approximation for small particles in low dielectric constant media. Absolute zeta potential values lower than 10 indicate neutral dispersion. Absolute zeta potential values higher than 30 indicate strongly ionic dispersion (Clogston, et al. 2010).

3.3.2 Stability Analyzer

The long-term stability of nanoemulsions without APG and with APGs (APG08, APG10 and APG12) were estimated using accelerated shell-life testing using Turbiscan stability analyzer. Other than Turbiscan that can assess stability under Earth's gravity, LUMizer can assess stabilities under Earth's gravity and under centrifugal force (Dammak et al., 2020).

The measurement of the Turbiscan stability analyser is based on multiple light scattering method, where a sample in a 60 mm standardized cell is scanned as a function of sample height for 72 h in the backscattering mode at room temperature. Stability analyzer Turbiscan Classic MA 2000 (Formulaction Co, France) was equipped with 850 nm laser light source. There were two detectors at 135° (backscattered light, BS) and 0° (transmitted light, T), as shown in **Figure 3.2**. equipped with 850 nm laser light source.
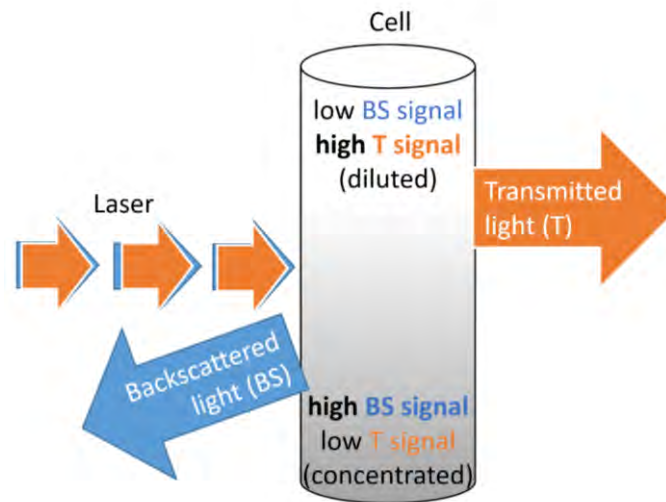
Figure 3.2: A schematic diagram of the operating principles of Turbiscan.

Based on Mie theory, both T and BS intensities are proportional to the dispersed phase volume fraction and inversely proportional to dispersed phase droplet size. In this research, delta backscattering, ΔBS was analysed. The main advantages of using Turbiscan are (1) non-destructive: it does not require sample dilution, thus more accurate determination of destabilization phenomena; (2) versatility; it can be used to pre-formulate and study dispersions of varying concentration and turbidity; and (3) efficiency: it is 20-50 times faster than the laborious and grossly accurate visual observation (Carbone et al, 2015; Kim et al, 2016; Sazalee et al, 2017).

The output data from Turbiscan stability analyzer was correlated with instability phenomena: particle migration (creaming or sedimentation) or particle variation (flocculation or coalescence). Particle migration is shown by local variations at the extremities: sedimentation is shown when the top part decreased while the bottom part increased; whereas creaming is shown when the top part increased while the bottom part decreased. Particle size variation is shown by global variations on the whole sample height: flocculation or coalescence is shown when the whole part decreased. No particle size change is shown when all scattering lines are superimposed.

3.3.3 Transmission Electron Microscope

Transmission electron microscopy (TEM) was performed to investigate the morphology of ibuprofen-loaded nanoemulsions by placing a drop of nanoemulsion suspension onto a 200 mesh formvar carbon-coated copper grid (Polyscience Inc, US) and the excess samples were removed after 10 min incubation. Then, samples were negatively stained with phosphotungstic acid solution, and the excess samples were removed after 5 min incubation. Excess liquid removal was done using Whatman filter paper No. 1 (Whatman International Ltd, UK) followed by drying at room temperature. Afterwards, a high-resolution transmission electron microscope HRTEM H-7100 (Hitachi Ltd, Japan) was used to visualize the morphology of ibuprofen-loaded nanoemulsion formulations. The acquired digital images were processed with Adobe Photoshop® software. **Figure 3.3** shows the principle of TEM.
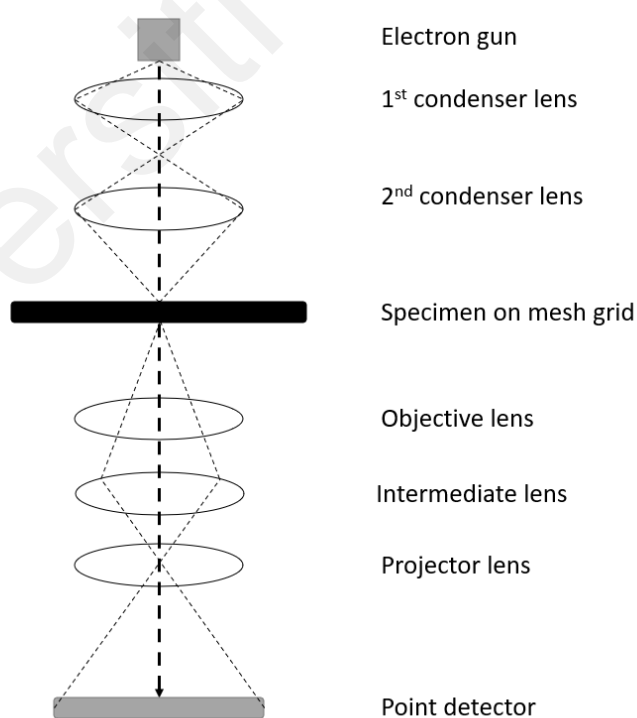
Figure 3.3: A schematic diagram of the operating principles of transmission electron microscopy (TEM).

3.3.4 UV-Visible Light Spectrophotometer

Turbidity is caused by scattering of light from the forward direction and reduction in the transmitted. Intensity of light can be calculated using Beer-Lambert equation (Hardesty & Attili, 2010) as shown in **Equation 3.12**.

$$A = \varepsilon cL = \log\frac{I_0}{I} \tag{3.12}$$

where A is the absorbance, ε is the molar absorption coefficient, c is the molar concentration, I and I_0 are the transmitted and incident light intensities, and L is the path length of light through a solution, which is usually 1 cm sample cell dimension. The absorbance profile presented in this work was scanned with the help of a Varian Cary 50 ultraviolet-visible (UV-Vis) spectrophotometer (Varian, USA). A schematic diagram of the instrument is shown in **Figure 3.4**. Under the given sets of conditions, the absorbance is the indirect measure of turbidity. The turbidimetric measurement of ibuprofen drug released from the nanoemulsions without and with APG08, APG10 and APG12 co-surfactants (NE0, NE1, NE2 and NE3) was performed at the 220 nm wavelength.
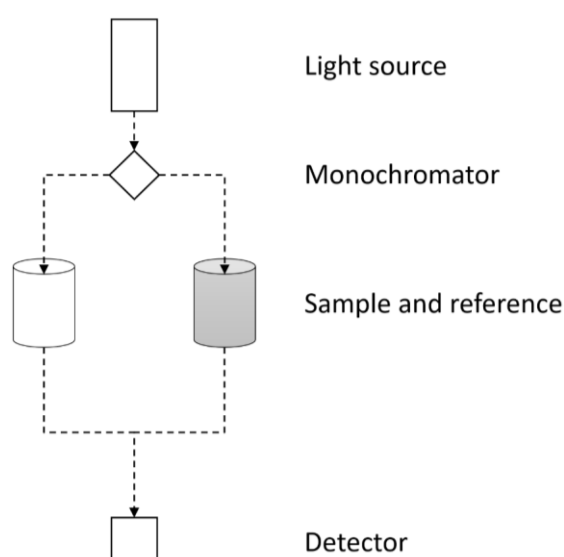
Figure 3.4: A schematic diagram of the operating principles of UV-Visible (UV-Vis) light spectrophotometer.

CHAPTER 4: RESULTS AND DISCUSSION

4.1   Phase Behaviour Study

Figure 4.1 shows the ternary phase diagram of CrEL/CO/W system which is the reference for the consequent phase diagrams of CrEL:APG08/CO/W system (**Figure 4.2**), CrEL:APG10/CO/W system (**Figure 4.3**), and CrEL:APG08/CO/W system (**Figure 4.4**). Based on visual inspection, there were two different regions present: the clear single-phase (1Φ) and the cloudy multiphase (MΦ) regions. The monophasic 1Φ region was studied due to relation with the phase transition during emulsification of nanoemulsion (Salim et al., 2018) and the unclear appearance showed incompatibility or breakdown in the system (Djekic et al., 2011). The successful formation of single-phase mixtures indicated the good compatibility of components in the designated systems for emulsification.
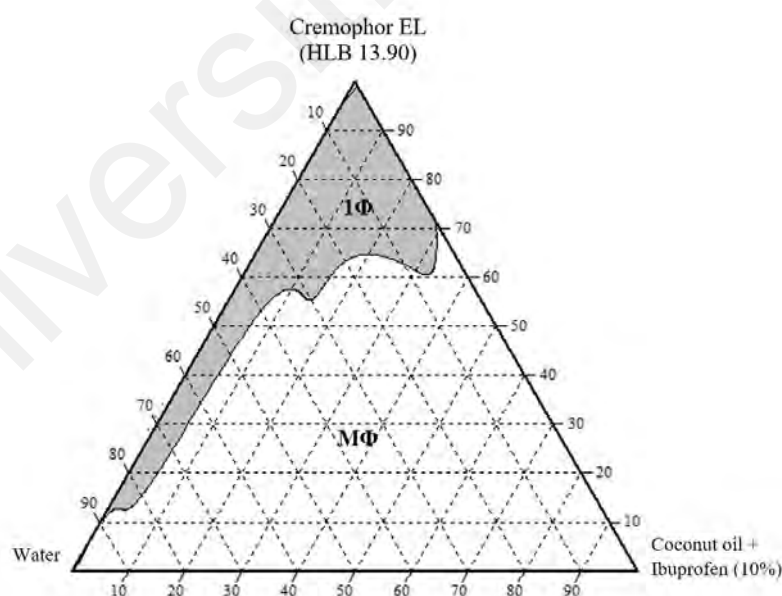
Figure 4.1: Phase diagram of system without APG co-surfactant: CrEL/CO/W system where Cremophor EL, coconut oil, water were abbreviated as CrEL, CO and W, respectively.
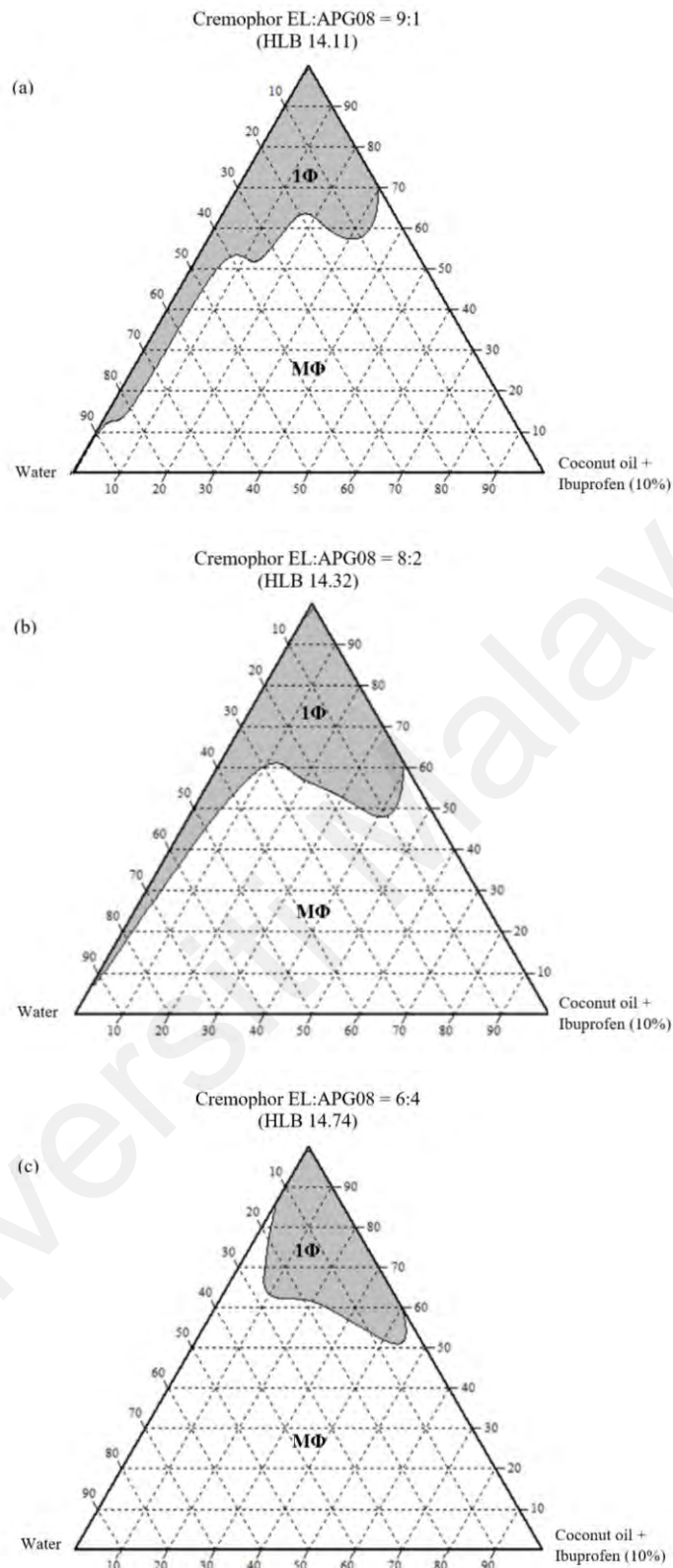
Figure 4.2: Phase diagrams of systems with APG08 co-surfactant: (a) (9:1)CrEL:APG08/CO/W, (b) (8:2)CrEL:APG08/CO/W, and (c) (6:4)CrEL:APG08/CO/W systems where Cremophor EL, commercial octyl decyl polyglucoside, coconut oil, and water were abbreviated as CrEL, APG08, CO, and W, respectively.
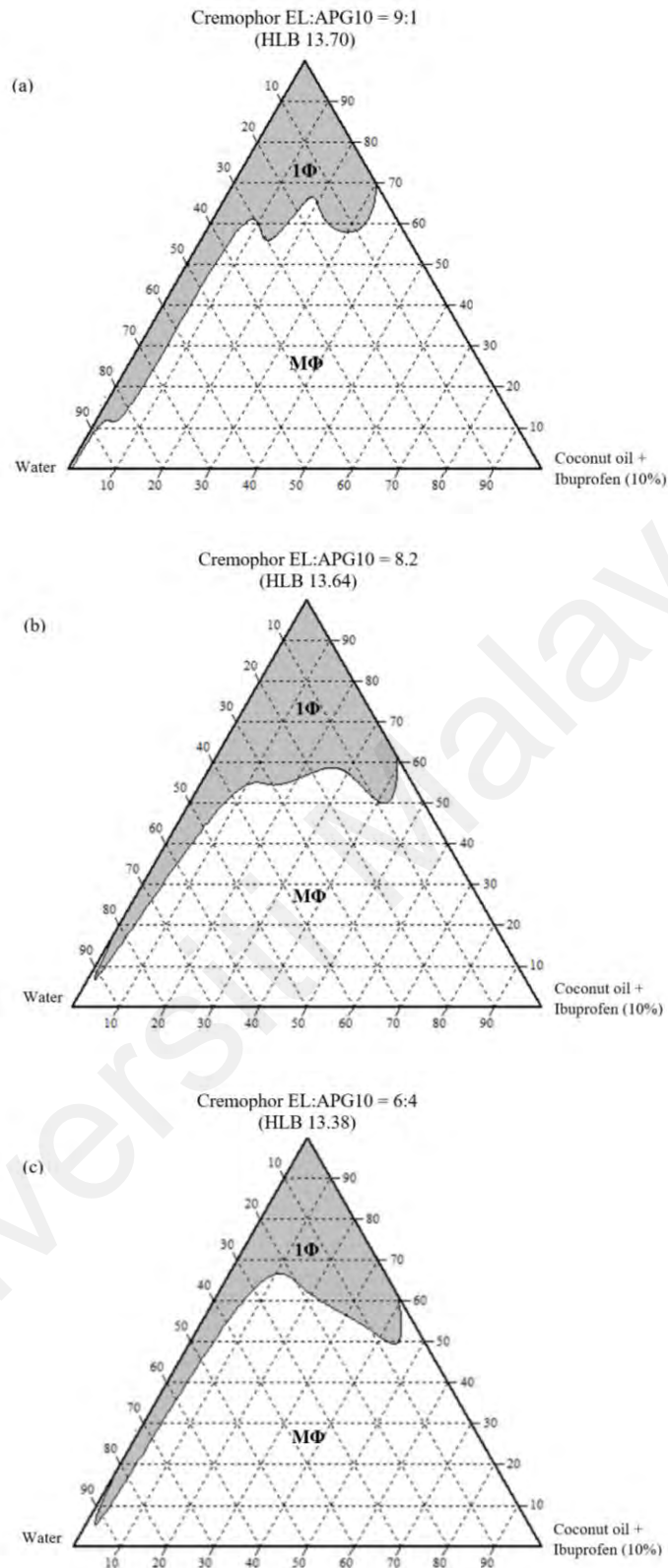
Figure 4.3: Phase diagrams of systems with APG10 co-surfactant: (a) (9:1)CrEL:APG10/CO/W, (b) (8:2)CrEL:APG10/CO/W, and (c) (6:4)CrEL:APG10/CO/W systems where Cremophor EL, commercial decyl polyglucoside, coconut oil, and water were abbreviated as CrEL, APG10, CO, and W, respectively.
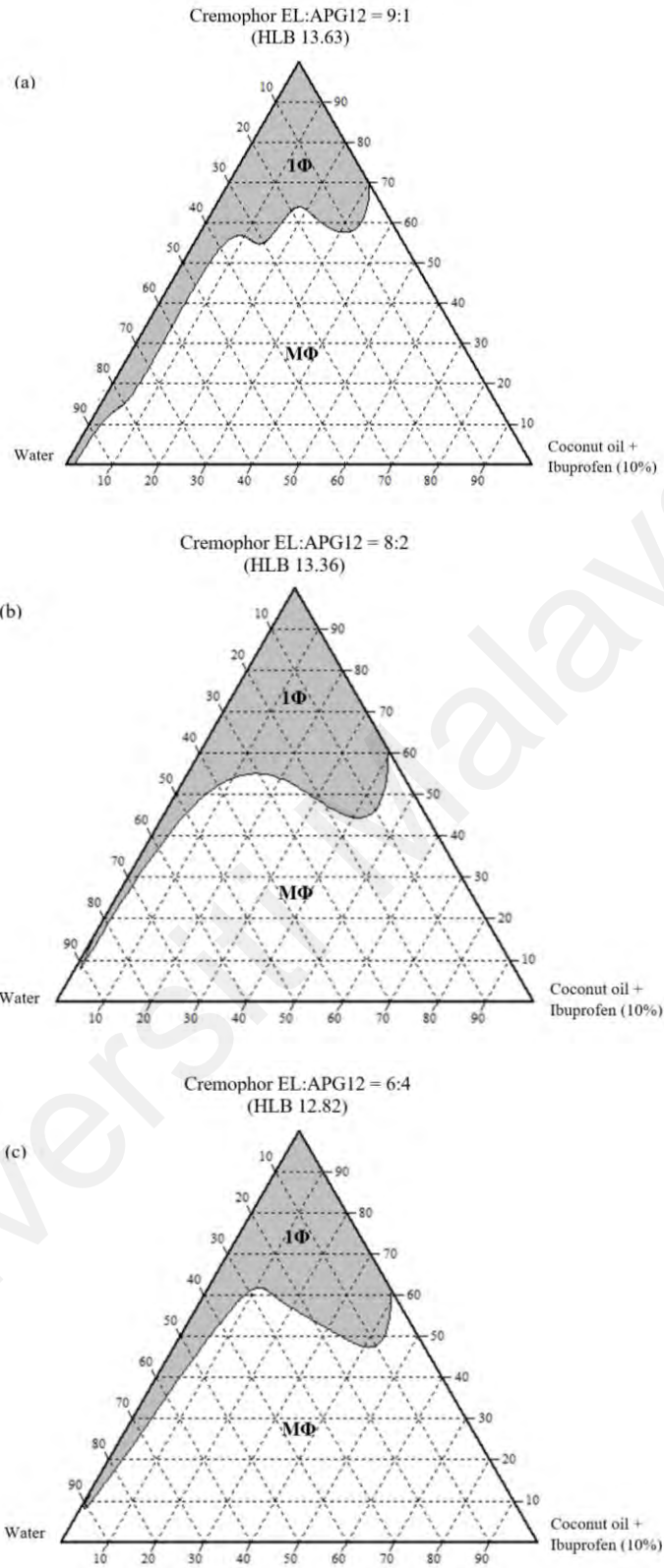
Figure 4.4: Phase diagrams of systems with APG12 co-surfactant: (a) (9:1)CrEL:APG12/CO/W, (b) (8:2)CrEL:APG12/CO/W, and (c) (6:4)CrEL:APG12/CO/W systems where Cremophor EL, commercial dodecyl polyglucoside, coconut oil, and water were abbreviated as CrEL, APG12, CO, and W, respectively.

APG directly affects the hydrophilic-lipophilic balance (HLB) values of the tensides and the single-phase regions. HLB values of surfactant(s) illustrate the solubility of the surfactants, and so predict the type of emulsion (Ahmad et al., 2012). The lower the HLB value of the surfactant, the more lyophilic it is, and hence the more likely it is to form an oil-in-water colloidal dispersion. **Figure 4.4(a)** (CrEL:APG12 = 9:1, HLB 13.63) showed the largest 1Φ region that extends from the surfactant-rich apex to the water-rich apex. Upon water addition along this emulsification path, phase transition occurred clear viscous mixtures to clear less-viscous mixtures. This visually observed phase transition is in agreement with studies employing nuclear magnetic resonance (Fanun, 2008) and optical polarizing microscopy (Salim et al., 2012). As phase transition occurred within this region, this is a crucial indicator for oil-in-water (O/W) emulsification.

Systems stabilized with CrEL:APG ratios of 8:2 and 6:4 (**Figure 4.2(b-c), Figure 4.3(b-c)** and **Figure 4.4(b-c)**) demonstrated trends with further increase of respective APG co-surfactant. The 1Φ regions in these systems shifted away from the water-rich vertex towards the oil-rich vertex. As APG surfactant exhibited lower HLB value than CrEL surfactant, further increase of APG decreased the hydrophilicity and increased the lipophilicity of these systems. These 1Φ regions shrunk in size due to the excess and the bulkiness of APG that disrupted the interfacial surfactant film. Excess APG surfactant proportion caused chain stiffness that affected the surfactant packaging in the interfacial film (Pajic et al., 2019). Other than the hydrophilic-lyophilic factor, the geometrical factor of the structural arrangement surfactants at the interface contributed synergistic effects in the surfactant film (Fanun, 2008). The APG08, APG10 and APG12 and CrEL surfactants possess approximately 8, 10, 12, and 17 carbon lengths in respective tails. The more hydrophilic and shorter-tailed APG surfactants complemented the less hydrophilic and longer-tailed CrEL surfactant, however both have bulky structures. Thus, delicate balance in mixed surfactants is crucial to maintain the structural arrangement of surfactant film.
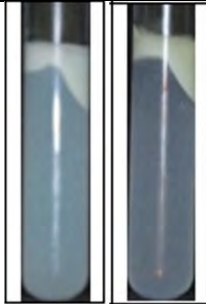
Phase behaviour study characterizes macroscopic properties of a colloidal system by observation (Kudo et al., 2014) such as the phase transitions of CO/CrEL/water are shown in **Figure 4.5**.

Figure 4.5: Visual appearances of CrEL/CO/W mixtures with S:O ratios of 1:9, 2:8, 3:7, 4:6: 5:5, 6:4, 7:3, 8:2 and 9:1 (from top to bottom) as increments of 5% water added (from left to right). Only mixtures with S:O ratios of 8:2 and 9:1 of remain as transparent single-phase mixtures.

Upon water dilution, samples changed differently based on their S:O ratios. For samples with S:O ratios of 9:1 and 8:2, homogeneous mixture of a single layer was formed throughout all water percentages, whereas for samples with S:O ratios of 7:3, 6:4, 5:5, 4:6, 3:7, 2:8, and 1:9, heterogeneous mixtures of multiple layers were formed. The layers formed when the mixtures contained low water percentages of about 10-20% were transparent liquid at the top layer and translucent-white sediment/gel at the bottom layer. The layers formed when the mixtures contained higher water percentages of more than 25% were opaque white at the top layer and translucent-bluish at the bottom layer.

Table 4.1: Visual appearance of coconut oil-based and yellow-coloured oil-based mixtures with S:O ratio of 9:1 at low (left) and high (right) percentages of water. Yellow-coloured oil was used for the purpose of qualitative observation of the oil layer before and after phase inversion composition (PIC) point.

Samples with S:O ratio of 9:1 and 20% W (before PIC point)	Samples with S:O ratio of 9:1 and 80% W (after PIC point)

The nature of the layers was qualitatively determined by comparing the samples of the same composition, but differently-coloured oils as shown in **Table 4.1**. The oily nature of the layer was confirmed when the yellow-coloured oil can be observed at the top layer. For mixtures formed at low water percentage, yellow colour could not be observed at the top layer. Thus, the less dense oily layer and the denser sediment layer described the Winsor type II system (biphasic water-in-oil emulsion with excess oil on top). For mixtures formed at higher water percentage, the yellow-coloured oil could not be observed at the top layer, hence the top layer was not the excess oil.

On the other hand, the bluish transparent liquid was characteristic of nanoemulsions (Ahmad et al., 2012). Thus, the less dense non-oily layer and the denser emulsion layer described the Winsor type I system (biphasic oil-in-water emulsion with excess water on top). From Winsor type II system to Winsor type I system, water addition inverted the dispersed and continuous phases crossing phase inversion composition (PIC) point.

4.2   Preparation and Physicochemical Characterization of Nanoemulsions

The low-energy emulsification method was employed to produce finer and more stable nanoemulsions with less cost and disruptive risks than the high-energy emulsification method (Tadros et al, 2014). Particle size distribution under the effects of varying compositional parameters was analyzed to screen for the optimum formulations.

i.   *Effect of water content*: Nanoemulsions without APG co-surfactants of 1:9, 2:8, 3:7, 4:6, 5:5, 6:4, 7:3, 8:2, and 9:1 of S:O ratios were compared at different water contents (90% and 80% water per total sample).

ii.   *Effect of ibuprofen content*: Nanoemulsions without APG co-surfactants of 1:9 and 9:1 of S:O ratios were compared at different ibuprofen contents (0, 2, 4, 6% ibuprofen per coconut oil).

iii.   *Effect of mixed surfactant content*: Nanoemulsions with APG co-surfactants of 95:05, 90:10, and 85:15 of S:O ratios were compared at different mixed surfactants contents (APG08, APG10 and APG12 at 9:1 and 8:2 CrEL:APG ratios).

4.2.1 Particle Size Analysis

4.2.1.1 Effect of Water Content

To identify the optimum water solubilization capacity, nanoemulsions were prepared at S:O ratios of 1:9, 2:8, 3:7, 4:6, 5:5, 6:4, 7:3, 8:1 and 9:1 at different water content (90% and 80% water). These nanoemulsions were stabilized by CrEL only.

Table 4.2: Composition, particle size and polydispersity index of nanoemulsions (S:O = 1:9, 2:8, 3:7, 4:6, 5:5, 6:4, 7:3, 8:1 and 9:1) containing different water content (90% and 80% water per total mass).

	Surfactant-to-oil ratio, S:O	Composition (wt.%)			Particle size (d, nm)	Polydispersity index, PDI
		S	CO	W		
Nanoemulsions containing 90% water	1:9	1	9	90	166.3 ± 4.6	0.32 ± 0.04
	2:8	2	8	90	178.5 ± 1.4	0.28 ± 0.01
	3:7	3	7	90	263.0 ± 4.5	0.35 ± 0.05
	4:6	4	6	90	287.3 ± 6.1	0.32 ± 0.02
	5:5	5	5	90	285.7 ± 3.7	0.29 ± 0.01
	6:3	6	4	90	249.1 ± 6.7	0.45 ± 0.05
	7:3	7	3	90	311.7 ± 3.9	0.52 ± 0.04
	8:2	8	2	90	305.0 ± 6.5	0.50 ± 0.03
	9:1	9	1	90	28.8 ± 0.3	0.63 ± 0.01
Nanoemulsions containing 80% water	1:9	2	18	80	161.9 ± 1.2	0.24 ± 0.01
	2:8	4	16	80	196.4 ± 5.3	0.40 ± 0.04
	3:7	6	14	80	268.2 ± 2.2	0.27 ± 0.01
	4:6	8	12	80	359.5 ± 5.1	0.27 ± 0.02
	5:5	10	10	80	398.9 ± 8.5	0.30 ± 0.01
	6:3	12	8	80	480.0 ± 11.1	0.37 ± 0.05
	7:3	14	6	80	404.7 ± 10.2	0.62 ± 0.04
	8:2	16	4	80	149.0 ± 14.2	0.97 ± 0.04
	9:1	18	2	80	21.0 ± 0.6	0.59 ± 0.02
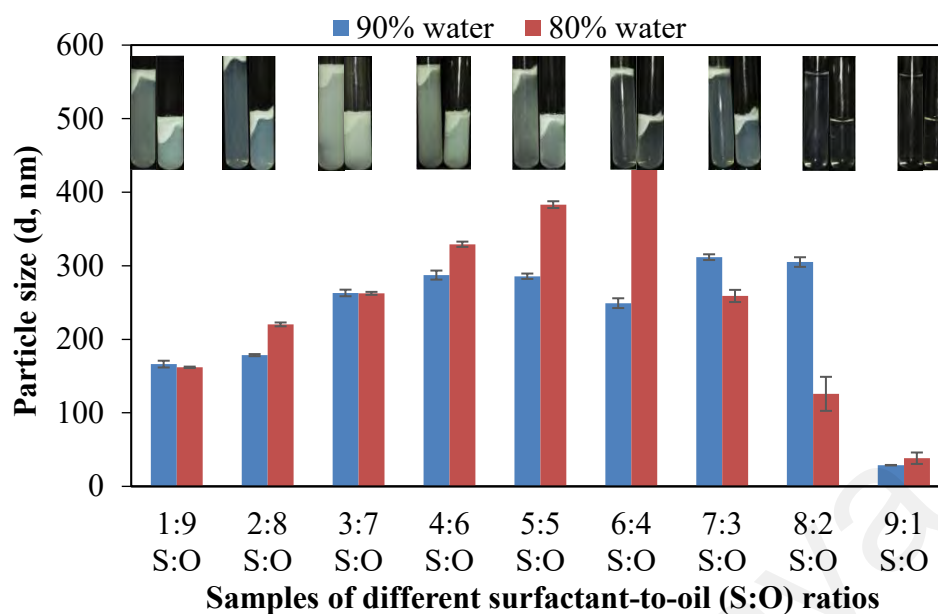
Figure 4.6: Particle size and images of nanoemulsions (S:O = 1:9, 2:8, 3:7, 4:6, 5:5, 6:4, 7:3, 8:1 and 9:1) containing different water content (90% and 80% water).

The particle size and visual images of the respective sample are shown in **Figure 4.6**. Most samples with higher water content (90% water) were smaller in size than samples with lower water content (80% water). This is due to a lesser oil droplet produced making it easier to be encapsulated as dispersed phase. Therefore, water content of 90% was selected as one of the optimum compositions. Samples with S:O ratio of 9:1 regardless of water content were extraordinarily smaller (<50 nm in diameter) than the rest (>100 nm in diameter). High amount of Cremophor EL induced ultralow interfacial tension to encapsulate bulky oil molecules, thus forming microemulsion. The particle size and appearance confirmed that the multiphase samples with S:O ratios of 7:3, 6:4, 5:5, 4:6, 3:7, 2:8 and 1:9 were Winsor I system, while the clear single-phase samples with S:O ratios of 9:1 and 8:2 were Winsor IV system. Previous phase behaviour study also showed that emulsification path exists along the water-dilution of these S:O ratios. However, the transparent nanoemulsion with S:O ratio of 9:1 and 90% water contained very low oil proportion and thus low drug capacity. Conversely, the translucent-bluish samples with S:O ratio of 1:9 and 90% water (nanoemulsion, NE) may have more drug capacity.

4.2.1.2 Effect of Ibuprofen Content

To observe how loading of ibuprofen drug influence the particle size of nanoemulsions with low- and high-surfactant ratios, nanoemulsions, that were stabilized by CrEL, were prepared at S:O ratios of 1:9 and 9:1 (NE-lowS and NE-highS) and loaded with different ibuprofen contents (0, 2, 4, and 6% ibuprofen in oil).

Table 4.3: Composition, particle size and polydispersity index of low- and high-surfactant nanoemulsions (S:O = 1:9 and 9:1) with different ibuprofen contents.

Ibuprofen (% per oil)		Composition (wt.%)				Particle size (d, nm)	Polydispersity index, PDI
		CrEL	Ibuprofen	CO	W		
NE-lowS (S:O = 1:9)	0	1	0.00	9.00	90	153.68 ± 0.01	0.26 ± 0.01
	2	1	0.18	8.82	90	205.63 ± 0.14	0.60 ± 0.14
	4	1	0.36	8.64	90	297.95 ± 0.03	0.68 ± 0.03
	6	1	0.54	8.46	90	168.90 ± 0.01	0.49 ± 0.01
NE-highS (S:O = 9:1)	0	9	0.00	1.00	90	14.49 ± 0.00	0.14 ± 0.00
	2	9	0.02	0.98	90	13.80 ± 0.01	0.11 ± 0.01
	4	9	0.04	0.96	90	13.60 ± 0.01	0.10 ± 0.01
	6	9	0.06	0.94	90	14.27 ± 0.01	0.13 ± 0.01
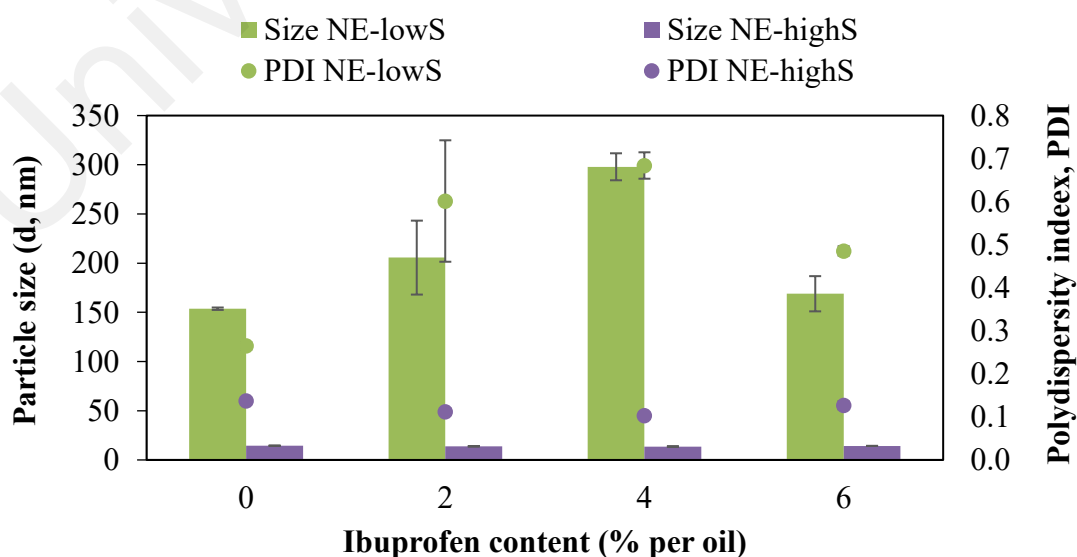
Figure 4.7: Particle size and polydispersity index of low- and high-surfactant nanoemulsions (S:O = 1:9 and 9:1) with different ibuprofen contents.

Table 4.3 and **Figure 4.7** show that ibuprofen content affected low-surfactant nanoemulsions with S:O ratio of 1:9 (NE-lowS) at greater extent than high-surfactant nanoemulsions with S:O ratio of 9:1 (NE-highS). Particle size of NE-lowS were larger of about 150-300 nm in diameter size with polydisperse distribution (PDI > 0.2). Particle size of NE-highS were 10 times smaller with a monodisperse distribution. Formulation that can retain its small and homogeneously distributed particles with drug loaded has potential to be utilised as carrier system.

4.2.1.3 Effect of APG Presence

To observe how APG surfactant influence the particle size of nanoemulsions with low- and high-surfactant ratios, CrEL-stabilized and CrEL:APG12-stabilized nanoemulsions were prepared at S:O ratio of 1:9 (NE0-lowS and NE3-lowS) and 9:1 (NE0-highS and NE3-highS). APG12 was selected for this particle size analysis because APG12 co-surfactant exhibited better stabilizing effect than APG08 and APG10 in the previous experiment. **Table 4.4** and **Figure 4.8** show the particle size measurement for 24 hours after sample preparation. PDI values for the low-surfactant nanoemulsions NE0-lowS (0.51) and NE3-lowS (0.74) showed polydisperse size distribution, while the PDI values for the high-surfactant nanoemulsions NE0-highS (0.20) and NE3-highS (0.24) showed monodisperse size distribution.

Table 4.4: Composition, particle size and polydispersity index of low- and high-surfactant nanoemulsions (S:O = 1:9 and 9:1) with and without APG12 surfactant.

	Composition (wt.%)					Particle size (d, nm)	Polydispersity index, PDI
	APG12	CrEL	Ibuprofen	CO	W		
NE0-lowS	-	0.9	0.91	8.19	90	50.0 ± 5.3	0.51 ± 0.08
NE3-lowS	0.1	0.8	0.91	8.19	90	70.6 ± 4.5	0.74 ± 0.01
NE0-highS	-	9.0	0.10	0.90	90	12.1 ± 0.1	0.20 ± 0.01
NE3-highS	1.0	8.0	0.10	0.90	90	12.4 ± 0.2	0.24 ± 0.03
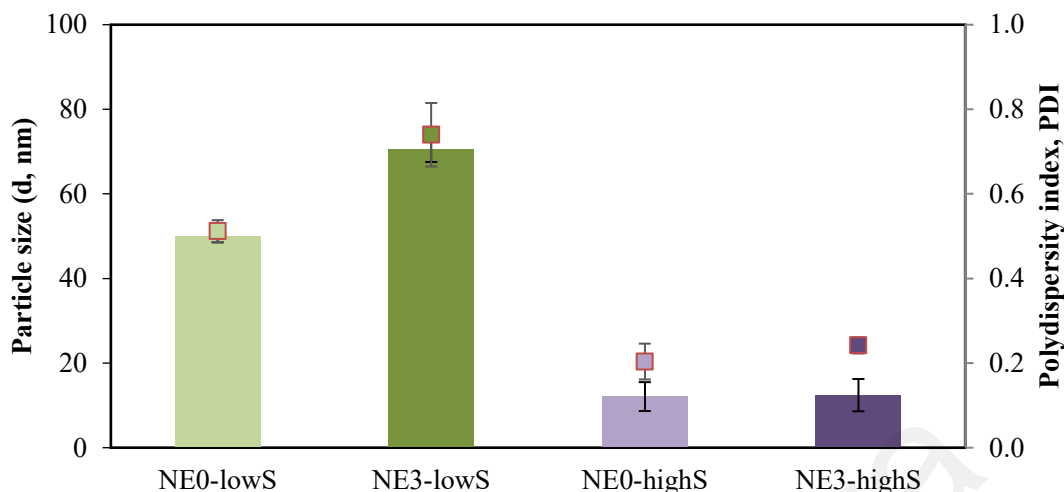
Figure 4.8: Particle size and polydispersity index of low- and high-surfactant nanoemulsions (S:O = 1:9 and 9:1) with and without APG12 surfactant.

The incorporation of APG surfactant showed a negative effect in low-surfactant ratio (S:O = 1:9). Formulation NE3-lowS was slightly larger in size than NE0-lowS because the bulky APG surfactant disturbed the thin surfactant packing, thus slightly decreased the curvature to solubilize the high proportion of oil. The presence of free fatty acids or esters of glyceride with ethoxylated ricinoleic acid in CrEL surfactant (Matsaridou et al., 2012) provided more significant oil-solubilizing effect than the APG incorporation when surfactant proportion is lower than oil proportion.

The incorporation of APG surfactant showed a positive effect in high-surfactant ratio (S:O = 9:1). Formulation NE3-highS exhibited smaller size than formulation NE0-highS. This is because the APG surfactant further lowered the interfacial tension while providing interface fluidity (Pajic et al., 2019). This shows the effect of APG surfactant which can separate well with oil, thus achieving proper surfactant packaging. The HLB value of APG surfactant is 11.2 and it is close to the required HLB value of coconut oil which is 12.5 wherein the similarity in the HLB values is imparted by the similarity in the carbon chains.

4.2.1.4 Effect of APG Content

To observe the influence of APG types and proportion, nanoemulsions were prepared at S:O ratios of 85:15, 90:10, 95:15 with different mixed surfactant contents as shown in **Table 4.5** and **Figure 4.9**. These nanoemulsions were stabilized by CrEL:APG08, CrEL:APG10, and CrEL:APG12 surfactants at 9:1 and 8:2 ratios.

Table 4.5: Composition, particle size and polydispersity index of APG-incorporated nanoemulsions (S:O = 85:15, 90:10 and 95:05) containing different mixed surfactant content.

Surfactant content	Surfactants-to-oil ratio, S:O	Composition (wt.%)			Particle size (d, nm)	Polydispersity index, PDI
		S	CO	W		
CrEL:APG08 = 9:1	85:15	8.5	1.5	90	28.1 ± 1.6	0.38 ± 0.01
	90:10	9.0	1.0	90	25.5 ± 3.0	0.27 ± 0.07
	95:05	9.5	0.5	90	14.2 ± 0.0	0.28 ± 0.01
CrEL:APG08 = 8:2	85:15	8.5	1.5	90	36.0 ± 0.2	0.76 ± 0.01
	90:10	9.0	1.0	90	16.1 ± 0.2	0.22 ± 0.02
	95:05	9.5	0.5	90	12.7 ± 0.1	0.12 ± 0.01
CrEL:APG10 = 9:1	85:15	8.5	1.5	90	27.4 ± 1.5	0.38 ± 0.02
	90:10	9.0	1.0	90	15.0 ± 0.4	0.19 ± 0.02
	95:05	9.5	0.5	90	12.9 ± 0.3	0.15 ± 0.02
CrEL:APG10 = 8:2	85:15	8.5	1.5	90	28.0 ± 0.8	0.18 ± 0.04
	90:10	9.0	1.0	90	15.0 ± 0.1	0.15 ± 0.00
	95:05	9.5	0.5	90	13.1 ± 0.4	0.23 ± 0.02
CrEL:APG12 = 9:1	85:15	8.5	1.5	90	13.5 ± 0.3	0.25 ± 0.00
	90:10	9.0	1.0	90	12.2 ± 0.1	0.12 ± 0.01
	95:05	9.5	0.5	90	12.3 ± 0.1	0.15 ± 0.02
CrEL:APG12 = 8:2	85:15	8.5	1.5	90	14.1 ± 0.3	0.28 ± 0.02
	90:10	9.0	1.0	90	12.5 ± 0.0	0.15 ± 0.01
	95:05	9.5	0.5	90	12.2 ± 0.1	0.21 ± 0.01

Table 4.5 shows the nanoemulsions with higher APG proportion (CrEL:APG = 8:2) were more polydisperse than nanoemulsions with lower APG proportion (CrEL:APG = 9:1). This indicated that too much APG molecules disrupted the interfacial film leading to different particle sizes, whether in terms of hydrophilicity balance or spatial arrangement. CrEL:APG ratio of 9:1 was chosen as one of the optimum mixing ratios.
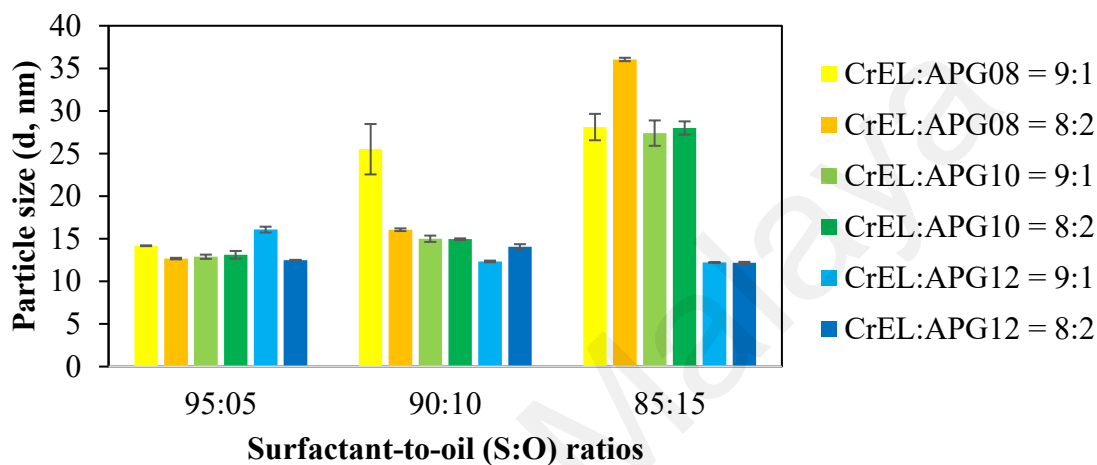
Figure 4.9: Particle size of APG-incorporated nanoemulsions with different mixed surfactant contents: CrEL:APG08, CrEL:APG10, and CrEL:APG12 surfactants at 9:1 and 8:2 mixed surfactant ratios.

Figure 4.9 shows different trends of particle sizes with increasing oil proportion from S:O 95:05 (left) to S:O 85:15 (right). The nanoemulsions incorporated with APG08 and APG10 co-surfactants increased in size due to swelling of oil core. In contrast, the nanoemulsions incorporated with APG12 co-surfactant decreased in size, due to possible synergism between APG12 molecules and coconut oil triglycerides. All samples with S:O ratio of 90:10 were smaller than 50 nm in diameter with PDI value less than 0.25. Therefore, S:O ratio of 90:10 was selected as the one of the optimum mixing ratios.

4.2.1.5 Effect of Ibuprofen Loading

Selected nanoemulsions NE0, NE1, NE2, and NE3 were nanoemulsions stabilized by CrEL, CrEL:APG08, CrEL:APG10, and CrEL:APG12 surfactants with the optimum composition (9:1 water-to-surfactant-oil ratio, 9:1 surfactant-to-oil ratio, and 9:1 mixed surfactant ratio). The optimized nanoemulsions were prepared with and without 10% ibuprofen loading in the oil phase as shown in **Table 4.6**.

Table 4.6: Composition, particle size and polydispersity index of selected nanoemulsions NE0, NE1, NE2, and NE3 with and without ibuprofen drug loading.

Nanoemulsions	Composition (wt. %)					Particle size, (d, nm)	Polydispersity index, PDI
	Ibuprofen	CO	APG	CrEL	W		
NE0	0.0	1.0	0.0	9.0	90.0	12.20 ± 0.03	0.14 ± 0.01
NE1	0.0	1.0	0.9	8.1	90.0	12.23 ± 0.06	0.10 ± 0.01
NE2	0.0	1.0	0.9	8.1	90.0	12.41 ± 0.16	0.18 ± 0.02
NE3	0.0	1.0	0.9	8.1	90.0	9.65 ± 0.04	0.19 ± 0.01
IB-loaded NE0	0.1	0.9	0.0	9.0	90.0	12.70 ± 0.03	0.10 ± 0.01
IB-loaded NE1	0.1	0.9	0.9	8.1	90.0	13.91 ± 0.12	0.20 ± 0.01
IB-loaded NE2	0.1	0.9	0.9	8.1	90.0	12.89 ± 0.05	0.13 ± 0.01
IB-loaded NE3	0.1	0.9	0.9	8.1	90.0	10.47 ± 0.09	0.20 ± 0.01

All nanoemulsions exhibited monodispersed particles with an average diameter lower than 20 nm and good homogeneity in particle size. All ibuprofen-loaded nanoemulsions were slightly larger than their respective ibuprofen-free nanoemulsions. This is in contrast with the expected sized reduction due to the interaction of carboxyl group of ibuprofen molecules with Cremophor EL molecules (Djekic et al., 2011). The incorporation of ibuprofen drug decreased the size of the palm kernel oil ester-based nanoemulsion (Salim et al., 2018) but increased the size of the coconut oil-based nanoemulsions formulated in this research despite both nanoemulsion systems stabilized

by Cremophor EL surfactant. The predicted interaction did not occur due to different oil phases encapsulated in different structural arrangements of surfactant film. Note that the APG08, APG10 and APG12 co-surfactants (8, 10, 12 carbon length respectively) possess similar alkyl chain length with the medium-chained triglycerides (6-12 carbon length) in coconut oil. However, different tail lengths could lead to different assemblies in the mixed nonionic surfactants configuration.
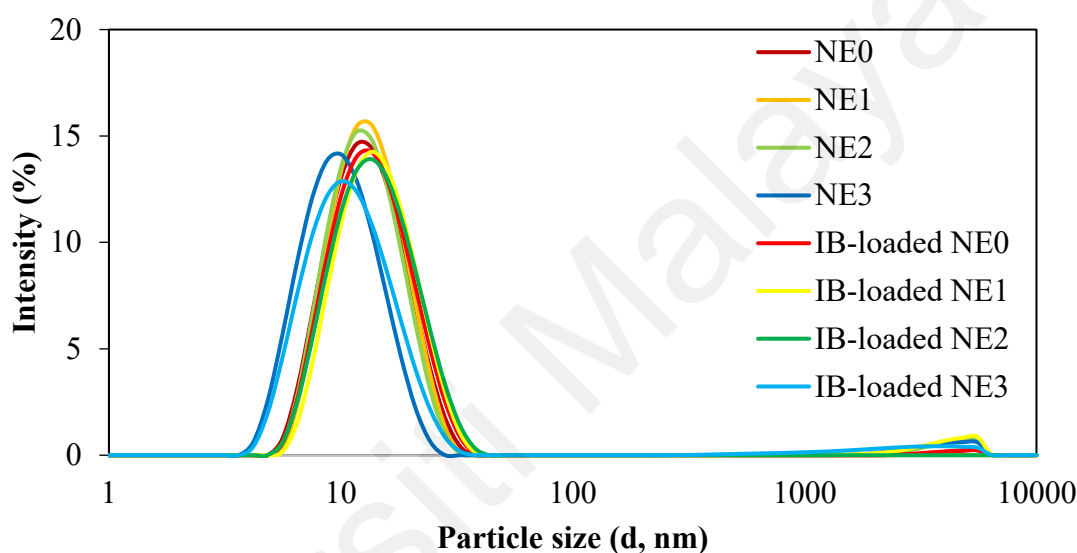
Figure 4.10: Particle size distribution profile of selected nanoemulsions NE0, NE1, NE2, and NE3 with and without ibuprofen loading.

Figure 4.10 shows the intensity-weighted size distribution profile plotted in logarithmic scale. APG12-incorporated nanoemulsions (NE3 and IB-loaded NE3) exhibited the smallest sizes. This is due to possible synergistic effect contributed by the alkyl chain lengths of APG12 (12 carbon atoms long) molecules and MCT (6-12 carbon atoms long) molecules in coconut oil. In the previous literatures, good drug carrier systems were also formulated using surfactant and oil of the same carbons in alkyl chain, for example C12/14 APG-mixed (myristyl glucoside and myristyl alcohol) and C16/18 APG-mixed (cetearyl glucoside and cetearyl alcohol) commercial emulsifiers (Tasić-Kostov et al, 2011 & 2012).

4.2.2 Zeta Potential Analysis

The selected nanoemulsions NE0, NE1, NE2, and NE3 were prepared and were diluted with water at dilution factors of 1 (undiluted), 10, 100 and 1000 (infinite dilution). **Table 4.7** shows that the zeta potential of NE0, NE2 and NE3 were more negative with more water dilution while the zeta potential of NE1 fluctuated. The negative value of zeta potential reflected the ability for electrostatic repulsion contributed by micellar or bicontinous structures (Moghimipour et al, 2013). The steady increase in zeta potential indicated a degree of stability of the nanoemulsions (Instrument, 2004). NE0, NE1, NE2 and NE3 at dilution factor of 10 and 100 exhibited small particle size of 10-70 nm and the polydispersity index lower than 0.25, which indicate monodisperse particles. As water can be added in without causing instability, these samples were confirmed to be oil-in-water nanoemulsion (Jaiswal, et al., 2015). NE0, NE1, NE2 and NE3 at dilution factor of 1000 exhibited large particle size of 300-400 nm and the polydispersity index higher than 0.4, which indicated a degree of instability at infinite dilution (Kotta et al., 2015). Despite this, the particle size of the nanoemulsions remained within nanoemulsion range of less than 500 nm (Chime et al. 2014).

Figure 4.11 shows the effect of dilution on zeta potential and particle size at dilution factors of 1, 10 and 100. When nanoemulsions were diluted 10 times, negligible changes in particle sizes were observed. When nanoemulsions were diluted 100 times, the particle sizes slightly increased but less than 100 nm diameter, indicating the nanoemulsions could withstand mild dilution. The influence of APG co-surfactant was correlated with how much the particle size of nanoemulsions changed due to dilution at 10 and 100 dilution factors. The particle size variability of nanoemulsions with APG08 (NE1, 64%), APG10 (NE2, 128%), and APG12 (NE3, 13%) were lower than nanoemulsions without APG (NE0, 807%). This proves that APG surfactants contribute to the improvement of nanoemulsion system stability.

Table 4.7: Zeta potential values, particle size and polydispersity index of selected nanoemulsions NE0, NE1, NE2, and NE3 diluted at different dilution factors.

Nanoemulsion	Dilution factor	Zeta potential (mV)	Particle size (d, nm)	Polydispersity index, PDI
NE0	×1	-3.5 ± 0.1	16.0 ± 0.2	0.33 ± 0.01
	×10	-13.3 ± 1.4	15.7 ± 0.2	0.19 ± 0.02
	×100	-15.1 ± 2.1	65.1 ± 26.6	0.15 ± 0.01
	×1000	-12.5 ± 0.7	294.4 ± 61.5	0.43 ± 0.07
NE1	×1	-4.4 ± 0.2	16.5 ± 0.5	0.31 ± 0.01
	×10	-12.9 ± 2.1	15.2 ± 0.2	0.13 ± 0.01
	×100	-7.8 ± 3.3	29.6 ± 2.6	0.34 ± 0.05
	×1000	-15.3 ± 0.9	299.5 ± 44.3	0.45 ± 0.08
NE2	×1	-3.7 ± 0.2	13.4 ± 0.2	0.20 ± 0.01
	×10	-12.9 ± 1.6	14.6 ± 0.2	0.10 ± 0.01
	×100	-21.5 ± 0.8	33.5 ± 4.4	0.21 ± 0.03
	×1000	-13.8 ± 1.2	416.1 ± 50.8	0.53 ± 0.05
NE3	×1	-4.7 ± 0.7	10.8 ± 0.1	0.25 ± 0.01
	×10	-12.0 ± 0.5	12.7 ± 0.2	0.22 ± 0.01
	×100	-15.7 ± 7.6	17.7 ± 0.4	0.31 ± 0.01
	×1000	-9.0 ± 2.9	399.3 ± 64.5	0.54 ± 0.07
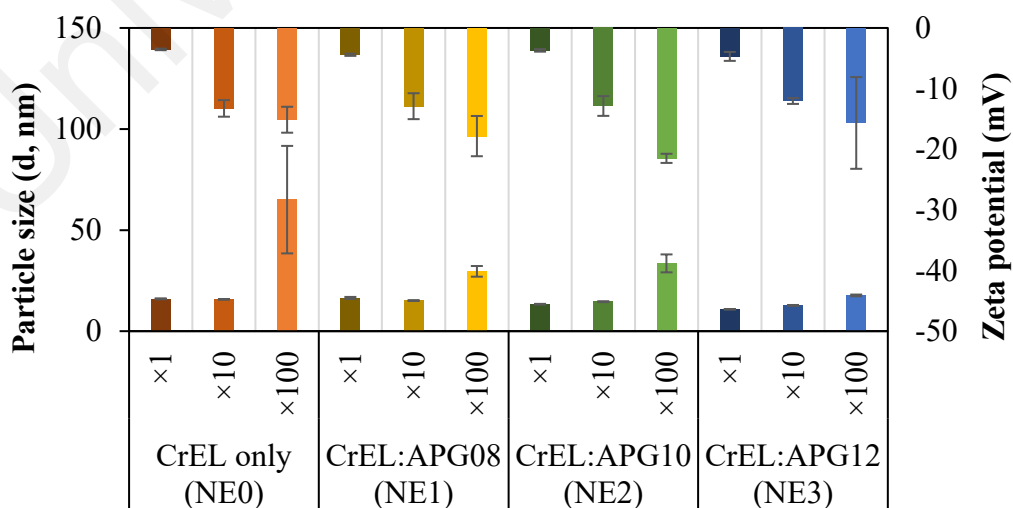
Figure 4.11: Zeta potential value and particle size of selected nanoemulsions NE0, NE1, NE2, and NE3 diluted at different dilution factors.

4.2.3   Morphology Analysis

To examine morphology of the nanoemulsions, direct method of transmission electron microscopic (TEM) analysis was performed to complement the indirect method of dynamic light scattering (DLS) analysis. Although reproducible DLS data gained after vigorous replication showed that the samples exhibited monodisperse particle size lower than 20 nm, it is prudent to consider that there might be a deviation from the spherical shape and the actual size may be deviated from the measured size (Turovsky et al, 2015). Non-sphericity can also be identified using multi-angle depolarized dynamic light scattering (Babick, 2019).

The TEM micrographs at 25,000 magnifications revealed that the ibuprofen-loaded nanoemulsions NE0, NE1, NE2 and NE3 exhibited varying nanostructures, where polymer-like globular structures were observed within interconnected particles. The ibuprofen-loaded formulation NE1 (with the presence of APG08) in **Figure 4.12(b)** exhibited more interconnected network than the ibuprofen-loaded formulation NE0 (with the absence of APG) in **Figure 4.12(a)**. This is because the hydrophilic APG08 surfactant promoted interdroplet attractive interaction and coalescence between droplets during hydrophobic drug incorporation (Wik et al., 2019). The ibuprofen-loaded formulations NE2 (with the presence of APG10) and N3 (with the presence of APG12) which are shown in **Figure 4.12(c-d)** exhibited rod-like structures within relatively larger interconnected particles. NE3 contained longer rods than NE2 and this can be correlated with the shared alkyl chains of the medium-chain triglycerides and the APG surfactant molecules (Zhang et al., 2019).
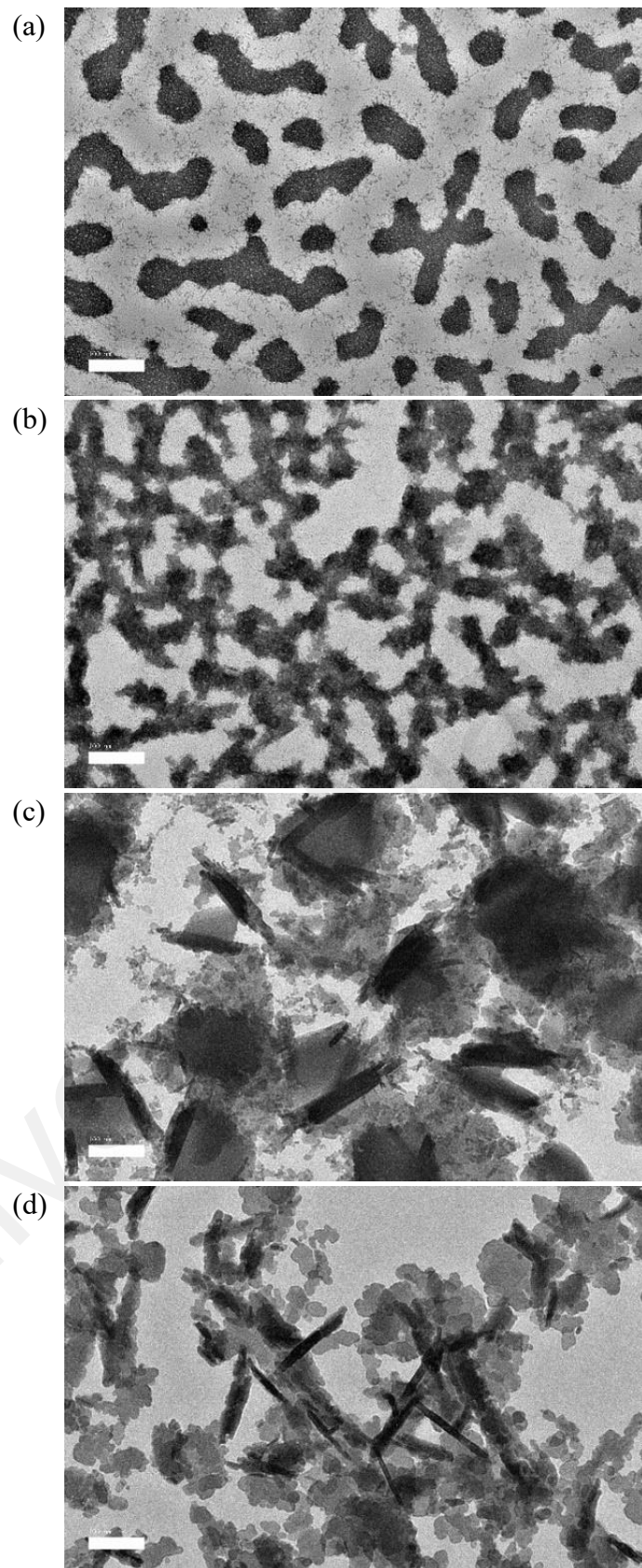
Figure 4.12: Transmission electron micrographs of ibuprofen-loaded nanoemulsions (a) NE0, (b) NE1, (c) NE2, and (d) NE3 stabilized with CrEL only, CrEL:APG08, CrEL:APG10, and CrEL:APG12 surfactants, respectively.

4.3 Stability Study

4.3.1 Centrifugation Result

In the centrifugation test, only samples with 90% water content appeared to remain homogeneous and transparent after centrifugation at 4000 rpm for 15 minutes. This indicated the good stability of the samples as the properties were retained (Bajaj et al., 2012). The transparent appearance was due to particle sizes well below the wavelength of visible light which is approximately $\lambda/15$ (40 nm).

4.3.2 Cooling-Heating Cycling Result

In the cooling-heating cycling test, all samples were unstable after cooling as the homogeneous samples turned from clear to opaque white. This indicated particle size increase due to interfacial film rupture under Laplace pressure. Aqueous continuous phase solidified easily in freezing condition, whereas non-aqueous dispersed phase collided rapidly in thawing condition (Azhar et al, 2018). The system was disrupted by ice crystal formation causing the irreversible increase in particle size (Pongsawatmanit & Srijunthongsiri, 2008). The signs of thermodynamic instability and the appearance indicated the nature of the systems as nanoemulsions. There was no recrystallization of coconut oil due to the low oil concentration and the reduction of crystallization temperature of oil fatty acid in the nanoemulsions (McClements, 2011).

4.3.3 Light Backscattering Analysis

Nanoemulsions NE0 (without APG), NE1 (with APG08), NE2 (with APG10) and NE3 (with APG12) were scanned using a Turbiscan stability analyzer for 72 hours to correlate destabilization processes from the light backscattering. **Figure 4.13** shows the delta light backscattering, ΔBS profiles as a function of time. **Figure 4.14** and **Figure**

4.15 show the kinetics of mean value and peak thickness plotted based on the relative backscattering at the middle (10-50 mm) ΔBS_{mean} and top (50-55 mm) ΔBS_{peak} segments of cell height.

Variation at the extremities (local variation) is indicative of particle migration reflecting sedimentation or creaming destabilization. A variation on the whole height (global variation) is indicative of particle variation reflecting flocculation or coalescence destabilization. No particle size change is shown when all scattering lines are superimposed (Ahmad et al., 2014). **Figure 4.13(a-c)** show the ΔBS profiles for formulations NE0 (without APG), NE1 (with APG08) and NE2 (with APG10), wherein global variation was detected. **Figure 4.13(d)** shows the ΔBS profile for formulation NE3 (with APG12) wherein the ΔBS signal did not change due to negligible particle variation detected. These profiles indicated that nanoemulsion without APG was destabilized by flocculation or coalescence, while nanoemulsion with APGs especially APG12 co-surfactant were more stable and robust. The complete overlap of ΔBS lines indicated long-term storage stability in the presence of APG12 surfactant.

The relative backscattering ΔBS_{mean} (shown in **Figure 4.14**) and ΔBS_{peak} (shown in **Figure 4.15**) showed the gradient of instability detected on the nanoemulsions in the following order: NE0 >> NE1 > NE2 > NE3. The calculated Turbiscan Stability Index (TSI) of NE0, NE1, NE2 and NE3 were approximately 1.76, 0.66, 0.19 and 0.16, respectively. Higher TSI value indicates lower stability (Wang et al, 2018), light backscattering analysis using Turbiscan supported that APG surfactant hindered instability. The decreasing of instability detected from NE1, NE2, and NE3 can also be correlated with the alkyl chain length of the APG08, APG10 and APG12 surfactants.
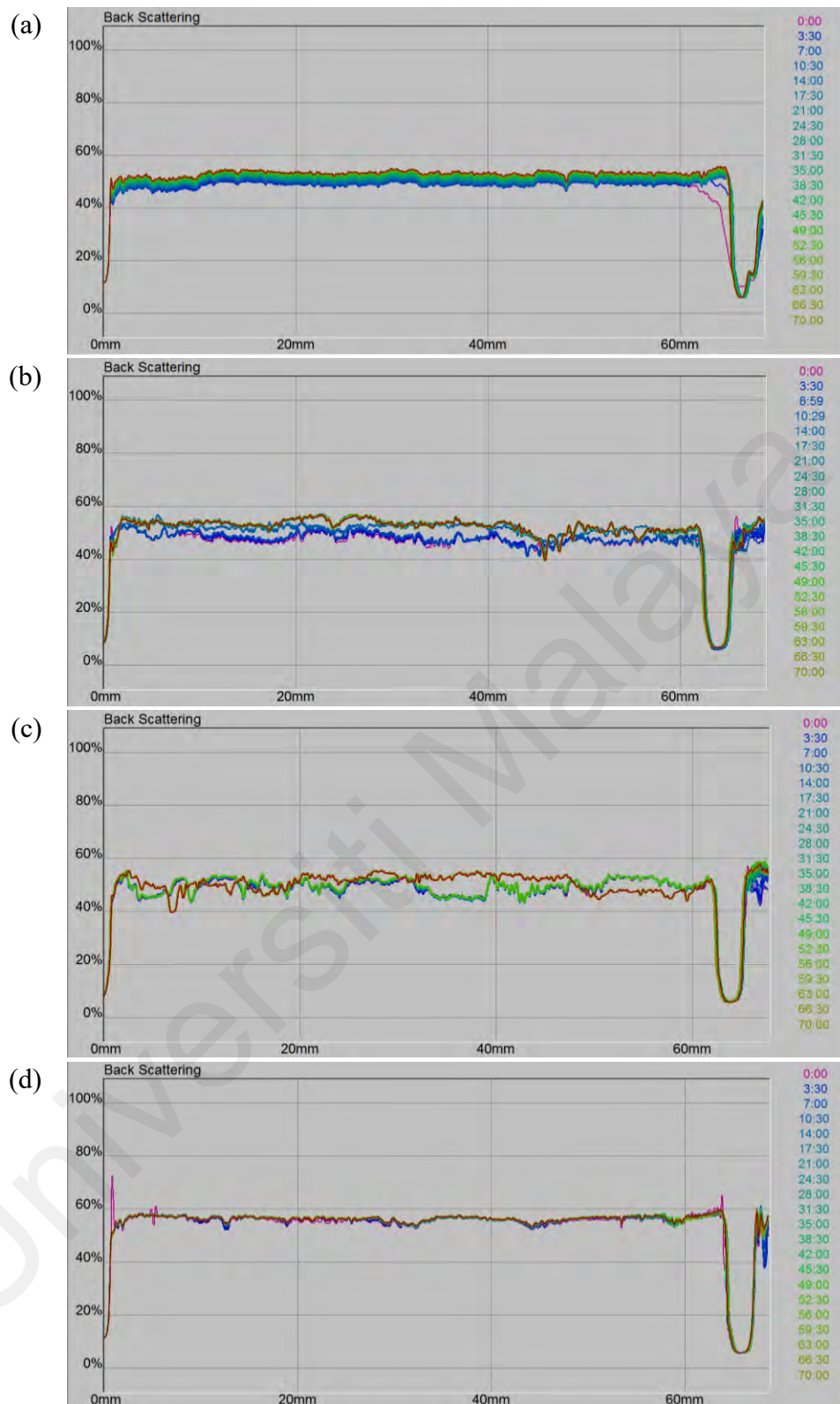
Figure 4.13: Backscattering light profiles of (a) NE0, (b) NE1, (c) NE2, and (d) NE3 nanoemulsions stabilized with CrEL only, CrEL:APG08, CrEL:APG10, and CrEL:APG12 surfactants, respectively.
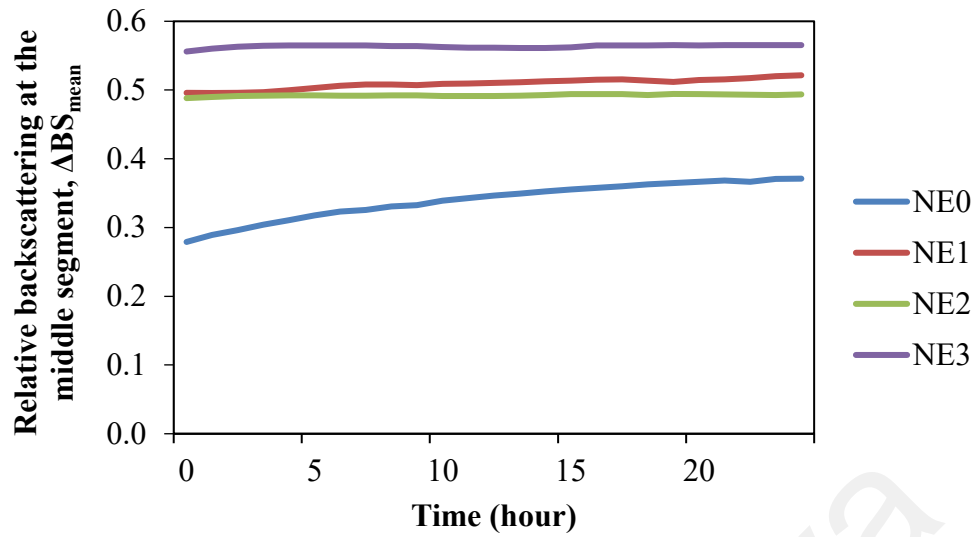
Figure 4.14: Mean value kinetics plot of NE0, NE1, NE2, and NE3 formulations based on the relative backscattering at the middle segment (10-50 mm of cell height).
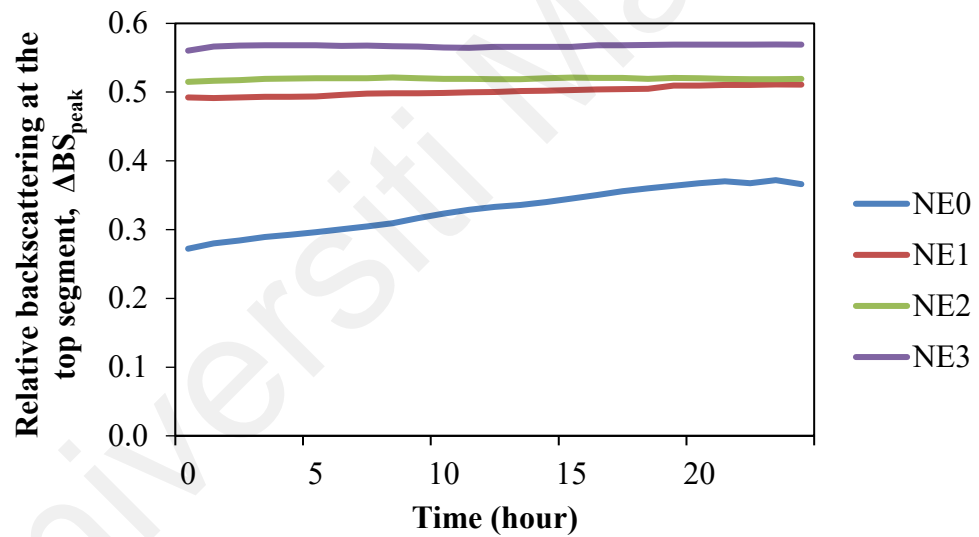
Figure 4.15: Peak value kinetics plot of NE0, NE1, NE2, and NE3 formulations based on the relative backscattering at the top segment (50-55 mm of cell height).

4.3.4 Dynamic Light Scattering Analysis

Nanoemulsions NE0, NE1, NE2 and NE3 (stabilized by CrEL only, CrEL:APG08, CrEL:APG10 and CrEL:APG12 surfactants) were subjected to accelerated ageing in different temperatures. The nanoemulsions showed no phase separation when stored at 4, 25, and 40°C for 90 days. Samples stored in 25 and 40°C appeared transparent with diameter sizes lower than 20 nm (**Figure 4.16(b-c)**). However, the same samples stored in 4°C appeared opaque-white with diameter sizes in 200-350 nm range, as shown in **Figure 4.16(a)**. This might be due to the rupture of interfacial film under the Laplace pressure and ice crystal formation in at low temperature, which also occurred in the freeze-thaw stability analysis. Coconut oil is prone to recrystallize at storage temperatures below 25°C (Brickmann et al., 2020).

NE0, NE1, NE2 and NE3 exhibited diameter size lower than 20 nm when stored at 25 and 40°C. However, different nanoemulsions showed different particles size increment when stored in different temperatures as shown in the **Table 4.8**.

Table 4.8: Particle size increment of nanoemulsions stored at different temperatures.

Temperature (°C)	Particle size increment of nanoemulsion (%)			
	NE0	NE1	NE2	NE3
4	+20.34	-19.70	+22.95	+24.66
25	+8.67	-4.72	-4.38	+0.14
40	+28.10	-20.53	+15.18	+16.83
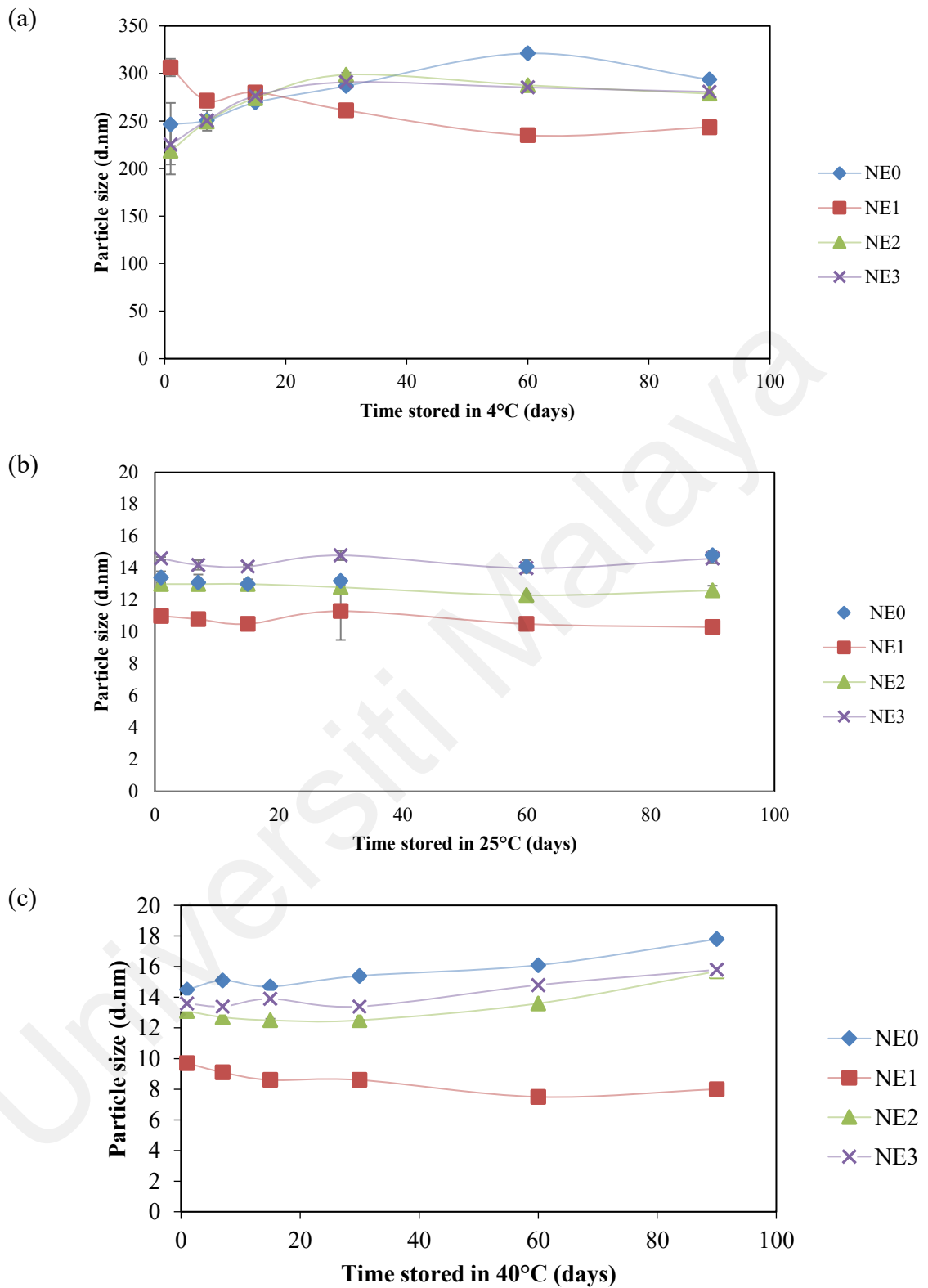
Figure 4.16: Changes in particle sizes of NE0, NE1, NE2, and NE3 formulations at (a) 4, (b) 25 and (c) 40°C within 90 days.

A decrease in size occurred when dispersed phase was able to leak out from the structure in prolonged time. When stored at 25°C, only nanoemulsion with APG08 (NE1) shrunk in size. When stored at 40°C, nanoemulsions with APG08 and APG10 (NE1 and NE2) decreased in size and the size reduction was directly proportional to the length of alkyl chain tail of surfactant, with drastic size reduction in APG08 sample. APG08 surfactant molecules have short 8-carbon alkyl chain tails that may not be able to retain its orientation in the oily core, thus causing distortion in interfacial arrangement. The different morphology of APGs also contributed to different direction (swelling or shrinking) and extent of size changes.

An increase in particle size can be explained by destabilization phenomena, such as flocculation and coalescence. This means that it is inevitable, especially when stored at elevated temperature over prolonged time. The size increment when stored at 40°C was relatively lower for nanoemulsions with APG10 and APG12 (NE2 and NE3) than nanoemulsions without APG (NE0). This proves that APG surfactants contributed to better size and resilience over time. The swelling might be due to water molecules diffusing in through the hydrophilic APG molecules in the film. Increase in particle size with aging is contributed by coalescence and Ostwald ripening, either simultaneously or in series (Santos et al., 2017). Further analysis was done to investigate these mechanisms of the irreversible increase in size.

4.3.4.1 Kinetic Analysis of Destabilization

Coalescence is the fusion of particles as continuous phase films ruptured. This destabilization phenomenon is driven by two processes: film rupture and droplet aggregation. The coalescence rate would follow first order kinetics when film rupture is the dominant process. The coalescence rate would follow second order kinetics when droplet aggregation is the dominant process (Wooster et al., 2016). The graphs of inverse of the square of radius ($1/r^2$) versus time (t) were plotted for coalescence rate analysis are shown in **Figure 4.17**.
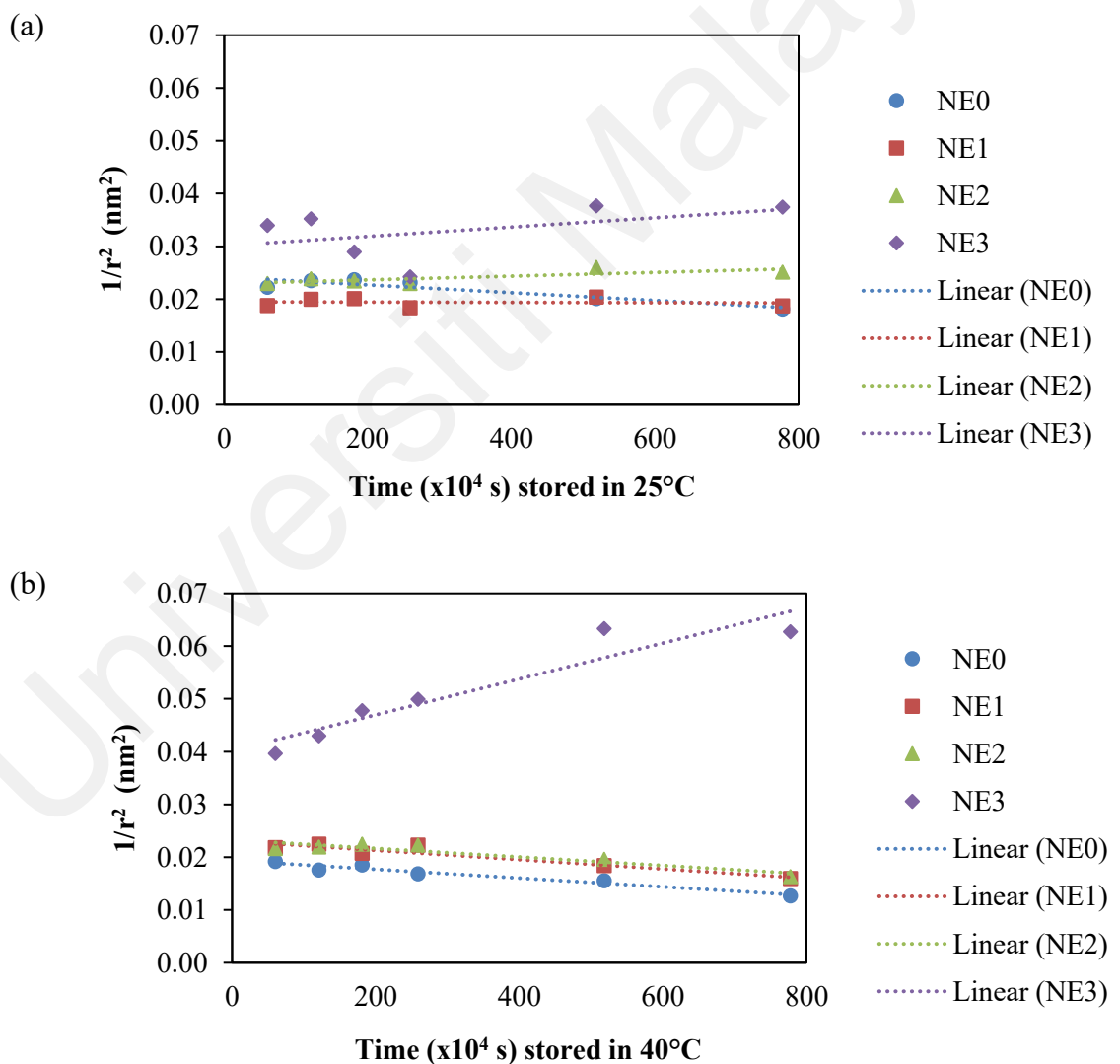
Figure 4.17: Coalescence curves of NE0, NE1, NE2, and NE3 formulations stored at (a) 25 and (b) 40°C for 90 days.

Ostwald ripening is the enlargement of particle size as dispersed phase transfers from smaller to larger particles. This destabilization mechanism is driven by Kelvin effect where the difference in Laplace pressure causes smaller particles to better solubilize local oil molecules than larger particles. Laplace pressure increased exponentially when particles reach 50-100 nm in size (Wooster et al., 2016). The graphs of cube of radius (r^3) versus time (t) were plotted for Ostwald ripening rate analysis are shown in **Figure 4.18**.
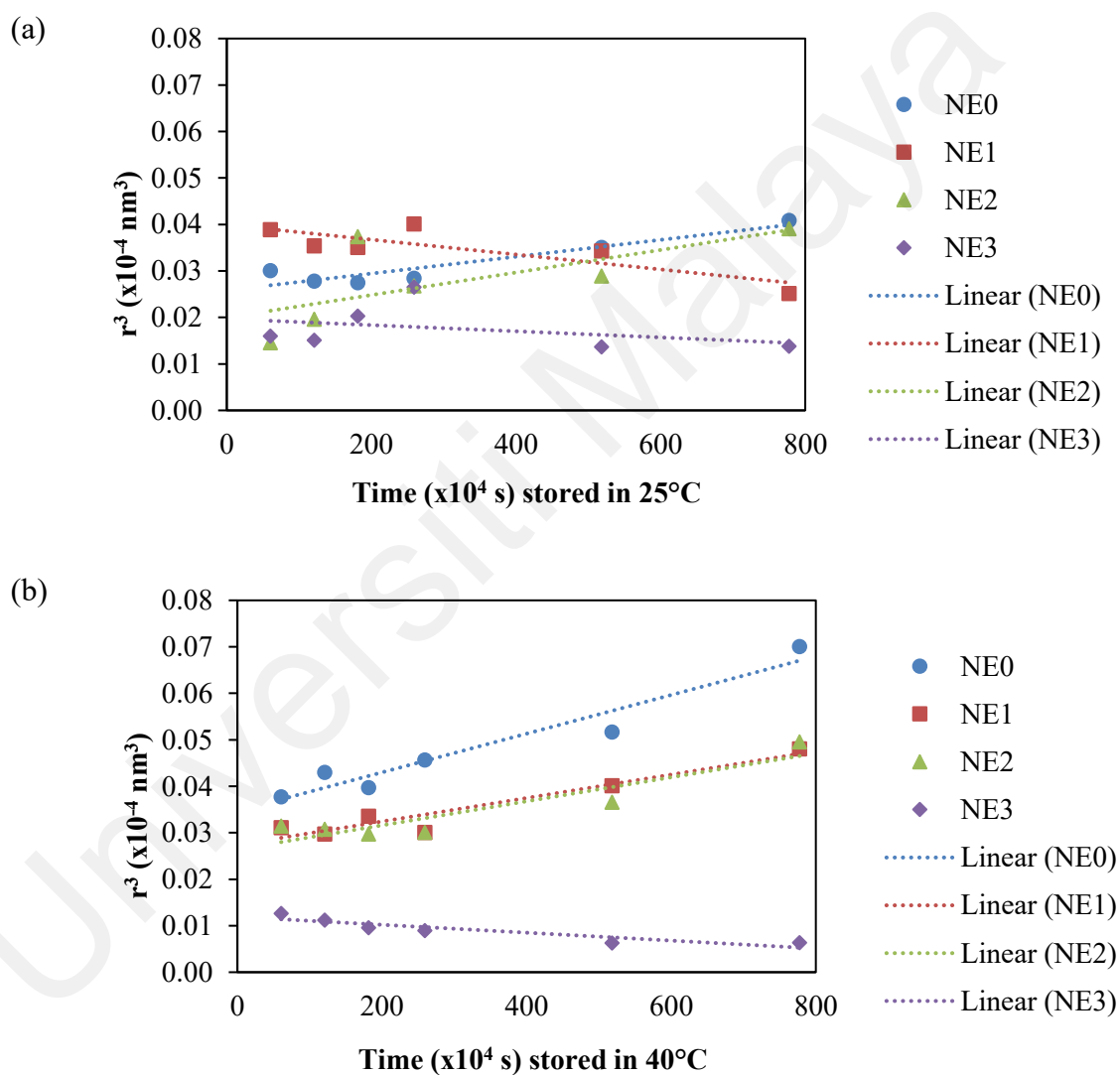
Figure 4.18: Ostwald ripening curves of NE0, NE1, NE2, and NE3 formulations stored at (a) 25 and (b) 40°C for 90 days.

The coefficients of determination of more than 0.9 showed linearity. **Table 4.9** shows that most nanoemulsions were not linear-fit to both kinetic rates at both temperatures which indicated that coalescence and Ostwald ripening processes were not the main destabilization phenomena. However, the trend of nanoemulsion without APG (NE0) stored in 40°C is linearly fit to both coalescence and Ostwald ripening processes while the trend of nanoemulsion without APG08 (NE1) stored in 40°C is linearly fit to Ostwald ripening process. This is expected as nanoemulsion without APG was found to be flocculated from the previous stability assessment using light backscattering. Coalescence may work consecutively or cooperatively with Ostwald ripening and Ostwald ripening process is promoted with the direct contact of flocculated oil droplets (Santos et al., 2017). As nanoemulsion particles absorb more energy at elevated temperature, higher effective collisions occur leading to more fusion (coalescence) and diffusion (Ostwald ripening) processes (Musa et al., 2017).

Table 4.9: Coefficient of determination for kinetic rates of destabilization (coalescence and Ostwald ripening rates).

Storage temperature	Coefficients of determination for coalescence rate (R_c) and Ostwald ripening rate (R_o)			
	NE0	NE1	NE2	NE3
R_c^2 at 25°C	0.8475	0.0073	0.6162	0.2095
R_c^2 at 40°C	0.9431	0.8906	0.8680	0.8847
R_o^2 at 25°C	0.8726	0.6982	0.4792	0.1322
R_o^2 at 40°C	0.9324	0.9097	0.8498	0.8302

4.4   *In-Vitro* Drug Release Study

In-vitro drug release was studied using the dialysis bag technique. This technique was chosen due to ease of handling and an inexpensive semi-permeable membrane to separate molecules based on differential diffusion. The released concentration of ibuprofen drug measured using UV-Vis spectrophotometer in the span of 24 hours. The patterns showed sustained release: initial fast release with steep gradient within the first 12 hours, then slower release afterwards. **Figure 4.19** shows biphasic pattern: initial fast release, then slower sustained release afterwards. At 24 hours, the release of ibuprofen from nanoemulsion with APG12 (NE3, 14.85%) was higher than nanoemulsion with APG10 (NE2, 14.50%), and nanoemulsion without APG (NE0, 13.11%). This shows that APG10 and APG12 could enhanced the ibuprofen drug release from the carrier system. Previous literatures showed that APG-based systems enhanced the permeation rates of diclofenac sodium and diclofenac diethylamine (Pantelic et al., 2014). On the other hand, the release of ibuprofen from nanoemulsion with APG08 (NE1, 12.07%) was the lowest because the release of the solubilized hydrophobic ibuprofen drug was obstructed by the oil core and surfactant film laced with highly hydrophilic APG08 molecules. The release of ibuprofen drug can be improved with the addition of hydrocolloid gums (Salim et al., 2012) or polymer matrix (Guerra-Ponce et a., 2016).
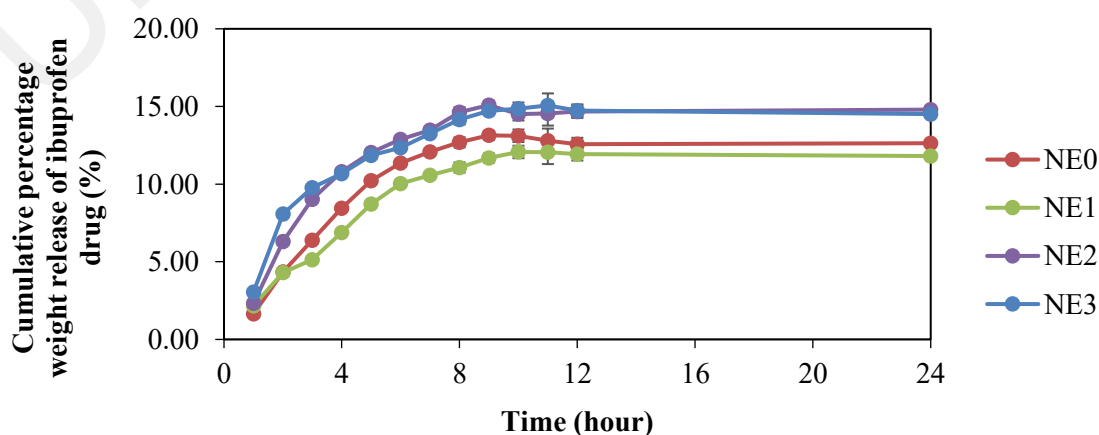
Figure 4.19: The release profile of ibuprofen from formulations NE0, NE1, NE2, and NE3 at 37°C.

The drug release mechanism was determined by fitting the release profiles within the first 12 hours' time to several kinetic models. **Table 4.10** shows the coefficient of determination for zero order, first order, Higuchi, Hixson-Crowell and Korsmeyer-Peppas models of drug release mechanisms. The highest R2 values were produced by Hixson-Crowell, followed by Korsmeyer-Peppas, Higuchi and first order models. The best linear fit to Hickson-Crowell model shows that dissolution is the main mechanism of the ibuprofen drug release resulting in a change in surface area and diameter of liquid crystalline systems. Other than that, the Korsmeyer-Peppas release exponent, n is more than 1 (super non-Fickian case II) shows that the release was also swelling-controlled along with the non-diffusion mechanism (Arbain et al., 2019). As a controlled and consistent drug release following the zero-rder model is ideal (Li et al., 2019) as shown in **Figure 4.20**, in which the formulated nanoemulsion can be modified further with permeation enhancers such as hydrocolloid gums (Salim et al, 2012).

Table 4.10: Coefficient of determination for kinetic model of drug release.

Ibuprofen loaded nanoemulsion	Coefficient of determination, R^2				
	Zero order	First-order	Higuchi	Hickson-Crowell	Korsmeyer-Peppas
NE0	0.8036	0.7660	0.9487	0.9836	0.9648
NE1	0.8872	0.7573	0.9648	0.9916	0.8743
NE2	0.7749	0.7573	0.9346	0.9836	0.8707
NE3	0.8074	0.7805	0.9487	0.9916	0. 8707
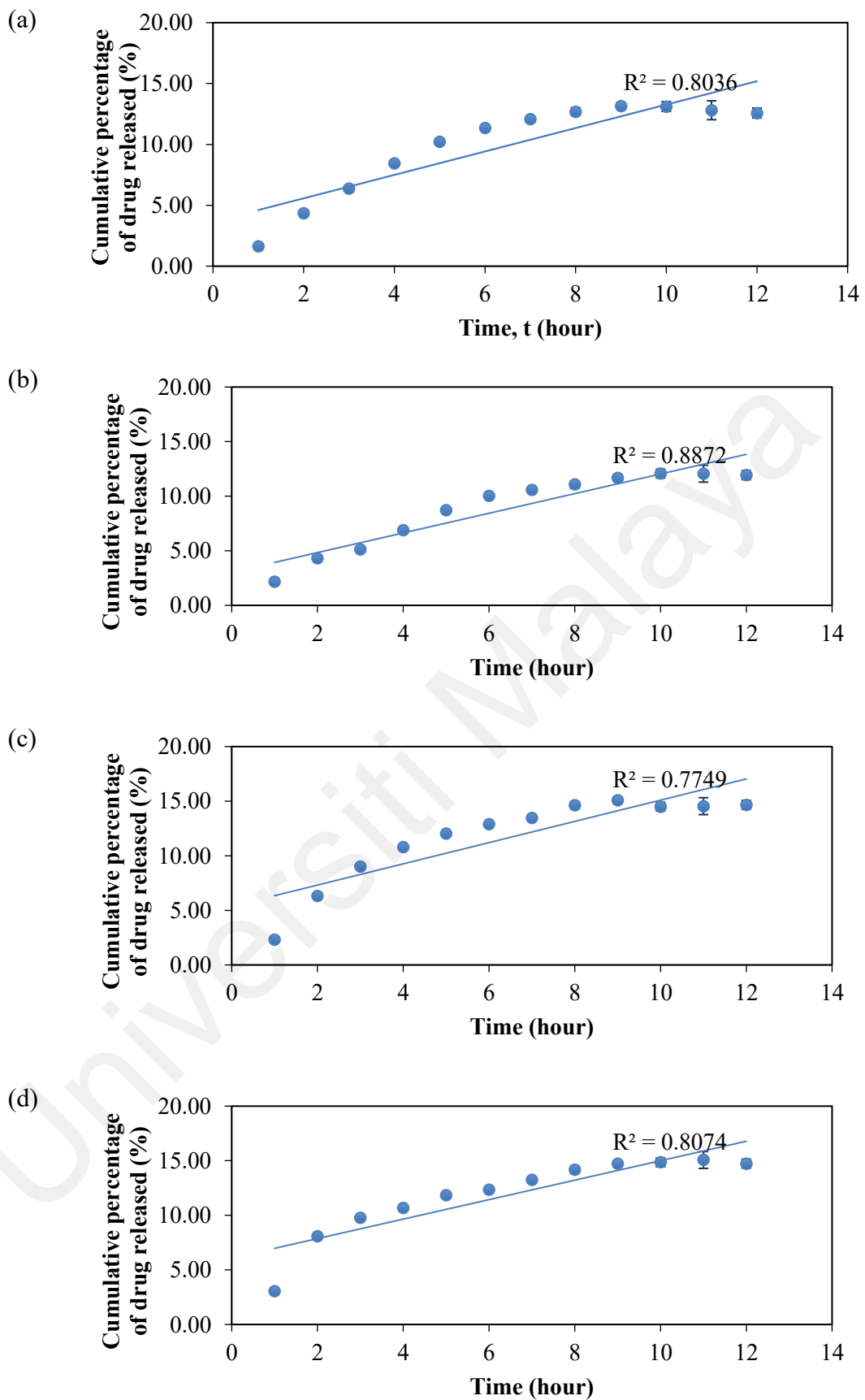
Figure 4.20: Drug release data of ibuprofen from (a) NE0, (b) NE1, (c) NE2, and (d) NE3 fitted to zero order model.

4.5 *In-vitro* Cytotoxicity Study

In order to assess the safety of nanoemulsions, an in-vitro cytotoxicity test was done on mouse embryonic fibroblast (3T3) cell line using MTT colorimetric assay after 72 hours of exposure. The cytotoxic effect of formulations NE03 and NE4 (without and with APG12, respectively) were compared with ibuprofen alone at varying concentrations. A formulation is considered less toxic when it exhibits 50% inhibition of cell viability, the IC_{50} value of more than 30 µg/mL concentration (Azhar et al., 2018). Based on **Figure 4.21**, no IC_{50} value was obtained up to the concentration of 500 µg/mL Therefore, it is concluded that there is no cytotoxic effect against 3T3 cell lines for both ibuprofen-loaded nanoemulsions in absence and presence of APG co-surfactant. This is because ibuprofen-loaded nanoemulsions NE0 (9% CrEL) and NE3 (8.1% CrEL and 0.9% APG12) consisted of minimal amount of CrEL to pose any adverse effect. In comparison, the toxic paclitaxel-loaded Toxol (50% CrEL) formulation needed to be diluted by 5 to 20-fold before administration (Ta-Chung et al., 2005; Mao et al, 2018). However, there is no significant difference in cell viabilities ($p < 0.05$) despite higher cell viability exhibited by NE3 exhibited than NE0 and ibuprofen alone.
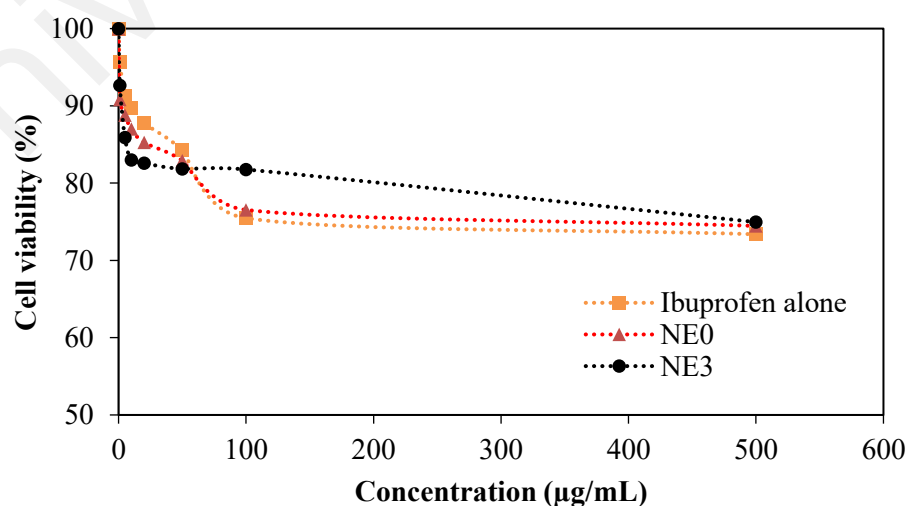
Figure 4.21: Cytotoxicity profile for nanoemulsions without APG (NE0) and with APG12 (NE3) when compared with ibuprofen alone.

CHAPTER 5: CONCLUSION

5.1 Conclusions

The synergistic potential of the sugar-based APG surfactants composed of short to medium-chained alkyl tails (C8-12) with the medium-chained triglycerides (C12) in coconut oil has been investigated. The right quality of APG co-surfactant type and the right quantity (optimized mixing ratios) overcame the toxic side effect concerning the use of polyethoxylated Cremophor EL (CrEL) surfactant in drug-carrying formulations has been discovered. The result of this study demonstrated that nanoemulsion containing ibuprofen was successfully formulated using low-energy phase inversion composition method and influenced by the incorporation of alkyl polyglucosides (APGs).

In the phase behaviour of coconut oil-based systems stabilized by Cremophor EL (CrEL), APG type (alkyl chain length of 8, 10 and 12 carbons) and APG proportion (CrEL:APG ratio of 9:1, 8:2 and 6:4) showed correlation with hydrophilicity-lipophilicity and geometrical influence on the system. In comparison with the system without APG, systems with APG12 and APG10 surfactants improved solubilization and formed larger one-phase regions, while system with APG08 surfactant exhibited smaller one-phase region. The mixed surfactants of CrEL and the more lipophilic APGs exhibited higher emulsifying ability than CrEL surfactant alone. The optimum CrEL:APG ratio mixed surfactants was 9:1. Further increase in APG surfactant proportion caused chain stiffness and one-phase regions shifted away from the water-rich vertex towards the oil-rich vertex. Winsor I and Winsor 4 systems were observed, and phase transitions were identified in the continuous emulsification path for 9:1 of S:O ratio only. The optimum nanoemulsions NE0, NE1, NE2 and NE3 were prepared at optimum composition of 90% water, 9:1 of S:O ratio, 9:1 of CrEL:APG ratio and 0.1% ibuprofen model drug in coconut oil.

The physicochemical characterizations comprised of particle size, polydispersity index, zeta potential and microscopic analyses showed that nanoemulsions exhibited interesting behaviour and microstructures. This can be correlated with the shared alkyl chains of the medium-chain triglycerides and the APG surfactant molecules as APG08, APG10 and APG12 co-surfactants (8, 10, 12 carbon length respectively) possess similar alkyl chain length with the medium-chained triglycerides (6-12 carbon length) in coconut oil. Stability studies indicated that the instability phenomena were hindered with incorporation of APG and the nanoemulsions possessed good stability and homogeneity against phase separation for 90 days storage. The suggested storage temperature for the nanoemulsions was at room temperature. The studies also showed that the optimum nanoemulsions exhibited suitable size for topical administration route, sustained release of ibuprofen and no cytotoxic effect. Based on the findings, nanoemulsion with APG12 (NE3) were more stable and robust than nanoemulsion without APG, with APG08 and with APG10 (NE0, NE1 and NE2). Thus, APG could be used as an alternative stabilizing agent and the APG-incorporated nanoemulsions could be used for topical applications.

5.2   Future Works

The stable formulations can be further modified with incorporation of additives such as hydrocolloid gums to enhance the viscosity for topical route of administration. The nanoemulsions can also be considered for parenteral route of administration with slight size modification as particle size must be larger than 30 nm to avoid leaking into blood capillaries (Yukuyama et al., 2017). Due to the neutral nonionic surfactants and the tiny particle size (< 20 nm in diameter size) of the drug carrier system produced, this system might also be used to carry targeted drug for more intrusive application such as brain-blood-barrier (BBB) routes with further development in target specificity. Due to its hydrophilicity, APG could be used as main surfactant in water-in-oil (W/O) emulsion or as o-surfactant in oil-in-water-in-oil (O/W/O) emulsion.

REFERENCES

Abbott, S. (2017). *Solubility science: principles and practice*. Ipswich, England: TCNF Ltd

Abbott, S. (2020). Solubility, similarity, and compatibility: A general-purpose theory for the formulator. *Current Opinion in Colloid & Interface Science*, *48*, 65-76.

Acharya, D. P., & Kunieda, H. (2006). Wormlike micelles in mixed surfactant solutions. *Advances in Colloid and Interface Science*, *123*, 401-413.

Ahmad, N., Ramsch, R., Esquena, J., Solans, C., Tajuddin, H. A., & Hashim, R. (2012). Physicochemical characterization of natural-like branched-chain glycosides toward formation of hexosomes and vesicles. *Langmuir*, *28*(5), 2395-2403.

Ahmad, N., Ramsch, R., Llinàs, M., Solans, C., Hashim, R., & Tajuddin, H. A. (2014). Influence of nonionic branched-chain alkyl glycosides on a model nano-emulsion for drug delivery systems. *Colloids and Surfaces, B: Biointerfaces*, *115*, 267-274.

Akrawi, S. H., Gorain, B., Nair, A. B., Choudhury, H., Pandey, M., Shah, J. N., & Venugopala, K. N. (2020). Development and optimization of naringenin-loaded chitosan-coated nanoemulsion for topical therapy in wound healing. *Pharmaceutics*, *12*(9), Article#893.

Ali, N., Bilal, M., Khan, A., Ali, F., & Iqbal, H. M. (2020). Effective exploitation of anionic, nonionic, and nanoparticle-stabilized surfactant foams for petroleum hydrocarbon contaminated soil remediation. *Science of the Total Environment*, *704*, Article#135391.

Amri, I. N. (2011). The lauric (coconut and palm kernel) oils. In Gunstone, F. D. (Ed.), *Vegetable oils in food technology composition, properties and uses* (pp. 169-194). Blackwell Publishing Ltd.

Anderson, B. D., & Marra, M. T. (1999). Chemical and related factors controlling lipid solubility. *Bulletin technique-Gattefossé Report, (92)*, 11-19.

Anton, N., & Vandamme, T. F. (2011). Nano-emulsions and micro-emulsions: clarifications of the critical differences. *Pharmaceutical Research*, *28*(5), 978-985.

Anuchatkidjaroen, S., & Phaechamud, T. (2013). Virgin coconut oil containing injectable vehicles for ibuprofen sustainable release. *Key Engineering Materials, 545*, 52-56

Arbain, N. H., Salim, N., Masoumi, H. R. F., Wong, T. W., Basri, M., & Rahman, M. B. A. (2019). In vitro evaluation of the inhalable quercetin loaded nanoemulsion for pulmonary delivery. *Drug Delivery and Translational Research*, *9*(2), 497-507.

Arbain, N. H., Salim, N., Wui, W. T., Basri, M., & Rahman, M. B. A. (2018). Optimization of quercetin loaded palm oil ester based nanoemulsion formulation for pulmonary delivery. *Journal of Oleo Science, 67*(8), 933-940.

Azhar, S. N. A. S., Ashari, S. E., & Salim, N. (2018). Development of a kojic monooleate-enriched oil-in-water nanoemulsion as a potential carrier for hyperpigmentation treatment. *International Journal of Nanomedicine*, *13*, Article#6465.

Babayan, V. K. (1987). Medium chain triglycerides and structured lipids. *Lipids*, *22*(6), 417-420.

Babick, F. (2019). Dynamic light scattering (DLS). In Hodoroaba, V. D., Unger, W., & Shard, A. (Eds.), *Characterization of Nanoparticles: Measurement Processes for Nanoparticles* (pp. 137-172). Elsevier Ltd.

Bajaj, S., Singla, D., & Sakhuja, N. (2012). Stability testing of pharmaceutical products. *Journal of Applied Pharmaceutical Science, 2*(3), 129-38.

Benita, S., & Levy, M. Y. (1993). Submicron emulsions as colloidal drug carriers for intravenous administration: comprehensive physicochemical characterization. *Journal of Pharmaceutical Sciences*, *82*(11), 1069-1079.

Bergonzi, M. C., Guccione, C., Grossi, C., Piazzini, V., Torracchi, A., Luccarini, I., ... & Bilia, A. R. (2016). Albumin nanoparticles for brain delivery: a comparison of chemical versus thermal methods and in vivo behavior. *ChemMedChem*, *11*(16), 1840-1849.

Brinker, C. J., Lu, Y., Sellinger, A., & Fan, H. (1999). Evaporation-induced self-assembly: nanostructures made easy. *Advanced Materials*, *11*(7), 579-585.

Brinkmann, J., Rest, F., Luebbert, C., & Sadowski, G. (2020). Solubility of pharmaceutical ingredients in natural edible oils. *Molecular Pharmaceutics*, *17*(7), 2499-2507.

Butt, H. J., Graf, K., & Kappl, M. (2013). *Physics and chemistry of interfaces*. John Wiley & Sons Ltd.

Callender, S. P., Mathews, J. A., Kobernyk, K., & Wettig, S. D. (2017). Microemulsion utility in pharmaceuticals: Implications for multi-drug delivery. *International Journal of Pharmaceutics*, *526*(1-2), 425-442.

Calogiuri, G., Foti, C., Nettis, E., Di Leo, E., Macchia, L., & Vacca, A. (2019). Polyethylene glycols and polysorbates: Two still neglected ingredients causing true IgE-mediated reactions. *Journal of Allergy and Clinical Immunology*, 7(7), 2509-2510.

Cao, Y., Marra, M., & Anderson, B. D., (2004). Predictive relationships for the effects of triglyceride ester concentration and water uptake on solubility and partitioning of small molecules into lipid vehicles. *Journal of Pharmaceutical Sciences, 93,* 2768–2779.

Chellapa, P., Mohamed, A. T., Keleb, E. I., Elmahgoubi, A., Eid, A. M., Issa, Y. S., & Elmarzugi, N. A. (2015). Nanoemulsion and nanoemulgel as a topical formulation. *IOSR Journal of Pharmacy*, *5*(10), 43-47.

Chen, S., Hanning, S., Falconer, J., Locke, M., & Wen, J. (2019). Recent advances in non-ionic surfactant vesicles (niosomes): Fabrication, characterization, pharmaceutical and cosmetic applications. *European Journal of Pharmaceutics and Biopharmaceutics*, *144*, 18-39.

Chime, S. A., Kenechukwu, F. C., & Attama, A. A. (2014). Nanoemulsions – Advances in formulation, characterization and applications in drug delivery. In Sezer A. D. (Ed.), *Application of Nanotechnology in Drug Delivery* (pp. 77-126). InTechOpen.

Clément, P., Laugel, C., & Marty, J. P. (2000). Influence of three synthetic membranes on the release of caffeine from concentrated W/O emulsions. *Journal of Controlled Release*, *66*(2-3), 243-254.

Clogston, J. D., & Patri, A. K. (2011). Zeta potential measurement. In McNeil S. E. (Ed.), Characterization *of Nanoparticles Intended for Drug Delivery* (pp. 63-70). Humana Press.

da Silva Marques, T. Z., Santos-Oliveira, R., de Siqueira, L. B. D. O., da Silva Cardoso, V., de Freitas, Z. M. F., & da Silva Ascenção, R. D. C. (2018). Development and characterization of a nanoemulsion containing propranolol for topical delivery. *International Journal of Nanomedicine*, *13*, Article#2827.

Dammak, I., Sobral, P. J. D. A., Aquino, A., Neves, M. A. D., & Conte-Junior, C. A. (2020). Nanoemulsions: Using emulsifiers from natural sources replacing synthetic ones—A review. *Comprehensive Reviews in Food Science and Food Safety*, *19*(5), 2721-2746.

Danaei, M., Dehghankhold, M., Ataei, S., Hasanzadeh Davarani, F., Javanmard, R., Dokhani, A., ... & Mozafari, M. R. (2018). Impact of particle size and polydispersity index on the clinical applications of lipidic nanocarrier systems. *Pharmaceutics*, *10*(2), Article#57.

Djekic, L., & Primorac, M. (2008). The influence of cosurfactants and oils on the formation of pharmaceutical microemulsions based on PEG-8 caprylic/capric glycerides. *International Journal of Pharmaceutics*, *352*(1-2), 231-239.

Djekic, L., Martinovic, M., Stepanović-Petrović, R., Tomić, M., Micov, A., & Primorac, M. (2015). Design of block copolymer costabilized nonionic microemulsions and their in vitro and in vivo assessment as carriers for sustained regional delivery of ibuprofen via topical administration. *Journal of Pharmaceutical Sciences*, *104*(8), 2501-2512.

Djekic, L., Primorac, M., & Jockovic, J. (2011). Phase behaviour, microstructure and ibuprofen solubilization capacity of pseudo-ternary nonionic microemulsions. *Journal of Molecular Liquids*, *160*(2), 81-87.

Djekic, L., Primorac, M., Filipic, S., & Agbaba, D. (2012). Investigation of surfactant/cosurfactant synergism impact on ibuprofen solubilization capacity and drug release characteristics of nonionic microemulsions. *International Journal of Pharmaceutics*, *433*(1-2), 25-33.

El-Aasser, M. S., Lack, C. D., Vanderhoff, J. W., & Fowkes, F. M. (1988). The miniemulsification process—different form of spontaneous emulsification. *Colloids and Surfaces*, *29*(1), 103-118.

Elkordy, A. A., & Essa, E. A. (2010). Dissolution of ibuprofen from spray dried and spray chilled particles. *Pakistan Journal of Pharmaceutical Sciences*, *23*(3), 284-290.

Elsayed, H. H., Elrahman, M. K. A., Emara, A. H., & El-Hafez, A. (2015). Compare effect of fatty acid composition (olive, coconut oil and butter) on adipose liver tissue, and serum lipid profile in albino rats. *IOSR Journal of Biotechnology and Biochemistry*, *1*, 28-38.

Fanun, M. (Ed.). (2008). *Microemulsions: Properties and applications* (Vol. 144). CRC Press.

Ferreira, T. M., Bernin, D., & Topgaard, D. (2013). NMR studies of nonionic surfactants. *Annual Reports on NMR Spectroscopy*, *79*, 73-127.

Fukuda, K., Olsson, U., & Ueno, M. (2001). Microemulsion formed by alkyl polyglucoside and an alkyl glycerol ether with weakly charged films. *Colloids and Surfaces, B: Biointerfaces*, *20*(2), 129-135.

Gelderblom, H., Verweij, J., Nooter, K., & Sparreboom, A. (2001). Cremophor EL: The drawbacks and advantages of vehicle selection for drug formulation. *European Journal of Cancer*, *37*(13), 1590-1598.

Gonzalez-Valdivieso, J., Girotti, A., Schneider, J., & Arias, F. J. (2021). Advanced nanomedicine and cancer: Challenges and opportunities in clinical translation. *International Journal of Pharmaceutics*, *599*, Article#120438.

Greenwald, H. L., Brown, G. L., & Fineman, M. N. (1956). Determination of hydrophile-lipophile character of surface-active agents and oils by water titration. *Analytical Chemistry*, *28*(11), 1693-1697.

Griffin, W. C. (1949). Classification of surface-active agents by "HLB". *Journal of the Society of Cosmetic Chemists*, *1*, 311-326.

Gudiña, E. J., Rangarajan, V., Sen, R., & Rodrigues, L. R. (2013). Potential therapeutic applications of biosurfactants. *Trends in Pharmacological Sciences*, *34*(12), 667-675.

Guerra-Ponce, W. L., Gracia-Vásquez, S. L., González-Barranco, P., Camacho-Mora, I. A., Gracia-Vásquez, Y. A., Orozco-Beltrán, E., & Felton, L. A. (2016). In vitro evaluation of sustained released matrix tablets containing ibuprofen: A model poorly water-soluble drug. *Brazilian Journal of Pharmaceutical Sciences*, *52*(4), 751-759.

Hadzir, N. M., Basri, M., Rahman, M. B. A., Salleh, A. B., Rahman, R. N. Z. R. A., & Basri, H. (2013). Phase behaviour and formation of fatty acid esters nanoemulsions containing piroxicam. *AAPS PharmSciTech*, *14*(1), 456-463.

Han, Z., Yang, X., Liu, Y., Wang, J., & Gao, Y. (2015). Physicochemical properties and phase behavior of didecyldimethylammonium chloride/alkyl polyglycoside surfactant mixtures. *Journal of Surfactants and Detergents*, *18*(4), 641-649.

Hardesty, J. H., & Attili, B. (2010). *Spectrophotometry and the Beer-Lambert Law: An Important Analytical Technique in Chemistry*. (Doctoral dissertation, Collin College). Retrieved from http://vfsilesieux.free.fr/1Seuro/BeerLaw.pdf.

Harun, S. N., Nordin, S. A., Abd Gani, S. S., Shamsuddin, A. F., Basri, M., & Basri, H. B. (2018). Development of nanoemulsion for efficient brain parenteral delivery of cefuroxime: Designs, characterizations, and pharmacokinetics. *International Journal of Nanomedicine*, *13*, Article#2571.

Hasan, H. M., Leanpolchareanchai, J., & Jintapattanakit, A. (2015). Preparation of virgin coconut oil nanoemulsions by phase inversion temperature method. In Sriamornsak P., Limmatvapirat S., & Piriyaprasart S., *Advanced Materials Research* (Vol. 1060, pp. 99-102). Trans Tech Publications Ltd.

Hashim, R., Hashim, H. H. A., Rodzi, N. Z. M., Hussen, R. S. D., & Heidelberg, T. (2006). Branched chain glycosides: Enhanced diversity for phase behavior of easily accessible synthetic glycolipids. *Thin Solid Films*, *509*(1-2), 27-35.

Hashim, R., Sugimura, A., Minamikawa, H., & Heidelberg, T. (2012). Nature-like synthetic alkyl branched-chain glycolipids: A review on chemical structure and self-assembly properties. *Liquid Crystals*, *39*(1), 1-17.

Hato, M. (2001). Synthetic glycolipid/water systems. *Current Opinion in Colloid & Interface Science*, *6*(3), 268-276.

Hato, M., Minamikawa, H., Tamada, K., Baba, T., & Tanabe, Y. (1999). Self-assembly of synthetic glycolipid/water systems. *Advances in Colloid and Interface Science*, *80*(3), 233-270.

He, G. S., Qin, H. Y., & Zheng, Q. (2009). Rayleigh, Mie, and Tyndall scatterings of polystyrene microspheres in water: Wavelength, size, and angle dependences. *Journal of Applied Physics*, *105*(2), Article#023110.

Henríquez, C. J. M. (2009). *W/O Emulsions: Formulation, Characterization and Destabilization* (Doctoral dissertation, Brandenburg University of Technology, Caracas, Venezuela). Retrieved from https://core.ac.uk/download/pdf/33428703.pdf

Holmberg, K. (2001). Natural surfactants. *Current Opinion in Colloid & Interface Science*, *6*(2), 148-159.

Holmberg, K., Lindman, B., & Kronberg, B. (2014). *Surface chemistry of surfactants and polymers*. John Wiley & Sons.

Ilic, D., Cvetkovic, M., & Tasic-Kostov, M. (2021). Emulsions with alkyl polyglucosides as carriers for off-label topical spironolactone–safety and stability evaluation. *Pharmaceutical Development and Technology*, 1-25.

Ilić, M., Haegel, F. H., Pavelkić, V., Zlatanović, D., Nikolić-Mandić, S., Lolić, A., & Nedić, Z. (2016). The influence of alkyl polyglucosides (and highly ethoxylated alcohol boosters) on the phase behavior of a water/toluene/technical alkyl polyethoxylate microemulsion system. *Chemical Industry & Chemical Engineering Quarterly*, *22*(1), 27-32.

Isailović, T. M., Todosijević, M. N., Đorđević, S. M., & Savić, S. D. (2017). Natural surfactants-based micro/nanoemulsion systems for NSAIDs—practical formulation approach, physicochemical and biopharmaceutical characteristics/performances. In *Microsized and Nanosized Carriers for Nonsteroidal Anti-Inflammatory Drugs* (pp. 179-217).

Jadhav, S. R., Bryant, G., Mata, J. P., Eldridge, D. S., Palombo, E. A., Harding, I. H., & Shah, R. M. (2021). Structural aspects of a self-emulsifying multifunctional amphiphilic excipient: Part II. The case of Cremophor EL. *Journal of Molecular Liquids*, *344*, Article#117881.

Jahan, R., Bodratti, A. M., Tsianou, M., & Alexandridis, P. (2020). Biosurfactants, natural alternatives to synthetic surfactants: Physicochemical properties and applications. *Advances in Colloid and Interface Science*, *275*, Article#102061.

Jaiswal, M., Dudhe, R., & Sharma, P. K. (2015). Nanoemulsion: An advanced mode of drug delivery system. *3 Biotech*, *5*(2), 123-127.

Jasmina, H., Džana, O., Alisa, E., Edina, V., & Ognjenka, R. (2017). Preparation of nanoemulsions by high-energy and lower-energy emulsification methods. *Proceedings of the International Conference on Medical and Biological Engineering 2017*, 317-322.

Jiang, L. C., Basri, M., Omar, D., Rahman, M. B. A., Salleh, A. B., & Rahman, R. N. Z. R. A. (2011). Self-assembly behaviour of alkylpolyglucosides (APG) in mixed surfactant-stabilized emulsions system. *Journal of Molecular Liquids*, *158*(3), 175-181.

Jintapattanakit, A., Hasan, H. M., & Junyaprasert, V. B. (2018). Vegetable oil-based nanoemulsions containing curcuminoids: Formation optimization by phase inversion temperature method. *Journal of Drug Delivery Science and Technology*, *44*, 289-297.

Jurado, E., Bravo, V., Vicaria, J. M., Fernandez-Arteaga, A., & Garcia-Lopez, A. I. (2008). Triolein solubilization using highly biodegradable non-ionic surfactants. *Colloids and Surfaces, A: Physicochemical and Engineering Aspects*, *326*(3), 162-168.

Keck, C. M., Kovačević, A., Müller, R. H., Savić, S., Vuleta, G., & Milić, J. (2014). Formulation of solid lipid nanoparticles (SLN): The value of different alkyl polyglucoside surfactants. *International Journal of Pharmaceutics*, *474*(1-2), 33-41.

Kiss, L., Walter, F. R., Bocsik, A., Veszelka, S., Ózsvári, B., Puskás, L. G., ... & Deli, M. A. (2013). Kinetic analysis of the toxicity of pharmaceutical excipients Cremophor EL and RH40 on endothelial and epithelial cells. *Journal of pharmaceutical sciences*, *102*(4), 1173-1181.

Kotta, S., Khan, A. W., Ansari, S. H., Sharma, R. K., & Ali, J. (2015). Formulation of nanoemulsion: a comparison between phase inversion composition method and high-pressure homogenization method. *Drug Delivery*, *22*(4), 455-466.

Kronberg, B., Holmberg, K., & Lindman, B. (2014). *Surface chemistry of surfactants and polymers*. John Wiley & Sons Ltd.

Kumar, M., Bishnoi, R. S., Shukla, A. K., & Jain, C. P. (2019). Techniques for formulation of nanoemulsion drug delivery system: a review. *Preventive Nutrition and Food Science*, *24*(3), Article#225.

Langevin, D. (1992). Micelles and microemulsions. *Annual Review of Physical Chemistry*, *43*(1), 341-369.

Ledet, G., Bostanian, L. A., Mandal, T. K., & Tiwari, A. (2013). *Nanoemulsions as a vaccine adjuvant* (pp. 125-148). CRC Press.

Li, M., McClements, D. J., Liu, X., & Liu, F. (2020). Design principles of oil-in-water emulsions with functionalized interfaces: Mixed, multilayer, and covalent complex structures. *Comprehensive Reviews in Food Science and Food Safety*, *19*(6), 3159-3190.

Lim, C. J., Basri, M., Omar, D., Rahman, M. A., Salleh, A. B., & Rahman, A. (2012). Phase behaviour of nonionic surfactants in new palm oil esters-based emulsion for glyphosate isopropylamine formulation. *Asian Journal of Chemistry*, *24*(10), Article#4601.

Lusas, E. W., Riaz, M. N., Alam, M. S., & Clough, R. (2017). Animal and vegetable fats, oils, and waxes. In Kent, J. A., Bommaraju, T. V., & Barnicki, S. D. (Eds.), *Handbook of Industrial Chemistry and Biotechnology* (pp. 823-932). Springer Publishing.

Malvern Instruments. (2004). *Zetasizer Nano User Manual MAN0317*. Retrieved from https://www.malvernpanalytical.com/en/learn/knowledge-center.

Mao, Y., Zhang, Y., Luo, Z., Zhan, R., Xu, H., Chen, W., & Huang, H. (2018). Synthesis, biological evaluation and low-toxic formulation development of glycosylated paclitaxel prodrugs. *Molecules*, *23*(12), Article#3211.

Marhamati, M., Ranjbar, G., & Rezaie, M. (2021). Effects of emulsifiers on the physicochemical stability of Oil-in-water Nanoemulsions: A critical review. *Journal of Molecular Liquids*, *340*, Article#117218.

Marina, A. M., Che Man, Y. B., Nazimah, S. A. H., & Amin, I. (2009). Chemical properties of virgin coconut oil. *Journal of the American Oil Chemists' Society, 86*(4), 301-307.

Mason, J. D., Cone, M. T., & Fry, E. S. (2016). Ultraviolet (250–550 nm) absorption spectrum of pure water. *Applied Optics*, *55*(25), 7163-7172.

Mason, T. G., Wilking, J. N., Meleson, K., Chang, C. B., & Graves, S. M. (2006). Nanoemulsions: formation, structure, and physical properties. *Journal of Physics: Condensed Matter*, *18*(41), R635-R666.

Matsaridou, I., Barmpalexis, P., Salis, A., & Nikolakakis, I. (2012). The influence of surfactant HLB and oil/surfactant ratio on the formation and properties of self-emulsifying pellets and microemulsion reconstitution. *AAPS PharmSciTech*, *13*(4), 1319-1330.

McClements, D. J. (2011). Edible nanoemulsions: Fabrication, properties, and functional performance. *Soft Matter*, *7*(6), 2297-2316.

McClements, D. J. (2012). Nanoemulsions versus microemulsions: Terminology, differences, and similarities. *Soft Matter, 8*(6), 1719-1729.

McClements, D. J. (2017). The future of food colloids: Next-generation nanoparticle delivery systems. *Current Opinion in Colloid & Interface Science*, *28*, 7-14.

McClements, D. J. (2020). Advances in nanoparticle and microparticle delivery systems for increasing the dispersibility, stability, and bioactivity of phytochemicals. *Biotechnology Advances*, *38*, Article#107287.

McClements, D. J., & Jafari, S. M. (2018). Improving emulsion formation, stability and performance using mixed emulsifiers: A review. *Advances in Colloid and Interface Science*, *251*, 55-79.

Moghimipour, E., Salimi, A., & Eftekhari, S. (2013). Design and characterization of microemulsion systems for naproxen. *Advanced Pharmaceutical Bulletin*, *3*(1), Article#63.

Moldes, A. B., Rodríguez-López, L., Rincón-Fontán, M., López-Prieto, A., Vecino, X., & Cruz, J. M. (2021). Synthetic and bio-derived surfactants versus microbial biosurfactants in the cosmetic industry: An overview. *International Journal of Molecular Sciences*, *22*(5), Article#2371.

Moore, J. E., McCoy, T. M., de Campo, L., Sokolova, A. V., Garvey, C. J., Pearson, G., ... & Tabor, R. F. (2018). Wormlike micelle formation of novel alkyl-tri (ethylene glycol)-glucoside carbohydrate surfactants: Structure–function relationships and rheology. *Journal of colloid and interface science*, *529*, 464-475.

Mosca, M., Cuomo, F., Lopez, F., & Ceglie, A. (2013). Role of emulsifier layer, antioxidants and radical initiators in the oxidation of olive oil-in-water emulsions. *Food Research International*, *50*(1), 377-383.

Musa, S. H., Basri, M., Masoumi, H. R. F., Shamsudin, N., & Salim, N. (2017). Enhancement of physicochemical properties of nanocolloidal carrier loaded with cyclosporine for topical treatment of psoriasis: in vitro diffusion and in vivo hydrating action. *International Journal of Nanomedicine*, *12*, Article#2427.

Myers, D. (2006). *Surfactant science and technology*. John Wiley & Sons Ltd.

Nainggolan, I., Radiman, S., Hamzah, A. S., & Hashim, R. (2009). The effect of the head group on branched-alkyl chain surfactants in glycolipid/n-octane/water ternary system. *Colloids and Surfaces, B: Biointerfaces*, *73*(1), 84-91.

Najjar, R. (Ed.). (2012). *Microemulsions: an introduction to properties and applications*. IntechOpen.

News-Medical.net (2014). Influence of concentration effects and particle interactions on DLS analysis of bioformulations. Retrieved from https://www.news-medical.net/whitepaper/20141218/Influence-of-Concentration-Effects-and-Particle-Interactions-on-DLS-Analysis-of-Bioformulations.aspx.

Nikam, T. H., Patil, M. P., Patil, S. S., Vadnere, G. P., & Lodhi, S. (2018). Nanoemulsion: A brief review on development and application in parenteral drug delivery. *Advance Pharmaceutical Journal*, *3*, 43-54.

Ontiveros, J. F., Pierlot, C., Catté, M., Molinier, V., Salager, J. L., & Aubry, J. M. (2014). A simple method to assess the hydrophilic lipophilic balance of food and cosmetic surfactants using the phase inversion temperature of C10E4/n-octane/water emulsions. *Colloids and Surfaces, A: Physicochemical and Engineering Aspects*, *458*, 32-39.

Pajić, N. B., Ilić, T., Nikolić, I., Dobričić, V., Pantelić, I., & Savić, S. (2019). Alkyl polyglucoside-based adapalene-loaded microemulsions for targeted dermal delivery: Structure, stability and comparative biopharmaceutical characterization with a conventional dosage form. *Journal of Drug Delivery Science and Technology*, *54*, Article#101245.

Pajić, N. B., Todosijević, M. N., Vuleta, G. M., Cekić, N. D., Dobričić, V. D., Vučen, S. R., ... & Savić, S. D. (2017). Alkyl polyglucoside vs. ethoxylated surfactant-based microemulsions as vehicles for two poorly water-soluble drugs: Physicochemical characterization and in vivo skin performance. *Acta Pharmaceutica*, *67*(4), 415-439.

Pal, A., Mondal, M. H., Adhikari, A., Bhattarai, A., & Saha, B. (2021). Scientific information about sugar-based emulsifiers: a comprehensive review. *RSC Advances*, *11*(52), 33004-33016.

Pantelic, I. (Ed.). (2014). *Alkyl polyglucosides: From natural-origin surfactants to prospective delivery systems*. Elsevier Ltd.

, N., & Bregni, C. (2009). The studies on hydrophilic-lipophilic balance (HLB): Sixty years after William C. Griffin's pioneer work (1949-2009). *Latin American Journal of Pharmacy*, *28*(2), 313-317.

Pasquali, R. C., Taurozzi, M. P., & Bregni, C. (2008). Some considerations about the hydrophilic–lipophilic balance system. *International Journal of Pharmaceutics, 356*(1-2), 44-51.

Patel, M. R., Patel, R. B., & Thakore, S. D. (2018). Nanoemulsion in drug delivery. In Asiri, A., *Applications of nanocomposite materials in drug delivery* (pp. 667-700). Woodhead Publishing.

Pengon, S., Chinatangkul, N., Limmatvapirat, C., & Limmatvapirat, S. (2018). The effect of surfactant on the physical properties of coconut oil nanoemulsions. *Asian Journal of Pharmaceutical Sciences*, *13*(5), 409-414.

Perazzo, A., Preziosi, V., & Guido, S. (2015). Phase inversion emulsification: Current understanding and applications. *Advances in Colloid and Interface Science*, *222*, 581-599.

Piazzini, V., Monteforte, E., Luceri, C., Bigagli, E., Bilia, A. R., & Bergonzi, M. C. (2017). Nanoemulsion for improving solubility and permeability of Vitex agnus-castus extract: formulation and in vitro evaluation using PAMPA and Caco-2 approaches. *Drug delivery*, *24*(1), 380-390.

Pongsawatmanit, R., & Srijunthongsiri, S. (2008). Influence of xanthan gum on rheological properties and freeze–thaw stability of tapioca starch. *Journal of Food Engineering*, *88*(1), 137-143.

Rajpoot, K., & Tekade, R. K. (2019). Microemulsion as drug and gene delivery vehicle: An inside story. In *Drug Delivery Systems* (pp. 455-520).

Ramisetty, K. A., Pandit, A. B., & Gogate, P. R. (2015). Ultrasound assisted preparation of emulsion of coconut oil in water: Understanding the effect of operating parameters and comparison of reactor designs. *Chemical Engineering and Processing: Process Intensification*, *88*, 70-77.

Rapp, B. E. (2017). *Microfluidics: Modeling, Mechanics and Mathematics*. Elsevier Ltd.

Rodriguez, V. B., Alameda, E. J., Requena, A. R., López, A. G., Bailón-Moreno, R., & Aranda, M. C. (2005). Determination of average molecular weight of commercial surfactants: alkylpolyglucosides and fatty alcohol ethoxylates. *Journal of Surfactants and Detergents*, *8*(4), 341-346.

Roohinejad, S., Greiner, R., Oey, I., & Wen, J. (Eds.). (2018). Emulsion-based systems for delivery of food active compounds: formation, application, health and safety.

Rootman, D. B., Lin, J. L., & Goldberg, R. (2014). Does the Tyndall effect describe the blue hue periodically observed in subdermal hyaluronic acid gel placement? *Ophthalmic Plastic & Reconstructive Surgery*, *30*(6), 524-527.

Rosen, M. J., & Kunjappu, J. T. (2012). *Surfactants and interfacial phenomena*. John Wiley & Sons Ltd.

Rosenholm, J. B. (2020). Critical evaluation of models for self-assembly of short and medium chain-length surfactants in aqueous solutions. *Advances in Colloid and Interface Science*, *276*, Article#102047.

Rosso, A., Lollo, G., Chevalier, Y., Troung, N., Bordes, C., Bourgeois, S., ... & Briancon, S. (2020). Development and structural characterization of a novel nanoemulsion

for oral drug delivery. *Colloids and Surfaces, A: Physicochemical and Engineering Aspects*, *593*, Article#124614.

Ruiz, C. C., & Molina-Bolívar, J. A. (2011). Characterization of mixed non-ionic surfactants n-octyl-β-d-thioglucoside and octaethylene–glycol monododecyl ether: Micellization and microstructure. *Journal of Colloid and Interface Science*, *361*(1), 178-185.

Sabjan, K. B., Munawar, S. M., Rajendiran, D., Vinoji, S. K., & Kasinathan, K. (2020). Nanoemulsion as Oral Drug Delivery-A Review. *Current Drug Research Reviews Formerly: current drug abuse reviews*, *12*(1), 4-15.

Sadurní, N., Solans, C., Azemar, N., & García-Celma, M. J. (2005). Studies on the formation of O/W nano-emulsions, by low-energy emulsification methods, suitable for pharmaceutical applications. *European Journal of Pharmaceutical Sciences*, *26*(5), 438-445.

Said Suliman, A., Tom, R., Palmer, K., Tolaymat, I., Younes, H. M., Arafat, B., ... & Najlah, M. (2020). Development, characterization and stability evaluation of ciprofloxacin-loaded parenteral nutrition nanoemulsions. *Pharmaceutical Development and Technology*, *25*(5), 579-587.

Salager, J. L. (2021). A Normalized Hydrophilic–Lipophilic Deviation Expression HLDN Is Necessary to Avoid Confusion Close to the Optimum Formulation of Surfactant-Oil–Water Systems. *Journal of Surfactants and Detergents*, *24*(5), 731-748.

Salager, J. L., Antón, R., Bullón, J., Forgiarini, A., & Marquez, R. (2020). How to use the normalized hydrophilic-lipophilic deviation (hldn) concept for the formulation of equilibrated and emulsified surfactant-oil-water systems for cosmetics and pharmaceutical products. *Cosmetics*, *7*(3), Article#57.

Salim, N., Ahmad, N., Musa, S. H., Hashim, R., Tadros, T. F., & Basri, M. (2016). Nanoemulsion as a topical delivery system of antipsoriatic drugs. *RSC advances*, *6*(8), 6234-6250.

Salim, N., Basri, M., Rahman, M. B., Abdullah, D. K., & Basri, H. (2012). Modification of palm kernel oil esters nanoemulsions with hydrocolloid gum for enhanced topical delivery of ibuprofen. *International Journal of Nanomedicine, 7*, Article#4739

Salim, N., Basri, M., Rahman, M.B., Abdullah, D.K., Basri, H., & Salleh, A.B. (2011). Phase behaviour, formation and characterization of palm-based esters nanoemulsion formulation containing ibuprofen. *Journal of Nanomedicine & Nanotechnology, 2*, 1-5.

Salim, N., García-Celma, M. J., Escribano, E., Nolla, J., Llinàs, M., Basri, M., ... & Tadros, T. F. (2018). Formation of nanoemulsion containing ibuprofen by PIC method for topical delivery. *Materials Today: Proceedings*, *5*, S172-S179.

Salunkhe, P. B., & Shembekar, P. S. (2012). A review on effect of phase change material encapsulation on the thermal performance of a system. *Renewable & Sustainable Energy Reviews*, *16*(8), 5603-5616.

Santos, J., Calero, N., Trujillo-Cayado, L. A., Garcia, M. C., & Muñoz, J. (2017). Assessing differences between Ostwald ripening and coalescence by rheology, laser diffraction and multiple light scattering. *Colloids and Surfaces, B: Biointerfaces*, *159*, 405-411.

Sarheed, O., Dibi, M., & Ramesh, K. V. (2020). Studies on the effect of oil and surfactant on the formation of alginate-based O/W lidocaine nanocarriers using nanoemulsion template. *Pharmaceutics*, *12*(12), Article#1223.

Savjani, K. T., Gajjar, A. K., & Savjani, J. K. (2012). Drug solubility: importance and enhancement techniques. *International Scholarly Research Notices Pharmaceutics*, Article#195727

Sazalee, S. A., Ahmad, N., & Hashim, R. (2017). Investigation of self-assembly properties and the effect of tween series co-surfactants on the stability of nonionic branched-chain glycolipid hexosomes. *Colloids and Surfaces, A: Physicochemical and Engineering Aspects*, *529*, 210-221.

Shakeel, F., Ramadan, W., Faisal, M. S., Rizwan, M., Faiyazuddin, M., Mustafa, G., & Shafiq, S. (2010). Transdermal and topical delivery of anti-inflammatory agents using nanoemulsion/microemulsion: an updated review. *Current Nanoscience*, *6*(2), 184-198.

Sheth, T., Seshadri, S., Prileszky, T., & Helgeson, M. E. (2020). Multiple nanoemulsions. *Nature Reviews Materials*, *5*(3), 214-228.

Siano, D. B. (1983). The swollen micelle—microemulsion transition. *Journal of Colloid and Interface Science*, *93*(1), 1-7.

Sing, A. J. F., Graciaa, A., Lachaise, J., Brochette, P., & Salager, J. L. (1999). Interactions and coalescence of nanodroplets in translucent O/W emulsions. *Colloids and Surfaces, A: Physicochemical and Engineering Aspects*, *152*(1-2), 31-39.

Skwarczynski, M., Hayashi, Y., & Kiso, Y. (2006). Paclitaxel prodrugs: toward smarter delivery of anticancer agents. *Journal of Medicinal Chemistry*, *49*(25), 7253-7269.

Solans, C., & Solé, I. (2012). Nano-emulsions: formation by low-energy methods. *Current Opinion in Colloid & Interface Science*, *17*(5), 246-254.

Solans, C., Izquierdo, P., Nolla, J., Azemar, N., & Garcia-Celma, M. J. (2005). Nano-emulsions. *Current Opinion in Colloid & Interface Science*, *10*(3-4), 102-110.

Sulek, M. W., & Wasilewski, T. (2006). Tribological properties of aqueous solutions of alkyl polyglucosides. *Wear*, *260*(1-2), 193-204.

Sułek, M. W., Ogorzałek, M., Wasilewski, T., & Klimaszewska, E. (2013). Alkyl polyglucosides as components of water-based lubricants. *Journal of Surfactants and Detergents*, *16*(3), 369-375.

Ta-Chung, C., Zyting, C., Ling-Ming, T., Tzeon-Jye, C., Ruey-Kuen, H., Wei-Shu, W., ... & Po-Min, C. (2005). Paclitaxel in a novel formulation containing less Cremophor EL as first-line therapy for advanced breast cancer: a phase II trial. *Investigational New Drugs*, *23*(2), 171-177.

Tadros, T., Izquierdo, P., Esquena, J., & Solans, C. (2004). Formation and stability of nano-emulsions. *Advances in Colloid and Interface Science*, *108*, 303-318.

Tasic-Kostov, M., Pavlovic, D., Lukic, M., Jaksic, I., Arsic, I., & Savic, S. (2012). Lactobionic acid as antioxidant and moisturizing active in alkyl polyglucoside-based topical emulsions: the colloidal structure, stability and efficacy evaluation. *International Journal of Cosmetic Science*, *34*(5), 424-434.

Tasić-Kostov, M., Reichl, S., Lukić, M., Jaksić, I., & Savić, S. (2011). Two alkyl polyglucoside natural surfactants varying in chain length in stabilization of lactobionic acid containing emulsions: physicochemical characterization and in vitro irritation potential assessment. *RSC Advances*, *88*(4), 256-264.

Turovsky, T., Khalfin, R., Kababya, S., Schmidt, A., Barenholz, Y., & Danino, D. (2015). Celecoxib encapsulation in β-casein micelles: structure, interactions, and conformation. *Langmuir*, *31*(26), 7183-7192.

Vanti, G. (2021). Recent strategies in nanodelivery systems for natural products: A review. *Environmental Chemistry Letters*, *19*(6), 4311-4326.

Velásquez, I., Muñoz, A., & Pereira, J. C. (2016). Tuning interfacial activity of polymeric resin–surfactant/n-alcohol solution interactions. *Journal of Surfactants and Detergents*, *19*(5), 1025-1032.

Vinceković, M., Viskić, M., Jurić, S., Giacometti, J., Kovačević, D. B., Putnik, P., ... & Jambrak, A. R. (2017). Innovative technologies for encapsulation of Mediterranean plants extracts. *Trends in Food Science & Technology*, *69*, 1-12.

von Rybinski, W., & Hill, K. (1998). Alkyl polyglycosides—properties and applications of a new class of surfactants. *Angewandte Chemie, International Edition*, *37*(10), 1328-1345.

Wang, K., Li, G., & Zhang, B. (2018). Opposite results of emulsion stability evaluated by the TSI and the phase separation proportion. *Colloids and Surfaces, A: Physicochemical and Engineering Aspects*, *558*, 402-409.

Wang, Z. N., Li, G. Z., Zhang, G. Y., Diao, Z. Y., Chen, L. S., & Wang, Z. W. (2005). Molecular interaction in binary surfactant mixtures containing alkyl polyglycoside. *Journal of Colloid and Interface Science*, *290*(2), 598-602.

Wik, J., Bansal, K. K., Assmuth, T., Rosling, A., & Rosenholm, J. M. (2019). Facile methodology of nanoemulsion preparation using oily polymer for the delivery of poorly soluble drugs. *Drug Delivery and Translational Research*, 1-13.

Winsor, P. A. (1948). Hydrotropy, solubilisation and related emulsification processes. *Transactions of the Faraday Society*, *44*, 376-398.

Wooster, T. J., Labbett, D., Sanguansri, P., & Andrews, H. (2016). Impact of microemulsion inspired approaches on the formation and destabilisation mechanisms of triglyceride nanoemulsions. *Soft Matter*, *12*(5), 1425-1435.

Wu, H. R., Wang, C. Q., Wang, J. X., Chen, J. F., & Le, Y. (2020). Engineering of long-term stable transparent nanoemulsion using high-gravity rotating packed bed for oral drug delivery. *International Journal of Nanomedicine*, *15*, 2391.

Yukuyama, M. N., Kato, E. T., Lobenberg, R., & Bou-Chacra, N. A. (2017). Challenges and future prospects of nanoemulsion as a drug delivery system. *Current Pharmaceutical Design, 23*(3), 495-508.

Zhang, J., Chai, J. L., Li, G. Z., Zhang, G. Y., & Xie, K. C. (2004). Phase behavior of the APG/alcohol/alkane/H2O system. *Journal of Dispersion Science and Technology*, *25*(1), 27-34.

Zhang, R., Zhang, L., & Somasundaran, P. (2004). Study of mixtures of n-dodecyl-β-d-maltoside with anionic, cationic, and nonionic surfactant in aqueous solutions using surface tension and fluorescence techniques. *Journal of Colloid and Interface Science, 278*(2), 453-460.

Zhang, Z., Li, K., Tian, R., & Lu, C. (2019). Substrate-assisted visualization of surfactant micelles via transmission electron microscopy. *Frontiers in Chemistry*, *7*, Article#242.

Zhao, L., Wei, Y., Huang, Y., He, B., Zhou, Y., & Fu, J. (2013). Nanoemulsion improves the oral bioavailability of baicalin in rats: In vitro and in vivo evaluation. *International Journal of Nanomedicine*, *8*, Article#3769.